OSMIUM GEOCHEMICAL BEHAVIOR AND GLOBAL ISOTOPIC CHANGES
ASSOCIATED WITH THE CRETACEOUS-PALEOGENE IMPACT

A THESIS SUBMITTED TO THE GRADUATE DIVISION OF THE UNIVERSITY OF
HAWAIʻI AT MĀNOA IN PARTIAL FULFILLMENT OF THE REQUIREMENTS FOR THE
DEGREE OF

MASTER OF SCIENCE

IN

GEOLOGY AND GEOPHYSICS

JUNE 2014

By

Jessica Zaiss

Thesis Committee:

Greg Ravizza, Chairperson

Ken Rubin

Eric Hellebrand

Abstract

The Re-Os isotopic system is a powerful tool for investigating impact events because of osmium enrichment in chondrites relative to upper continental crust and large isotopic differences between these two end-members. Physical mixing models of chondrites and upper continental crust predict that the $^{187}Os/^{188}Os$ ratio of sediments found at terrestrial Cretaceous-Paleogene (K-Pg) impact horizons should be ≈0.13. This is thought to represent the Os isotopic composition of the ejecta plume fallout that results from the impact event. Results reported here do not support a chondritic Os composition for the ejecta plume but rather suggest a slightly elevated $^{187}Os/^{188}Os$ ratio of ≈0.14. This is consistent with previously reported data. This has significant implications for Os-based estimates of impactor size. These results require a bolide greater than three times more massive than previous Os based estimates. These estimates are based on impact induced global changes in the $^{187}Os/^{188}Os$ ratio of seawater. Profiles of $^{187}Os/^{188}Os$ of marine sediments across the K-Pg boundary exhibit an excursion from ~0.4 before the impact, to ~0.15-0.17 immediately following the impact, and then recovery back to pre-impact values of ~0.4. This excursion has been documented for many sites and is therefore thought to be homogeneous throughout global seawater. Results here suggest that the Os inventory of the Indian sector of the Southern Ocean was more unradiogenic than the rest of the global ocean for at least the first 3 myr of the Paleogene as $^{187}Os/^{188}Os$ ratios recover only to ~0.32. However, reworking of sediment with inherently low $^{187}Os/^{188}Os$ composition cannot be precluded as an alternative explanation at this time.

Table of Contents

List of Tables

List of Figures

Chapter 1. Introduction & Overview

1.1 The Re-Os system

The versatility of the rhenium-osmium (Re-Os) isotopic system makes it a useful tool for studying a variety topics including early solar system, platinum group element (PGE) fractionation processes (Chen et al., 1998), continental erosion (e.g. Peucker-Ehrenbrink and Blum, 1998), chondrite impact events (Koeberl et al., 2012), large igneous province emplacement (e.g. Cohen and Coe, 2002). The broad application of the Os isotopic system results from its distinct characteristics in many geologic settings.

Osmium is one of six platinum group elements (PGE). Though not directly considered a member of the PGE group, Re is commonly associated with PGE due to similar geochemical behavior and the parent-daughter relationship of Re and Os. Rhenium has two naturally occurring isotopes, ^{185}Re (37.4% atomic abundance) and ^{187}Re (62.6% atomic abundance; Berglund and Wieser, 2011). ^{187}Re decays to ^{187}Os with a half-life of 41.8 Gyr (Smoliar et al., 1996). Osmium has seven naturally occurring isotopes (^{184}Os - 0.02%; ^{186}Os- 1.6%; ^{187}Os - 1.51%; ^{188}Os - 13.29%; ^{189}Os - 16.22%; ^{190}Os – 26.38%; ^{192}Os – 40.98%; Shirey and Walker, 1998). ^{187}Os is not the only Os isotope that is the product of radioactive decay, ^{190}Pt decays to ^{186}Os with a half-life of 450 Gyr (Carlson, 2005). In early work variations in the abundance of ^{187}Os were reported as ^{187}Os/^{186}Os ratios (e.g. Luck and Turekian, 1983). However, with the development of the ^{190}Pt-^{186}Os system, a shift was made to utilizing ^{187}Os/^{188}Os ratios because ^{188}Os is unaffected by naturally long-lived radioactive decay schemes. Rhenium and Os differ from other long-lived radiogenic isotope systems in that Re and Os are highly siderophile (prefer iron phases), whereas other pairs tend to be lithophile (concentrate in silicate phases). However, in the absence native metal phases, Re and Os will concentrate in sulfur phases as they are also highly chalcophile elements. They are also unlike other parent-daughter isotope pairs in that instead of having similar melt compatibilities, Re is moderately incompatible whereas Os is highly compatible during partial melting of the mantle. In the

following sections, I will discuss how these, and other properties, govern Re and Os behavior in both high- and low-temperature geochemical settings.

1.2 High-Temperature Re-Os Geochemistry

Rhenium and Os are both refractory elements with low-pressure melting points of 1819 and 1814 K, respectively (Wasson 1985). Their siderophile nature means that Re and Os are strongly partitioned into Fe-metal and its alloys when these phases are present. This allows the Re-Os system to be used as a tool for studying the origin and differentiation of planetesimals in the early solar system, as well as the conditions of the solar nebula in which the materials formed. As asteroid cores begin to cool, the fractional crystallization of solid metal separates Re from Os as Os preferentially goes into the solid phase. This permits the use of the Re-Os isotopic system as an tool for determining ages of iron meteorites iron meteorites (e.g. Shen et al., 1996). However, the small range of Re/Os ratios in chondrites limits the precision of Re-Os ages for chondrites. Instead, the long-term evolution of Os isotopic composition for different types of chondrites is a useful tool for studying the behavior of highly siderophile elements during the early Solar System and can provide information about relative formation ages through model age calculations and materials added to planetary mantles via accretion (Shirey and Walker, 1998 and references therein). The range of present-day $^{187}Os/^{188}Os$ values is small across all types of chondrites centering around 0.1270 ±0.0040, 2σ (n= 40; Horan et al., 2003), although there are slight variations among different types of chondrites. Carbonaceous chondrites exhibit more radiogenic $^{187}Os/^{188}Os$ ratios with an average ratio of ~0.126 (n=19, Horan et al., 2003 and Meisel et al., 1996) than entstatite and ordinary chondrites ($^{187}Os/^{188}Os$ ≈ 0.128, n = 42, Horen et al., 2003 and Meisel et al., 1996). This has important implications on the core-mantle formation processes which will be discussed in more detail below.

As a result of their siderophile nature, almost all (99.8%) of the Os and other PGE were extracted from the mantle and into the core during planetary differentiation. The net result of this process is believed to be strong Os enrichment in the Earth's core (estimated concentration of 2.2-2.4 µg/g; Palme 2008; Lorand et al., 2008) relative to the Earth's mantle. The compatibility differences between Re and Os predict that the liquid outer core has a higher Re/Os ratio than the inner core and, as such, a higher $^{187}Os/^{188}Os$ ratio, but still low compared to upper continental crust (Walker et al., 1997; Carlson et al., 2008). However, mantle Os concentration and $^{187}Os/^{188}Os$ measurements in peridotites (Figures 1.1 and 1.2) are higher and closer to chondritic, respectively, than predicted by partition coefficients to be the sole result of core-mantle separation (Carlson, 2005; Palme 2008). The bulk mantle is observed to have a $^{187}Os/^{188}Os$ ratio of 0.1269 and $^{187}Re/^{188}Os$ ratio of 0.4353 (Meisel et al., 2001), approximately the same as chondrites. Rhenium and Os are nearly 100 times more abundant in the mantle than predicted by low pressure metal-silicate distribution coefficients (Carlson 2005 and references therein). The current understanding of PGE solubility in silicate melts remains poorly constrained. Recent studies have shown that the solubility of PGE in silicate melts may increase with increasing temperature and pressure (Palme 2008 and references therein). Although differences in the partitioning behavior of Os and other PGE may have been different during core formation, this explanation would require that the behavior of all PGE change in the exact same way T and P increases. Alternatively, the accretion of a small amount (~1 wt%) of chondritic material to the earth, after core formation, could account for the measured $^{187}Os/^{188}Os$ and Re/Os compositions (Carlson 2005 and references therein).

Once the native metals have been removed to the core, the chalcophilic nature of Os and Re becomes important and they are partitioned into sulfide phases. Sulfide-melt partition coefficients for Re are high (43-325; Roy-Barman et al., 1998 and Burnham et al., 1998) but remain significantly lower than Os (10^3 – 10^5; Ballhaus et al., 2006 and Roy-Barman et al., 1998). The presence of 0.001% of sulfide can account for observed PGE depletions in komatiitic basalt melts (Putchel and Humayun, 2001). Rhenium and Os

4

fractionation increases with increasing extent of melting. Previously melted mantle sources exhibit lower Re/Os ratios compared to unmelted mantle. Additionally, as the sulfide phases gradually enter the melt, the remaining sulfides become more enriched in Os and other PGE and ultimately form alloys (Peregoedova et al., 2004) or go micrometer sized Os sulfides which then go into residual peridotite (Luguet et al., 2007). Chromite is the next best option for an Os host once sulfur has been depleted. The effect of sulfides on the Os budget can be seen at mid-ocean ridges where eruption of basalts that result from lower degrees of melting can be in equilibrium with sulfides that have yet to be consumed and, therefore, are less PGE rich (Lorand et al., 2008). Conversely, magmas that are formed by high degrees of partial melting (20% +/- 5%, Lorand et al., 2008), and therefore have consumed sulfide phases, are PGE rich with concentrations approaching those predicted for primitive mantle (Pruchtel et al., 2004). Although sulfides host a portion of Re in igneous rocks, it is more commonly associated with silicates such as orthopyroxene, garnet, and phlogopite (Carlson 2008 and references therein).

Due to the differences in compatibility, Re is concentrated in crustal rocks relative to Os. The enrichment of Re over Os has a profound effect on the Os isotopic composition of UCC over time compared to mantle rocks or chondrites (Figure 1.3). Rhenium has a concentration of ~200 pg/g whereas Os has ~30-50 pg/g (Peucker-Ehrenbrink and Jahn, 2001) in upper continental crust (UCC). As a result, the $^{187}Os/^{188}Os$ ratio of UCC is ~1.2-1.4 with a $^{187}Re/^{188}Os$ ratio of ~34.5 (Peucker-Ehrenbrink and Jahn, 2001).

1.3 Marine Re-Os Geochemistry

Osmium is present in modern seawater in trace concentrations ranging from 6.2 to 14.3 fg/g depending on ocean basin and depth (Chen and Sharma, 2009) with a present-day seawater average $^{187}Os/^{188}Os$ composition of 1.075 ± 0.275 (2σ, n=14; Chen and Sharma, 2009). Compared to Sr, Os has a shorter residence time, between <10 and 40 kyr (Oxburgh, 2001; Levasseur et al., 1999) but still longer than the approximate ~1000 yr mixing time of the oceans. As a result, Os in the ocean is assumed to be well-

mixed. However, slight regional variations exist (Paquay and Ravizza, 2012) and are suggested to reflect isotopic differences actively weathered terrain in the form of continental runoff (e.g. Martin et al., 2001). The most prominent source of Os to the oceans is via river runoff (Figure 1.4). Rivers are responsible for 70-80% of the total flux of Os to the global ocean and have radiogenic $^{187}Os/^{188}Os$ ratios similar to UCC (Levasseur et al., 1999, Sharma et al., 1997). Though the mass balance of seawater Os remains poorly constrained, hydrothermal vents, mid-ocean ridges, and cosmic dust are likely the main contributors of unradiogenic Os (Peucker-Ehrenbrink and Ravizza, 2000). Os removal mechanisms from seawater to underlying sediments are poorly understood. However, Os and Re have an affinity for reducing environments and are often associated with organic-rich sediments, which have been shown to exhibit large Os and Re burial fluxes that are consistent with anoxic sediments being the main sink of Os and Re from seawater (Colodner et al., 1993, Lee et al., 2002; Morford et al., 2012; Ravizza and Turekian, 1992).

Reconstructions of the seawater $^{187}Os/^{188}Os$ ratio through time reflect global changes in the sources of dissolved Os delivered to the oceans as seawater $^{187}Os/^{188}Os$ ratio reflects a balance of radiogenic and unradiogenic inputs. The short residence time of Os enables rapid shifts in the Os supply to the global ocean to be recorded in marine sediments. The marine Os isotope record has been applied to identify and/or quantify perturbations to the marine Os isotope balance associated with three distinct types of phenomena: continental weathering, impact events, and large igneous province (LIP) emplacement. During glacial periods, the silicate weathering intensity decreases which corresponds to a decreased supply of radiogenic to the global ocean. In support of this, sedimentary records show local minima in $^{187}Os/^{188}Os$ ratios during glacial maxima (e.g. Burton et al., 2010; Dalai et al., 2005; Oxburgh et al., 2007) suggesting that marine sediments record shifts in seawater $^{187}Os/^{188}Os$ compositions. Other examples of weathering induced Os isotopic shifts in seawater are the Paleocene-Eocene thermal maximum (Ravizza et al., 2001) and during the early-Jurassic (Cohen et al., 2004). Large igneous province emplacement are

marked by prominent shifts to lower $^{187}Os/^{188}Os$ ratios that remain low for timescales of millions of years (e.g. Cohen and Coe, 2002, 2007; Du Vivier et al, 2014; Kuroda et al., 2010; Ravizza and Peucker-Ehrenbrink, 2003; Tejada et al., 2009, Turgeon and Creaser, 2008). During LIP eruptions, a large amount of unradiogenic, mantle-like Os is thought to be introduced to seawater creating an overall shift to lower $^{187}Os/^{188}Os$ ratios. Large impact events caused by chondrites or iron meteorites are also recorded in the marine sedimentary record (e.g. Paquay et al., 2008; Sato et al., 2013). For this type of event, large amounts of extraterrestrial Os enter the global ocean and cause a rapid decline in $^{187}Os/^{188}Os$ composition that immediately begins to recover. The use of Os isotopes for LIP emplacement and large impact event studies are discussed in more detail below. Reconstructions of the marine $^{187}Os/^{188}Os$ record through time are a valuable tool to investigate major geologic events throughout the earth's history.

1.4 Rhenium-Os geochemistry of impact events

For this thesis, I focused mainly on the application of the Os isotopic system to large impact events and, to a lesser extent, the Os isotope excursion induced by LIP emplacement. In the following sections, I will review previous work related to this topic, and frame the questions that motivated this master's thesis.

Large enrichments of Os, Ir, and other PGE in extraterrestrial (ET) material relative to UCC make these elements sensitive indicators of ET material in sediments. This was first suggested by Alavarez at al. (1980) who recognized the globally distributed Ir anomaly associated with the Cretaceous-Paleogene (K-Pg) impact event at 66.04 Ma. When the PGE enriched chondrite impacted the earth, vaporized chondritic material mixed with vaporized target rock in the ejecta plume which then fell back to the earth. Because of the large PGE concentration and Os isotopic composition differences between upper-continental crust and chondrites, it only takes a small amount of chondritic material to create a sedimentary boundary layer enriched in PGE with an associated low $^{187}Os/^{188}Os$ ratio (Koeberl and

Shirey, 1997; Koeberl et al., 2012). Though it has since been demonstrated many times, Luck and

Turekian (1983) were one of were the first to analyze the Os isotopic compositions across the K-Pg

boundary and documented a shift towards chondritic values associated with the maximum Ir

concentration. The K-Pg impact event is not the only impact for which this Os isotopic excursion can be

identified. Similar excursions have been identified for the late-Eocene impact event (Paquay et al., 2008)

as well as a late-Triassic event (Sato et al., 2013). In all three impact events, the sedimentary record

shows $^{187}Os/^{188}Os$ ratios that decline rapidly near the time of the impact event, to a local minimum and

then recover to pre-impact values. The impact-induced $^{187}Os/^{188}Os$ minimum need not be the same for

each impact event. There are two main factors that control the $^{187}Os/^{188}Os$ impact excursion, the pre-

impact Os isotopic composition of the ocean and the amount of chondritic Os added to the global

oceans, i.e. impactor size. The size of the impactor can be estimated from the fractional increase of Os

added to the oceans during an impact event compared to the pre-impact budget, assuming the fraction

of the projectile Os that dissolves in the ocean is known (Paquay et al., 2008; Paquay et al., *In Review*)

(Equation 1)

$$M_{impactor} = M(Os)_{impactor}/(f_{Os-soluble} * C(Os)_{projectile}) \qquad (1)$$

Where $M_{impactor}$ is the mass of the bolide (kg), $M(Os)_{impactor}$ is the mass of projectile-derived Os

thatdissolves in seawater (in moles of Os), $f_{Os-soluble}$ is the fraction of the Os in the projectile that is

soluble in water, and $C(Os)_{projectile}$ is the average concentration of Os in chondrites (mol Os). The fraction

of impact-derived Os in the post-impact seawater can be estimated as

$$f = (R_{post-impact} - R_{pre-impact})/(R_{impactor} - R_{pre-impact}) \qquad (2)$$

Where $R_{post-impact}$ is the $^{187}Os/^{188}Os$ ratio of the seawater immediately after the impact event (also

denoted as R_o in Figure 1.5), $R_{pre-impact}$ is the $^{187}Os/^{188}Os$ ratio of seawater immediately before the impact

event (R_{ss} in Figure 1.5), $R_{impactor}$ is the $^{187}Os/^{188}Os$ ratio of the bolide, assumed to be chondritic ($\approx$0.127,

R_m in Figure 1.5).

$M(Os)_{impactor}$ is estimated by multiplying the fraction of the total impact-derived Os by the total seawater

Os inventory (Equation 3)

$$M(Os)_{impactor} = (f/1-f) * 7.3 * 10^7 \text{ mol Os} \tag{3}$$

The total amount of Os in seawater results from assuming a concentration of 10 fg Os/g of seawater

with a total ocean seawater amount of $1.4 * 10^{23}$ g seawater (V = $1.335*10^9$ km^3, NOAA; ρ = 1.027

kg/cm^3).

A value of $3.34 *10^{-9}$ mol Os/g is used for $C(Os)_{proj}$. This value comes from averaging reported Os

concentrations for chondrites (Horan et al., 2003). Using the reported data from Paquay et al. (2008),

the calculated estimate for the K-Pg $M_{impactor}$ is as follows:

$$f = (R_{post-impact} - R_{pre-impact})/(R_{impactor} - R_{pre-impact}) \tag{4}$$

f = (0.15 -0.4)/(0.127-0.4)

f = 0.92

$$M(Os)_{impactor} = (f/1-f) * 7.3 *10^7 \text{ mol Os} \tag{5}$$

$M(Os)_{impactor} = (0.92/1-0.92) *7.3 *10^7$ mol Os

$M(Os)_{impactor}$ = 7.95 * 10^8 mol Os

$$M_{impactor} = M(Os)_{impactor}/(f_{Os-soluble} * C(Os)_{projectile}) \tag{6}$$

$M_{impactor} = 7.95*10^8$ mol Os/(1 * $3.34*10^{-9}$ mol Os/g) (assume 100% of Os is soluble)

$M_{impactor}$ = 2.38 * 10^{17} g = 2.38 * 10^{14} kg

From the mass of the impactor, assumptions can be made about the shape (typically assume spherical) and density of the bolide to predict a total bolide diameter. However, Morgan (2008) suggests that using a total bolide mass is more useful.

For the late-Eocene impact, the ^{187}Os/^{188}Os composition decreased from 0.5 to 0.28. The Os estimated impactor diameter is 2.8-3.0 km (Paquay et al., 2008). The excursion for the K-Pg boundary impact is from 0.4 to ~0.16 caused by an Os estimated bolide 4.1 -4.4 km in diameter (Paquay et al., 2008). Lastly, the late-Triassic impact event induced an Os isotopic excursion from 0.47 -0.13 with an Os estimated impactor size of 3.3-7.8 km in size (Sato et al., 2013). One assumption of these calculations is that the Os entering the oceans is of chondritic isotopic composition. Impact related spinel are thought to form by direct condensation from vaporized projectile material, crystallization of liquid droplets from the impact vapor plume, or from ablated impact debris (Quitte et al., 2007 and references therein). Therefore, these spinel most likely reflect the direct Os isotopic composition of the impactor. For the K-Pg impact event, Quitté et al. (2007) report a ^{187}Os/^{188}Os composition 0.165 for Ni-rich spinel. They suggest significant Os loss due to volatilization, as Os is highly volatile in oxidizing conditions, as a possible mechanism for the super-chondritic Os isotopic composition. Another way to test this would be to look at data from a terrestrial site.

1.5 Motivation for studying the Bowring Pit outcrop

The Bowring Pit outcrop is located within the West Bijou K-Pg site, ~40 km to the southeast of Denver, CO. The objective of my work on the Bowring Pit outcrop section was to better constrain the ^{187}Os/^{188}Os ratio and the chemical form of Os delivered to a non-marine K-Pg section. Simple two-component mixing between UCC and chondrites suggest that fallout from the K-Pg impact ejecta plume should be chondritic. In fact, only 6 wt% chondritic material would be enough to create chondritic Os isotopic

compositions at the boundary horizon (Figure 1.6). However, data reported for terrestrial sites all record super chondritic ^{187}Os/^{188}Os compositions (see Table 2.2 in Chapter 2). Of these eight data points, only three of them also gave Re concentrations to allow corrections to be made for the *in situ* decay of ^{187}Re to ^{187}Os. Even after these corrections are made, the ^{187}Os/^{188}Os ratios remain super-chondritic. However, all but one of these terrestrial data come from older studies (c.a. 1983 and 1989). It should be taken into account that analytical techniques have improved drastically since the time of these studies. This led me to the first research question I wanted to answer; do measurements of ^{187}Os/^{188}Os ratios in a terrestrial K-Pg section record chondritic initial ^{187}Os/^{188}Os ratios? Also, could a study like this provide information on the solubility of impact-derived Os? The most recent data point that exhibits super-chondritic ^{187}Os/^{188}Os ratios (^{187}Os/^{188}Os = 0.167, Moore et al., 2014) was published well after the onset of this project.

1.6 Motivation for studying post-impact ^{187}Os/^{188}Os recovery in the Southern Ocean

My original objective for investigating post-impact ^{187}Os/^{188}Os recovery was to apply a recently proposed "Os clock" model that utilized the ^{187}Os/^{188}Os recovery to pre-impact, steady state values, as a method of keeping time in the earliest-Paleogene (Ravizza and VonderHaar, 2012). The effect of the impact on seawater has been well-documented. Recently, more work has focused on the post-impact seawater recovery profiles. The Ir anomaly, most commonly used to locate the K-Pg impact horizon within pelagic sediments, typically exhibits an asymmetrical shape instead of a singular peak directly at the K-Pg horizon. Hull et al. (2011) modeled Ir profiles and determined that sediment mixing is the dominant factor in the profile shape opposed to bioturbation, diffusion/diagenesis, prolonged volcanic addition and other proposed processes. That is, Ir is redeposited as discrete particles that experience local mixing. A different view was offered by Ravizza and VonderHaar (2012) in which post-impact changes in seawater ^{187}Os/^{188}Os result from the Os isotopic composition of seawater itself changing as a result of

removing chondritic Os from the water column to the underlying sediments (Figure 1.5). In this model, the main control of the ^{187}Os/^{188}Os recovery time was the Os enrichment in the post-impact ocean versus the pre-impact ocean, and the residence time of Os. When this model was applied to ODP sites 1262, 1209, and 690, the results show ^{187}Os/^{188}Os ratios recover to pre-impact values in roughly 200 kyr, consistent with an Os residence time of 40 kyr , similar to that of the modern ocean. If this model is accurate, it would provide a novel method of time-keeping in the earliest-Paleogene that did not require biostratigraphy which can be difficult to obtain accurate ages with. My original second research question became: Can the "Os clock" model be applied to other sites? ODP 738C offered a unique opportunity to test this out. The K-Pg boundary here was defined by a large Ir anomaly (Schmitz et al., 1991) that occurred within a 15 cm of finely laminated, clay-rich section of the core. The laminations eliminated the problem of possible sediment reworking allowing for an unbiased approach to apply the Os clock model. However, the results were surprising in that the post-impact ^{187}Os/^{188}Os ratio never recovered to the expected pre-impact value and thus the model could not be applied. Consequently, the focus of my work on ODP 738 shifted to trying to understand the reason for the persistently low ^{187}Os/^{188}Os ratios.

The results from this work are discussed in detail in Chapter 3

Chapter 2. A complete Os excursion across a terrestrial Cretaceous-Paleogene boundary at the West

Bijou Site, Colorado, with evidence for recent open system behavior*

Jessica Zaiss[1], Greg Ravizza[1], Steven Goderis[2], Justine Sauvage[2], Philippe Claeys[2] Kirk Johnson[3]

[1]Department of Geology and Geophysics, SOEST, University of Hawaii-Manoa Honolulu, HI USA

[2]Earth System Science, Vrije Universiteit Brussel, Brussels, Belgium

[3]National Museum of Natural History, Smithsonian Institution, Washington D.C. USA

*This chapter is based on a submitted manuscript.

Abstract

The few previously reported values of $^{187}Os/^{188}Os$ ratios from non-marine K-Pg boundary sections are distinctly higher than the range of $^{187}Os/^{188}Os$ ratios measured in chondrites and the range of ratios predicted by models of physical mixing between chondrites and upper crust. Here, Re-Os data from the West Bijou continental K-Pg boundary site, located within the Denver Basin, are used to better constrain the Os isotopic composition of fallout from the Chicxulub ejecta plume. For the first time, full vertical profiles of $^{187}Os/^{188}Os$ ratios and Re and Os concentrations across a continental K-Pg boundary section are reported. Within this section of lignite, the lowest measured $^{187}Os/^{188}Os$ ratio (0.182) coincides with the K-Pg boundary interval as previously determined by palynology and the distribution of shocked quartz in a nearby outcrop. However, sediments with elevated Os concentrations and measured $^{187}Os/^{188}Os$ below 0.23 extend over a 30 cm interval, from ~ 5 cm above the clay-rich boundary interval (~ 5 cm thick) to ≈ 25 cm below. Maximum Ir and Os concentration occur 3 cm and 10 cm below the K-Pg boundary, respectively, demonstrating greater diagenetic mobility of Os relative to Ir. Low $^{187}Os/^{188}Os$ above the K-Pg boundary suggests that accumulation of impact derived Os at this site persisted after the impact event, perhaps due to redistribution of impact debris in the surrounding area. Importantly, calculated initial $^{187}Os/^{188}Os$ ratios throughout most of the section are impossibly low and require open system behavior, likely in the form of Re addition within the last 10 million years. Within the boundary interval, Re concentrations are among the lowest measured at Bowring Pit and calculated initial $^{187}Os/^{188}Os$ ratios are very similar to those previously reported from the western interior of the United States K-Pg boundary material (~0.14), suggesting super-chondritic $^{187}Os/^{188}Os$ is characteristic of the Chicxulub ejecta plume. Beyond implications for our understanding of Os as an impact tracer, this study emphasizes the dramatic effect diagenesis can have on the Re-Os system in organic-rich environments, especially through post-depositional addition of Re.

14

2-1. Introduction

An iridium (Ir) concentration anomaly marks the Cretaceous-Paleogene (K-Pg) impact horizon in sediment sequences globally (e.g., Alvarez et al., 1980). Multiple independent geochemical and petrologic means of recognizing impact horizons, developed and tested since this pioneering work, substantiate this interpretation (See Koeberl et al. 2012 for a recent review). Carbonaceous chondrites, such as the bolide responsible for the impact at the K-Pg boundary (Kyte, 1998; Quitté et al., 2007; Shukolyukov and Lugmair, 1998; Trinquier et al., 2006), at 66.043 ± 0.043 Ma (Renne et al., 2013), are highly enriched in Ir and Os, (~400-900 ng/g, Horan et al., 2003) relative to upper-continental crust, (~30 pg/g, Peucker-Ehrenbrink and Jahn, 2001). This accounts for the anomalously high Os and Ir concentrations associated with the K-Pg impact ejecta. While recent studies have demonstrated Ir mobility at the K-Pg boundary (Miller et al., 2010; Racki et al., 2011), comparatively little work has investigated Os mobility at the K-Pg boundary. Osmium and Ir are platinum group elements (PGE) that often exhibit similar geochemical behavior to one another, and are as such, together with Ru, sometimes termed the Ir-group PGE. However, in aqueous systems there is evidence that Os and Ir behave very differently from one another (Lee et al., 2003).

An important distinction between Os and Ir as geochemical markers of impact horizons is the use of $^{187}Os/^{188}Os$ ratios to constrain PGE sources within sediments (Koeberl and Shirey, 1997). The average $^{187}Os/^{188}Os$ ratio of upper-continental crust is ~1.4-1.9 (Esser and Turekian, 1993; Peucker-Ehrenbrink and Jahn, 2001), while mantle and chondritic sources are characterized by ratios closer to ~0.12 (Horan et al., 2003; Walker et al., 2002). In rocks affected by impacts, low $^{187}Os/^{188}Os$ ratios and high PGE concentrations are, to first order, the result of two component mixing of crustal and meteoritic material (Koeberl and Shirey, 1997).

The Os isotope and concentration excursions associated with the K-Pg impact have been studied extensively in marine environments (e.g., Frei and Frei, 2002; Lichte et al., 1986; Luck and Turekian, 1983; Meisel et al., 1995; Peucker-Ehrenbrink et al., 1995; Ravizza and VonderHaar, 2012) but rarely at terrestrial sites (e.g., Esser and Turekian, 1989; Ferrow et al., 2011; Luck and Turekian, 1983). Globally, the K-Pg boundary sample with the lowest measured ratio ($^{187}Os/^{188}Os$ = 0.1369) is from Sumbar, Turkmenistan which is characterized as a marine environment at the time of deposition (Meisel et al., 1995). Although this ratio is very low compared to typical crustal values, it is also distinctly higher than the known range of chondritic values of 0.1198-0.1297 (Horan et al., 2003). Minimum ratios from other marine K-Pg boundary horizons range from 0.1502 (DSDP 596, Peucker-Ehrenbrink et al., 1995) to 0.2170 (ODP 1209C, Ravizza and VonderHaar, 2012). One view (Paquay et al., 2008; Ravizza and VonderHaar, 2012) is that super-chondritic $^{187}Os/^{188}Os$ ratios recorded in marine sediments result from mixing of ambient hydrogenous (seawater-derived) Os ($^{187}Os/^{188}Os$ ~ 0.4, Robinson et al., 2008) with soluble impact-derived Os. This mixing causes an overall decrease in the global $^{187}Os/^{188}Os$ ratio of seawater, but the ratio remains elevated above chondritic levels (Paquay et al., 2008; Ravizza and VonderHaar, 2012).

Compared to marine K-Pg boundary sites, terrestrial sites should exhibit a more nearly chondritic Os isotopic composition because the influence of seawater derived Os is unlikely. Physical mixing between chondritic and continental crustal Os should result in nearly chondritic $^{187}Os/^{188}Os$ ratios over nearly a full order of magnitude of elevated Os concentrations (Figure 2.1) due to the large Os concentration difference between the two end-members. However, reported $^{187}Os/^{188}Os$ ratios for terrestrial sites range from 0.1378 (Raton, Esser and Turekian, 1989) to 0.2040 (Compressor Creek, Ferrow et al., 2011). One explanation for this discrepancy is production of ^{187}Os by *in situ* decay of its parent ^{187}Re (half-life 41.8 Gyr, Smoliar et al., 1996) since deposition of K-Pg boundary sediments . The average $^{187}Re/^{188}Os$ ratio of upper continental crust is ~34.5 (Peucker-Ehrenbrink and Jahn, 2001) but

16

can be much higher in organic-rich sediments. Baioumy et al. (2011) report ^{187}Re/^{188}Os ratios up to 2851

in late-Cretaceous marine black and gray shales, while non-marine shales and coals have much lower

^{187}Re/^{188}Os ratios (mean ^{187}Re/^{188}Os of 51 ± 29 (1 SD), n = 10 with exclusion of an outlier with a

^{187}Re/^{188}Os ratio of 977); these data are especially relevant to this work because they are lithologically

similar to samples investigated here. ^{187}Re/^{188}Os ratios for carbonaceous chondrites are much lower,

approximately 0.4 (Horan et al., 2003). Large ^{187}Re/^{188}Os ratios in crustal rocks and organic rich

sediments cause ^{187}Os/^{188}Os ratios in these lithologies to increase much faster than the ^{187}Os/^{188}Os ratio

of chondrites. Often, Re data for terrestrial K-Pg boundary sediments are not reported (e.g., Esser and

Turekian, 1989; Ferrow et al., 2011; Luck and Turekian, 1983). This lack of Re data prevents calculation

of initial ^{187}Os/^{188}Os ratios of these K-Pg boundaries, and hampers direct comparison to the Os isotopic

composition of chondrites.

This study aims to better constrain the Os isotopic composition of the fallout from the ejecta

plume by measuring Os and Re abundances, in combination with ^{187}Os/^{188}Os and ^{187}Re/^{188}Os ratios

across a continental K-Pg boundary site. This is the first study to report the Re and Os concentrations

and ^{187}Os/^{188}Os composition variations across a terrestrial K-Pg section. We hypothesized that careful

analysis of ^{187}Os/^{188}Os and the concentrations of Re and Os across a complete continental K-Pg boundary

section would yield essentially chondritic ^{187}Os/^{188}Os initial ratios after correction for *in situ* decay of

^{187}Re. This hypothesis was motivated by the possibility that early measurements of single discrete

samples from continental K-Pg boundary sections (Luck and Turekian 1983; Esser and Turekian 1989),

might not have captured minimum ^{187}Os/^{188}Os ratios. As detailed below, results reported here show that

this hypothesis is false. Instead, our best estimate of the initial ^{187}Os/^{188}Os at the West Bijou K-Pg

boundary (~ 0.14) is elevated above the chondrite field and very similar to previously reported values for

other continental K-Pg boundary sections across the western United States. An additional unexpected

result of this study was clear evidence of post-depositional redistribution of Re and Os.

2-2. Geologic Setting and Sampling

The Rocky Mountains experienced uplift during the Laramide Orogeny from the Late Cretaceous to the early Paleogene (Hicks et al., 2003). Sediments deposited in the Denver basin at this time are a part of the D1 sequence (Raynolds, 2002) characterized by heterogeneous, synorogenic sediment. Sediments in the eastern part of the Denver basin are characterized by coal-rich facies known as the Denver Lignite Zone (Kirkham and Ladwig, 1979). The West Bijou K-Pg boundary impact site is located within the Denver Lignite Zone, located approximately 60 km east of Denver, Colorado (39° 34'14"N, 104° 18'09"W). The sediments studied here are lignites with the exception of the clay-rich K-Pg boundary interval and two distinct volcanic ash horizons (Fig 2). The K-Pg boundary at this site is well defined by palynology and the occurrence of the iridium anomaly and shocked quartz (Barclay et al., 2003). K-Pg boundary sections from the western interior of the United States are often characterized by a 1 to 2 cm-thick dual layer stratigraphy; a lower kaolinitic clay layer and a thinner overlying layer that contains the maximum Ir concentration (Smit, 1999). In the late 1980s, this Ir-rich layer was often referred to as the "magic layer" (Schmitz 1992). Since the discovery of the Chicxulub impact crater, this horizon is generally regarded as the impact horizon.

The Bowring Pit outcrop (Figure 2.2) studied here, is one of a series of K-Pg exposures located on the western slope of the West Bijou Creek escarpment south of Strasburg, Colorado. This location is atypical of most previously studied K-Pg boundary sites in the western United States because the boundary layer is ~5cm thick and lacks a distinct upper layer. The Ir anomaly at Bowring Pit spans ~30 cm (Figure 2.3) and peaks at a concentration of 0.375 ng/g approximately 3 cm below the K-Pg boundary as defined by the thick claystone layer (Sauvage, 2010). The Ir concentrations at Bowring Pit resemble values reported for kaolinitic clays at other sites from the western United States (ranging from 0.22 ng/g to 2.5 ng/g), but are consistently an order of magnitude lower than the anomalies reported for the

18

impact layer at those same sites (ranges from 1.1 ng/g to 26.4 ng/g, Schmitz, 1992). This site was chosen

for our study despite its atypical characteristics because it is the target of high precision U-Pb zircon

dating of multiple volcanic ash layers that bracket the K-Pg boundary (Bowring et al. 2007, Dalton,

2007). In addition the palustrine depositional setting should be associated with higher sediment

accumulation rates and a more highly resolved record of the K-Pg impact event. Sampling at the Bowring

Pit was continuous with ~5 cm resolution over a 90 cm interval centered about the K-Pg boundary. In

order to minimize the potential influence of Re and Os mobilization associated with oxidative

weathering, the outcrop was dug back to reveal unweathered surfaces prior to sampling. Note that

fracture surfaces (cleats) commonly extend throughout coals even in the subsurface and in cored

material (Laubach et al., 1998) and are not features of surficial weathering. During sampling, exposed

outcrop was removed (>5 cm to as much as a meter) before samples were taken to minimize bias due to

weathering processes at the surface.

2-3. Methods

Inductively couple plasma mass spectrometry was used to determine Re and Os concentrations

by isotope dilution, as well as $^{187}Os/^{188}Os$ and $^{187}Re/^{188}Os$ ratios, on the same powdered lignite samples

studied by Sauvage et al. (2010). Carius tube digestion was used to obtain Re/Os data on same-sample

aliquots (Shirey and Walker 1995). This study employed a H_2O_2/HNO_3 digestion solution as outlined in

Ravizza and VonderHaar (2012, Supplemental Material). Osmium data were obtained by transferring the

digestion solution to a Teflon vial, followed by sparging the solution to introduce volatile OsO_4 (Hassler

et al., 2002) into a *Thermo Scientific* Element 2 ICP-MS at the School of Ocean and Earth Sciences

(SOEST) at the University of Hawaii at Manoa. Rhenium was purified from the post-sparging solution via

anion exchange chromatography, as described in Ravizza and Paquay (2008). These methods allow

corrections for the in situ decay of ^{187}Re to ^{187}Os to be made. Because this was the first application of this method to coals and lignites, nickel-sulfur fire assay digestion was also performed to determine if systematic biases occurred between Os data obtained from carius tube digestions and fire assay. Nickel-sulfur fire assay is a well-established digestion method commonly applied at the SOEST laboratory (Ravizza and Pyle, 1997). Average procedural Os blanks for Carius tube analyses were 0.38 ± 0.25 pg (2σ) and Re blanks were 3.8 ± 1.1 pg (2σ). Procedural blanks were ~2% and <1% of the lowest Os and Re concentrations, respectively. The fusion Os blank was 1.32 ± 0.03 pg (2σ) per gram sample. Regardless of the digestion method used, the total analyte exceeded analytical detection limits by more than a factor of 10. Consequently, analytical detection limits do not influence data quality in any meaningful way in this study. Measured ^{187}Re/^{185}Re ratios yielded an average of 1.6907 ± 0.0063 (1 SD; n = 6) compared to 1.6739 measured for natural samples (Gramlich et al. 1973). This difference was attributed to instrumental mass bias and measured sample Re isotope ratios were corrected accordingly. Measured ^{187}Os/^{188}Os ratios for standard analyses yielded a mass-bias-corrected average ratio of 0.1073 ± 0.0005 (1 SD; n = 18) compared to an accepted value of 0.1069 for the Leoben Os standard (Nowell et al., 2008). Although rock standards were not analyzed as a part of this study, previous analyses of the TDB-1 diabase standard (n = 5) by NiS fire assay yield Os concentrations and ^{187}Os/^{188}Os of 101 -137 pg Os/g and 0.73 – 0.83, respectively. This compares well with TDB-1 results reported by Peucker-Ehrenbrink et al. (2003): Os 107 - 127 pg/g and ^{187}Os/^{188}Os 0.78 – 0.89.

Weight percent carbon data (wt% C) were obtained on an Exeter Analytical model CE 440 elemental analyzer at the University of Hawaii at Manoa in the SOEST laboratory for analytical biogeochemistry following the methodologies of Gordon (1969) and Sharp (1974). Standard analysis for wt% C on NIST marine sediment reference materials MESS-3 and 1941b yielded 2.77 ± 0.02 (1 SD, n = 5) and 3.12 ± 0.08 (1 SD, n = 5), respectively. The accepted values for these materials are 2.99 and 3.3, respectively.

2-4. Results

2-4.1 Osmium

Concentrations of Os vary between 16 pg/g and 605 pg/g in a broad, downwardly skewed peak along the sample profile in the Bowring Pit section (Figures 2.3 and 2.4). The maximum of the profile occurs 12 cm below the boundary, and then gradually decreases with depth through the sample section. Although Os concentrations of most samples analyzed exceed that of average upper continental crust concentrations (~30-50 pg/g, Esser and Turekian, 1993; Peucker-Ehrenbrink and Jahn, 2001), background Os concentrations near the top of the sample profile are similar to those reported for Jurassic coals from a wet forest swamp located in a delta plain (18-47 pg/g, Baioumy et al., 2011). The Bowring Pit K-Pg boundary displays Os concentrations ~3.5 times higher than at Compressor Creek (172 pg/g at the boundary, Ferrow et al., 2011); a terrestrial K-Pg site located in New Zealand that was a paleo-floodplain with sediments characterized by carbonaceous mudstone, siltstones and coal seams. The maximum concentration found at Bowring Pit is significantly lower than those measured at other continental K-Pg sites in the western United States (Table 2.2). For example, in the Raton Basin, Os concentrations at the impact boundary range from 12,000 to 36,000 pg/g (Esser and Turekian, 1989).

Measured $^{187}Os/^{188}Os$ values vary from 0.1819 (BP 13) to 0.7091 (BP 17) (Figure 2.4). Shallower samples display $^{187}Os/^{188}Os$ ratios higher than those of than the deeper samples, with exception of BP 14 and BP 15 that are both located immediately above the boundary. Beginning at the deepest part of the sample section and moving upward, the measured Os isotopic ratio gradually decreases to a minimum at the boundary, and then increases abruptly ~ 10 cm above the boundary. Although the range of measured ratios is large, the highest $^{187}Os/^{188}Os$ ratio is still distinctly lower than average upper continental crustal values. The shift towards less radiogenic values near the boundary is expected and similar to observations at other K-Pg sites. Nevertheless, the measured K-Pg boundary isotopic

compositions at the Bowring Pit are distinctly higher than those measured for chondrites and other K-Pg

sites from the Western United States which vary from 0.1378 (Raton Basin, Esser and Turekian, 1989) to

0.1553 (Raton Basin, Luck and Turekian, 1983).

^{187}Os/^{188}Os ratio data obtained from both Carius tube digestion and nickel-sulfur fire assay

digestion on the same sample are similar to one another. Variations between the two methods are small

relative to the variation of the data (Table 2.1 and Figure 2.4). For the eight samples on which both

digestion methods were used, the average difference between ^{187}Os/^{188}Os ratios obtained from Carius

tube digestion and those from nickel-sulfur fire assay was 2.6%. The Os concentration data for these

samples show a higher mean difference of 9.4%, however the higher variability is likely due to smaller

sample mass used for carius tube digestion (~0.5 g) compared to the fire assay digestions (~5 g). When

larger sample masses are used, the results seem less affected by PGE clumping into micrometer-sized

pieces, known as the "nugget effect," known to increase variability among aliquots (Hall and Pelchat,

1994; Lorand et al., 2008; Tagle and Claeys, 2005)

2-4.2 Osmium/Ir ratios

A comparison between the Os concentration data determined in this study and the Ir

concentration data reported by Sauvage (2010) yields super-chondritic Os/Ir ratios (chondrites ~ 1,

Horan et al., 2003) ranging from 1.3 to 3.5 throughout the profile, with the exception of two samples (BP

11 and BP 18, Table 2.1). In general, the upper portion of the sample profile, close to the K-Pg boundary,

exhibits nearly chondritic Os/Ir ratios compared to the lower portion of the section. It should be noted

that while Os data were obtained on the same powdered samples as Sauvage (2010), Ir and Os data

were from different sample aliquots, which could introduce some bias. Nevertheless, the inference of

Os/Ir ratios larger than the chondritic ratio of ~1 are likely robust. The Ni-S fire assay method used to

produce the Ir data has been proven to yield accurate results when compared to rock standards (Tagle

and Claeys, 2005; Goderis et al., 2013) and the data from Sauvage (2010) are similar to independent Ir data reported in Barclay et al. (2003). Similarly, Os concentrations for TDB-1 rock standard from the UH lab agree with data from other labs (see methods section above). The Os/Ir ratios found at Bowring Pit are systematically lower than those reported for Jurassic wet-swamp coals (Baioumy et al., 2011), consistent with the addition of a chondritic component at Bowring Pit. Although Os and Ir concentrations for K-Pg boundary sites in the western United States have been previously reported separately, we believe this is the first time analyses of both elements on same powders have been reported. Osmium/Ir ratios inferred for other K-Pg sites from the western United States, based on previously published data and different sample data, exhibit super- chondritic ratios as well, varying between 1.3 and 33 (Table 2.2).

2-4.3 Rhenium concentrations and $^{187}Re/^{188}Os$ ratios

Rhenium concentrations vary along the profile between 2 ng/g and 48 ng/g (Figure 2.3), one to two orders of magnitude higher than average upper continental crustal values (0.2-0.4 ng/g, Esser and Turekian, 1993; Peucker-Ehrenbrink and Jahn, 2001). Bowring Pit Re concentrations are much higher than anticipated based on reported data of previous studies on coals (Baioumy et al., 2011) and other K-Pg sites from the western United States (Esser and Turekian, 1989). In Jurassic wet-swamp coals, Re contents range from 0.1 to 4.82 ng/g (Baioumy et al., 2011). The highest Re concentrations in these Jurassic coals are similar to those found near the K-Pg boundary at Bowring Pit, but remain consistently lower than background samples at the top and bottom of the Bowring Pit sample profile. K-Pg sections at Madrid and Berwind Canyon have Re concentrations similar to the lower concentration end-members of Bowring Pit with concentrations of 2.09 ng/g and 2.05 ng/g, respectively (Esser and Turekian, 1989).

The $^{187}Re/^{188}Os$ ratios throughout the sample profile are elevated above values for upper crust ($^{187}Re/^{188}Os$ ~ 34.5; Peucker-Ehrenbrink and Jahn, 2001), with the exception of BP 11, $^{187}Re/^{188}Os$ = 33.3

(Table 2.1). The Re/Os ratios are unexpectedly high because they not only exceed upper continental crust but also exceed the values previously reported fresh water coals. The majority (~67%) of $^{187}Re/^{188}Os$ ratios reported for Jurassic coals are also higher than those reported for average upper crust, but remain systematically lower than those from Bowring Pit (Baioumy et al., 2011). To compare Bowring Pit to other K-Pg sites from the western United States, we calculated $^{187}Re/^{188}Os$ ratios based on reported Re concentrations for Madrid and Berwind Canyon (Esser and Turekian, 1989). The resulting $^{187}Re/^{188}Os$ ratios (0.8 for Madrid and 0.5 for Berwind Canyon) were well below those of upper continental crust and Bowring Pit, but at the same time distinctly higher than chondrites (0.31-0.44, Horan et al., 2003).

2-4.4 Weight percent carbon

Total wt% C is variable across the sample profile ranging from as low as 5.45 wt%, found 13 cm above the boundary interval in an ash layer, to as high as 42.23 wt%, found 25 cm below the impact interval (Table 2.1). The wt% C corresponds to organic carbon as these samples are devoid of calcium carbonate. Compared to the rest of the profile, total C is relatively low immediately above and below the K-Pg boundary. Unfortunately, the sample representing the boundary interval and the one immediately below were depleted during Re and Os analyses, but based on the appearance of this part of the section it is likely that organic carbon content at the K-Pg boundary is similarly low. Rhenium and Os concentrations increase with increasing wt% carbon with the exception of samples adjacent to the K-Pg boundary. This is consistent with previously recognized affinity of these elements to carbon rich, reducing sediments (Cohen et al., 1999; Kendall et al., 2004; Peucker-Ehrenbrink and Hannigan, 2000; Ravizza and Turekian, 1989; Selby, 2007).

2-5. Discussion

24

Most Os isotope studies of the K-Pg impact event have focused narrowly on the impact horizon (Frei and Frei, 2002; Luck and Turekian, 1983; Quitté et al., 2007), while the data reported here extend approximately 40 cm above and below the boundary horizon. Cretaceous-Paleogene Os isotope studies that span longer time/depth intervals have thus far been limited to marine sections (Peucker-Ehrenbrink et al., 1995; Ravizza and Peucker-Ehrenbrink, 2003; Ravizza and VonderHaar, 2012). The interest in these marine studies was to track the temporal evolution of the seawater Os isotope composition following the Chicxulub impact event. This work on marine K-Pg sections uses the marine Os isotope record of impact events to estimate projectile sizes (Paquay et al., 2008) and as a chronologic tool for dating marine sediments in the aftermath of the K-Pg boundary impact (Ravizza and VonderHaar, 2012). Both approaches depend on the assumptions that much of the Os carried by the ejecta plume was soluble in seawater, and that the $^{187}Os/^{188}Os$ ratio of the ejecta plume was chondritic. Results reported here strongly support the first of these assumptions. Although the paleo-depositional environment of the West Bijou K-Pg site was palustrine (marsh-like) rather than marine, the downward diagenetic mobility of Os, and the vertical separation of Os from Ir we have documented, requires that a significant fraction of the impact-derived Os is water-soluble. Unfortunately, rigorous testing of the second assumption is not possible due to significant post-depositional addition of Re to the West Bijou K-Pg boundary section. As discussed in more detail below, this complicates efforts to better constrain the $^{187}Os/^{188}Os$ of the Chicxulub impact ejecta plume. Nonetheless, calculated initial $^{187}Os/^{188}Os$ for samples close to the K-Pg boundary are elevated above the range measured in chondrites, and similar to previously reported values for the western interior of the United States.

2-5.1 Osmium Mobility

This K-Pg section displays strong evidence for remobilization of impact-derived Os down section. Not only does the maximum Os concentration occur 12 cm below the boundary, but most (~75%) of the

Os inventory resides in a broad peak that extends tens of centimeters below the K-Pg boundary, rather than in a well-defined peak centered at the boundary (Figures 2.3 and 2.4). Os isotope ratio variations are also consistent with down-section mobilization of impact-derived Os. Instead of a sudden drop in the ^{187}Os/^{188}Os ratio directly at or near the boundary, the ratio gradually decreases from the bottom of the section to the local minimum at the boundary. If remobilization was solely the result of diffusion away from the boundary interval, then a nearly symmetric profile across the boundary should be observed, as vertical direction does not affect diffusion rates. The large vertical extent of low measured ^{187}Os/^{188}Os ratios may reflect the presence of both soluble and insoluble impact derived components. An insoluble component of impact-derived Os seems to be retained near the boundary and a soluble component mobilized down-section, perhaps as water percolated through the sediment pile (Figure 2.4). Ideally initial ^{187}Os/^{188}Os ratio could be used to assess the vertical distribution on impact derived Os. However, as detailed below, most of the calculated initial ^{187}Os/^{188}Os ratios are unreasonably low. Nevertheless, measured ^{187}Os/^{188}Os ratios less than 0.24 extending 20 cm below the K-Pg boundary are strong evidence of a mobile component of impact-derived Os, especially because these samples also have the highest Os concentrations. Correction for in situ decay of ^{187}Re would only shift ^{187}Os/^{188}Os ratios to lower values.

We propose that soluble, chondritic Os was mobilized down section and reduced to a less soluble form by sedimentary organic matter. This suggestion is motivated by previous work showing that Os has an affinity for reducing environments caused by organic rich material (e.g., Cohen et al., 1999; Kendall et al., 2004; Peucker-Ehrenbrink and Hannigan, 2000; Ravizza and Turekian, 1989; Selby, 2007). High Os concentrations found in the interval with the highest wt% C below the K-Pg boundary horizon also support this interpretation. In previous studies, the shift in maximum PGE concentration was explained as the result of bioturbation or diffusion (Lee et al., 2003). However, we suggest that the complex Os concentration profile seen here results from differences in the solubility of more than one

Os-carrying phase and we speculate that Os retained at the boundary interval is, at least in part, contained in insoluble particles from the ejecta plume. In contrast, projectile-derived Os that occurs tens of centimeters below the boundary and below the downward extent of shocked quartz must have been mobilized down-section by aqueous solutions. Assuming that Os would be just as soluble in this swamp-like environment as it would in seawater, aqueous mobility of Os in this section supports the existence of soluble Os in the ejecta plume.

The Bowring Pit Os profile also shows prolonged accumulation of impact-associated Os above the boundary horizon (Figure 2.4).   Sample BP 14 immediately above the K-Pg boundary (5.5 cm above) displays an elevated Os concentration coupled with a low $^{187}Os/^{188}Os$ ratio compared to the rest of the upper portion of the profile. The basin setting of the West Bijou K-Pg site and the swamp-like depositional environment for the Bowring Pit indicates that the sample section was probably located at a topological local minimum at the time of deposition. Therefore, impact-derived Os (and other PGE) could have been carried by river and rain runoff from the surroundings could have accumulated above the K-Pg boundary at this site in the aftermath of the impact. This is consistent with the interpretation of Sauvage (2010), who also reports prolonged addition of Ir (and other PGE, including Ru, Rh, Pd, and Pt), perhaps due to reworking of impact debris in the surrounding area.

2-5.2 Osmium/Ir fractionation

Although variability in Os/Ir ratio throughout the section reflects differential mobility of Ir and Os (Fig. 3), the Os/Ir ratio of most samples is elevated above the chondritic value (~ 1, Horan et al. 2003). The super-chondritic Os/Ir ratios found throughout the profile (with the exception of BP 11, Table 2.1) suggest fractionation of Os from Ir in the ejecta plume and/or after deposition (Peucker-Ehrenbrink et al., 1995). Additionally, higher Os/Ir ratios down section of the boundary compared to those up section suggest that Os is more mobile than Ir in these sediments. Elevated Os relative to Ir is

consistent with the observations of Lee et al. (2003), who propose that Os/Ir ratio variations in K-Pg

sediments from the open ocean are caused by preferential Ir take-up in open ocean sediments

compared to Os, which is deposited in anoxic, organic rich sediments found on oceanic margins. In this

study, we observe preferential accumulation of Os to Ir in an organic-rich lacustrine setting. Some

marine K-Pg sites also indicate deviations from chondritic Os/Ir ratios directly at the boundary (e.g.,

Ferrow et al., 2011; Kyte et al., 1985). It is not possible to compare the distribution of Os and Ir down

section from the K-Pg boundary in these earlier studies, as data are limited to the boundary horizon.

In studies where concentration profiles are established, fluence calculations allow direct

comparisons of element inventories to be made in a given section. This approach is useful to apply to

Bowring Pit profile because the data indicate that vertical redistribution of Os and Ir has occurred. The

fluence calculation makes it possible to compare the total amount of Os and Ir integrated over the

entire sample profile rather than relying only on comparisons at the boundary eliminating bias due to

the differential vertical mobility of Os and Ir. Fluence for the Bowring Pit was calculated by Equation 1.

$$F = \rho \sum_{n=20}^{1} \Delta z_n c_n \qquad (1)$$

Where F is the fluence (ng /cm^2), ρ (g/cm^3) is the density of the sediment, Δz_n (cm) is the width of

sample interval n, and c_n (ng/g) is the concentration of sample n. For this calculation we assume that the

density of the lignite profile is 1.29 g/cm^3 (Kolin 2007). Fluence calculations for Os (24.9 ng Os/cm^2) and

Ir (10.4 ng Ir/cm^2) over the length of the Ir-sampled profile result in a super-chondritic overall Os/Ir ratio

of 2.4 requiring Os and Ir fractionation. Calculated oxygen fugacities indicate that conditions in the

ejecta plume were sufficiently oxidizing to allow formation of OsO_4 (Ebel and Grossman, 2004). In

contrast, Ir does not form a volatile oxide and is expected to condense with refractory spinels. Ebel and

Grossman (2004) cite a previously reported sub-chondritic Os/Ir spinel composition as evidence

validating their inference of a highly oxidizing vapor plume. We note that the condensation of a spinel component with sub-chondritic Os/Ir ratios would require the Os/Ir ratio of the remaining material to be super-chondritic.

2-5.3 Rhenium mobility and open system behavior

The Re results for Bowring Pit suggest recent open system behavior, either as Re addition or Os loss, sometime between the present day and 10 Ma. *In situ* decay of ^{187}Re to ^{187}Os can change ^{187}Os/^{188}Os ratios drastically over time in this section because corresponding Re/Os ratios are high. Consequently, it is important to calculate initial ^{187}Os/^{188}Os ratios at the time of the sediment deposition. Age corrections, which assume closed system behavior for Re and Os since the time of deposition, result in impossibly low ^{187}Os/^{188}Os values for 14 out of 21 samples in the Bowring Pit section (Figure 2.5). The four samples immediately surrounding and including the boundary sample yield initial ^{187}Os/^{188}Os ratios ranging from 0.142 – 0.160. The impossibly low initial ratios calculated for samples above and below the boundary can only be caused by over-correcting for the amount of ^{187}Re decay due to open system behavior either via Re addition or Os loss. Negative initial ^{187}Os/^{188}Os values due to remobilization open system behavior were also reported for Paleogene dark Egyptian marine shales and organic-rich Upper Devonian sediments (Jaffe et al., 2002; Schmitz et al., 2004). Age corrections for the Bowring Pit samples for successively younger ages constrain the maximum amount of time that has passed since Re addition/Os loss. Correcting for 10 Ma of *in situ* ^{187}Re decay yields initial ^{187}Os/^{188}Os values that are all chondritic or higher (Figure 2.5), indicating disturbance of the Re-Os system occurred sometime in the last 10 million years. However, this analysis does not enable us to determine whether Re addition/Os loss occurred gradually over the last 10 Myr, or abruptly at 10 Ma.

To confirm open system behavior, we determined overall ^{187}Re/^{188}Os and ^{187}Os/^{188}Os values for the sample profile (172 and 0.2469, respectively) by dividing the ^{187}Re and ^{187}Os fluences by the ^{188}Os

fluence. Then, these values were used to calculate a single initial ^{187}Os/^{188}Os ratio for the entire section.

Age corrections still resulted in an impossibly low initial ^{187}Os/^{188}Os ratio of 0.0578. This confirms that

the whole section was affected by open system behavior and eliminates the possibility of purely vertical

redistribution of Re and Os within the sampled profile. The ^{187}Re/^{188}Os ratio of the entire profile is

higher than crustal averages, demonstrating that the Re added to the system is unrelated to the impact

event as the Re/Os ratios in chondrites are typically 0.3-0.4 (Horan et al., 2003). It is possible, though

unlikely, that the system has experienced both Re addition and Os loss as both elements exhibit mobility

in organic-rich sediment (Jaffe et al., 2002).

We favor the Re addition interpretation for several reasons. First, as noted above, Re

concentrations are extremely high compared to both average crustal material and non-marine coals, as

reported by Baioumy et al. (2011). Second, Os/Ir ratios are elevated relative to chondritic Os/Ir ratios.

Given the expectation that most of the Os and Ir content in the section is projectile-derived, this places

strong constraints on the likely degree of Os loss. Last, Os loss seems to occur only in deeply weathered

samples that have experienced nearly complete Re loss (Jaffe et al. 2002). To our knowledge there is no

empirical evidence showing both net Os loss and net Re addition.

2-5.4 Calculated initial ^{187}Os/^{188}Os proximal to the K-Pg boundary

Available data from the Bowring Pit section suggest that the ^{187}Os/^{188}Os ratios of samples closest

to the K-Pg boundary are relatively unaffected by redistribution of Re and Os. The sample that

corresponds to the K-Pg boundary and those samples immediately above and below the boundary are

unique among the samples analyzed in that they exhibit Re concentrations that are lower than other

samples from the profile. Relatively lower wt% C compared to the rest of the sample profile may

account for the observed low Re concentrations across the K-Pg boundary at the Bowring Pit. The two

samples immediately surrounding the impact horizon exhibit elevated Os concentrations relative to other samples with similar carbon content consistent with Os enrichment via an impact event (Figure 2.6). The Os within these samples likely is comprised of more insoluble, impact-derived Os leading to the generally lower ^{187}Os/^{188}Os compared to the rest of the profile. Due to the relatively low wt% C of these samples, soluble Re migrating through the sediment would be more likely to by-pass this section of the sample profile and instead accumulate in a more reduced (C-rich) part of the section. These two factors produce a local minimum in Re/Os ratio across the K-Pg boundary, reducing corrections for in situ Re decay.

Although we cannot rule out the possibility that open system behavior with respect to Re and Os in samples closest to the K-Pg boundary has biased calculated initial ^{187}Os/^{188}Os ratios based on an age of 66 Ma, we suggest that the calculated initial ^{187}Os/^{188}Os ratios of these samples closely approximate the ^{187}Os/^{188}Os value of the Chicxulub ejecta plume. Due to the low ^{187}Re/^{188}Os ratios of samples proximal to the K-Pg boundary, corrections associated with in situ ^{187}Re decay over the last 66 million years are small and the calculated initial ^{187}Os/^{188}Os ratio close to the boundary reach as low as 0.142 ± 0.003. Several nearby samples yield similar initial ^{187}Os/^{188}Os ratios, and these ratios are only slightly elevated compared to previously reported ^{187}Os/^{188}Os ratios for other K-Pg boundary section in the Western United States (Table 2.2; 0.138-0.140: Esser and Turekian 1989; Luck and Turekian 1983). Obtaining such similar ^{187}Os/^{188}Os ratios over such a large range of absolute Os concentrations (Fig 1) is not consistent with physical mixing between chondrite and upper crustal end members. Instead the similarity of the Os isotope composition among terrestrial K-Pg boundary sites over such a large range in Os concentrations suggests that samples analyzed are capturing the Os isotope composition of the ejecta plume itself. While this is admittedly speculative and other interpretations are possible, this interpretation is testable because it leads to the prediction that the lowest ^{187}Os/^{188}Os ratios measured

31

in K-Pg boundary sections throughout the western United States should be close to 0.14, and clearly elevated above the know range of chondrites which extends to nearly 0.13.

If the inference that the Chicxulub ejecta plume deposited Os with a bulk $^{187}Os/^{188}Os$ value close to 0.14 over much of the western interior of the United Stated is correct, then the super-chondritic character of the K-Pg ejecta plume can be explained in several ways. One option is that the bulk $^{187}Os/^{188}Os$ ratio of the K-Pg bolide is elevated above the measured $^{187}Os/^{188}Os$ range in chondrites, which exhibits an upper bound close to 0.13. A second option is that target material assimilated into the ejecta plume upon impact carried enough Os to shift the $^{187}Os/^{188}Os$ ratio of the ejecta plume to super-chondritic values. A third possibility is that the ejecta plume is inhomogeneous with respect to its $^{187}Os/^{188}Os$ ratio. Although we cannot discern between these various possibilities at this time, confidently determining the $^{187}Os/^{188}Os$ of the ejecta plume remains an important goal because this piece of information is essential to using Os isotope data to estimate projectile size (Paquay et al. 2008; Sato et al. 2013). Specifically, if the Chicxulub ejecta plume is as high as 0.14, rather than being chondritic with respect to $^{187}Os/^{188}Os$, then Os isotope-based estimates of K-Pg projectile size increases substantially compared to the range calculated by Paquay et al. (2008).

2-6. Conclusions

The Bowring Pit K-Pg site displays strong evidence for remobilization of Os and Ir as well as open system behavior with respect to Re. Concentration profiles along the sample section suggest Os and Ir were dominantly subjected to vertical redistribution, while Re appears more susceptible to lateral movement based on evidence for net addition of Re to the system. Despite this mobility, the $^{187}Os/^{188}Os$ ratios clearly delineate the K-Pg boundary Os excursion. Age corrections for the $^{187}Os/^{188}Os$ ratio for the boundary sample result in an initial $^{187}Os/^{188}Os$ ratio of 0.1436 ± 0.0033, very similar to values reported for other sites from the western interior of the United States, suggesting that the $^{187}Os/^{188}Os$ value of

the Chicxulub ejecta plume was elevated compared to chondrites. Age corrections for the rest of the

sample profile result in impossibly low $^{187}Os/^{188}Os$ ratios above and below the K-Pg boundary requiring

open system behavior, most likely due to Re addition, within the last 10 Myr. Elevated Os concentration

and a relatively low $^{187}Os/^{188}Os$ ratio extending ~ 5 cm above the K-Pg boundary suggest that Os

accumulation at the Bowring Pit section continued after the impact event. This is most likely due to

accumulation of impact-derived Os released from weathering of nearby sediment or local sediment

redistribution.

2.7 Effect on impactor size

Rejecting the hypotheses that the $^{187}Os/^{188}Os$ composition the Os entering the ocean immediately after

the impact is both spatially homogeneous and of chondritic nature has large implications on the Os

estimated size of the impactor. The distribution of K-Pg impact ejecta has been numerically modeled

with impactor sizes ranging as big as 12-16 km (e.g. Artemieva and Morgan, 2009). Iridium and Os based

estimates were 6 km and 4.1 – 4.4, respectively (Paquay et al., 2008). However, these Os estimations are

based on chondritic $^{187}Os/^{188}Os$ composition entering the ocean. As the $^{187}Os/^{188}Os$ ratio of the impact-

related Os increases, the absolute difference between background Os and impact-related Os becomes

smaller, requiring more impact-related Os to obtain the same impact-induced $^{187}Os/^{188}Os$ minimum than

if chondritic Os were entering the ocean. Results from my first study indicate that total mass of the

impacting bolide should be three times the size of that predicted by Paquay et al. (2008). The Bowring

Pit study also helps constrain the amount of impact-related Os that is in a water soluble phase. By

integrating under the portion of the Os concentration profile that represents the water soluble portion

of Os and doing the same thing for the Os bound in particulate phases, I can compare the inventories of

these two types of impact-related Os. From this calculation I found that approximately 75% of the

impact related Os is in a water soluble phase. However, because this is only one study site, more work should be done to better constrain this number.

$$f = (R_{post\text{-}impact} - R_{pre\text{-}impact})/(R_{impactor} - R_{pre\text{-}impact}) \tag{7}$$

f = (0.15 -0.4)/(0.14-0.4)

f = 0.96

$$M(Os)_{impactor} = (f/1\text{-}f) * 7.3 * 10^7 \text{ mol Os}$$

$$M(Os)_{impactor} = (0.96/1\text{-}0.96) * 7.3 * 10^6 \text{ mol Os} \tag{8}$$

$M(Os)_{impactor}$ = 1.83 * 10^9 mol Os

$$M_{impactor} = M(Os)_{impactor}/(f_{Os-soluble} * C(Os)_{projectile}) \tag{9}$$

$$M_{impactor} = 1.83*10^9 \text{ mol Os}/(0.75 * 3.34*10^{-9} \text{ mol Os/g})$$

$M_{impactor}$ = 7.24 * 10^{17} g = 7.24 * 10^{14} kg versus 2.38 * 10^{14} kg for Paquay et al. (2008)

This calculation should be considered an upper limit estimate whereas results from Paquay et al. (2008) should be considered a lower limit. Inherent in this estimation is that all the Os in the ejecta plume being added to the ocean is from the projectile. However, a large amount of crust was vaporized during the impact event, as suggested by the ~180 km in diameter crater that was created. This crustal Os could have "contaminated" the ejecta plume adding to the total Os that was introduced to the oceans. Additionally, as the post-impact $^{187}Os/^{188}Os$ ratio approaches the $^{187}Os/^{188}Os$ ratio of the impactor, these calculations are subject to significant error amplification. As Paquay et al. (*In Review)* point out, a 13% decrease in the post-impact $^{187}Os/^{188}Os$ ratio results $M_{impactor}$ mass four times larger.

7. Acknowledgements

Alvarez, L., Alvarez, W., Asaro, F., Michel, H., 1980. Extraterrestrial Cause for the Cretaceous-Tertiary Extinction. Science, 208: 1095-1108.

Baioumy, H., Eglinton, L., Peucker-Ehrenbrink, B., 2011. Rhenium-osmium isotope and platinum group element systematics of marine and non-marine organic-rich sediments and coals from Egypt. Chemical Geology, 285: 70-81.

Barclay, R., Johnson, K., Betterton, W., Dilcher, D. 2003. Stratigraphy and megaflora of a K-T boundary section in the eastern Denver Basin, Colorado. Rocky Mountain Geology, 38:45-71.

Bowring, S. Crowley, J. Condon, D., Ramezani, J. Johnson, K. 2007. Geochronology of the Maastrichtian-Paleocene rocks of the Denver Basin: an opportunity for high-precision calibration of climate change and extinction ca. 69-64 Ma. Geological Society of America Abstracts with Programs, 39:26.

Cohen, A., Coe, A., Bartlett, J.M., Hawkesworth, C.J., 1999. Precise Re-Os ages of organic-rich mudrocks and the Os isotope composition of Jurassic seawater. Earth and Planetary Science Letters, 167: 159-173.

Dalton, R. 2007. Time Traps, Nature, 449:20-21.

Ebel, D., Grossman, L. 2004. Spinel-bearing spherules condensed from the Chicxulub impact-vapor plume. Geology, 33:293-296.

Esser, B., Turekian, K., 1989. Osmium isotopic composition of the Raton Basin Cretaceous-Tertiary boundary interval [abs.]. EOS: Transactions, American Geophysical Union, 70: 717.

Esser, B., Turekian, K., 1993. The osmium isotopic composition of the continental crust. Geochimica et Cosmochimica Acta, 57: 3093-3104.

Ferrow, E., Vajda, V., Koch, C., Peucker-Ehrenbrink, B., Willumsen, P. 2011. Multiproxy analysis of a new terrestrial and a marine Cretaceous-Paleogene (K-Pg) boundary site from New Zealand. Geochimica et Cosmochimica Acta, 75: 657-672.

Frei, R., Frei, K., 2002. A multi-isotopic and trace element investigation of the Cretaceous-Tertiary boundary layer at Stevns Klint, Denmark-inferences for the origin and nature of siderophile and lithophile element geochemical anomalies. Earth and Planetary Science Letters, 203(2): 691-708.

Gramlich, J., Murphy, T., Garner, E., Shields, W. 1973. Absolute isotopic abundance ratio and atomic weight of a reference sample of rhenium. Journal of Research National Bureau of Standards, 77A:691-698.

Goderis S., Tagle R., Belza J., Smit J., Montanari A., Vanhaecke F., Erzinger J., and Claeys Ph. 2013. Reevaluation of siderophile element abundances and ratios across the Cretaceous-Paleogene (K-Pg) boundary: Implications for the nature of the projectile. Geochimica et Cosmochimica Acta 120: 417-446.

Gordon, Jr. D.C. (1969) Examination of methods of particulate organic carbon analyses. Deep Sea Research, 16:661-665.

Hall, G.E.M., Pelchat, J.C., 1994. Analysis of geological materials for gold, platinum and palladium at low ppb levels by fire assay-ICP mass spectrometry. Chemical Geology, 115(1-2): 60-72.

Hassler, D., Peucker-Ehrenbrink, R., Ravizza G. 2000. Determination of Os isotope composition by sparging OsO_4 in a magnetic sector ICP-MS. Chemical Geology, 166:1-14.

Horan, M., Walker, R., Morgan, J., Grossman, J., Rubin, A., 2003. Highly siderophile elements in chondrites. Chemical Geology, 196(1-4): 27-42.

Hicks, J., Johnson, K., Obradovich, J., Miggins, D., Tauxe, L. 2003. Magnetostratigraphy of Upper Cretaceous (Maastrichtian) to lower Eocene strata of the Denver Basin, Colorado. Rocky Mountain Geology, 38: 1-27.

Jaffe, L., Peucker-Ehrenbrink, B., Petsch, S., 2002. Mobility of rhenium, platinum group elements and organic carbon during black shale weathering. Earth and Planetary Science Letters, 198(3-4): 339-353.

Kendall, B.S., Creaser, R.A., Selby, R.D., 2004. Constraints on the timing of Marinoan 'Snowball Earth' glaciation by 187Re-187Os dating of Neoproterzoic post-glacial black shale in Western Canada. Earth and Planetary Science Letters, 222(3-4): 729-740.

Kirkham, R. and Ladwig, L. 1979. Coal resources of the Denver and Cheyenne Basins, Colorado. Colorado Geological Survey Resource Series, 5: 1-70.

Koeberl, C., Claeys, P., Hecht, L., McDonald, I. 2012. Geochemistry of Impactites. Elements, 8: 37-24.

Koeberl, C., Shirey, S. 1997. Re-Os systematics as a diagnostic tool for the study of impact craters and distal ejecta. Palaeogeography, Palaeoclimatology, Palaeoecology, 132: 25-46.

Kyte, F., 1998. A meteorite from the Cretaceous/Tertiary boundary. Nature, 396: 237-239.

Kolin, K. 2007. Report NI 43-101 Technical Report Limon Lignite Project Elbert County, Colorado USA. Prepared by Tetra Tech for Radar Acquisitions Corp, 97 Pages, www.canamcoal.com/i/pdf/43-101-Final.pdf, accessed 1/24/14.

Kyte, F., Smit, J., Wasson, J., 1985. Siderophile interelement variations in the Cretaceous-Tertiary boundary sediments from Caravaca, Spain. Earth and Planetary Science Letters, 73(2-4): 183-195.

Laubach, S., Marrett, R., Olson, J., Scott, A. 1998. Characteristics and origins of coal cleat: A review. International Journal of Coal Geology, 35:175-207.

Lee, C., Wasserburg, G., Kyte, F., 2003. Platinum-group elements (PGE) and rhenium in marine sediments across the Cretaceous–Tertiary boundary: Constraints on Re-PGE transport in the marine environment. Geochimica et Cosmochimica Acta, 67(4): 655-670.

Lichte, F. et al., 1986. New method for the measurement of osmium isotopes applied to a New Zealand Cretaceous/Tertiary boundary shale. Nature, 322(6082): 816-817.

Lorand, J.P., Luguet, A., Alard, O., Bezos, A., Meisel, T., 2008. Abundance and distribution of platinum-group elements in orogenic lherzolites; a case study in a Fontete Rouge Iherzolite (French Pyrenees). Chemical Geology, 248(3-4): 174-194.

Luck, J.M., Turekian, K.K., 1983. Osmium-187/Osmium-186 Manganese Nodules and the Cretaceous Tertiary Boundary. Science, 222(4624): 613-615.

Nowell, G., Luguet, A., Pearson, D., Horstwood, M. 2008. Precise and accurate ^{186}Os/^{188}Os and ^{187}Os/^{188}Os measurements by multi-collector plasma ionisation mass spectrometry (MC-ICP-MS) part I: Solution analyses. Chemical Geology, 248: 363-393.

Meisel, T., Kraehenbuel, U., Nazarov, M., 1995. Combined osmium and strontium isotopic study of the Crectaceous-Tertiary boundary at Sumbar, Turkmenistan: A test for an impact vs. a volcanic hypothesis. Geology, 23(4): 313-316.

Miller, K.G.S., R. M. et al., 2010. Relationship between mass extinction and iridium across the Cretaceous-Paleogene boundary in New Jersey. Geology, 38(10): 867-870.

Paquay, F.S., Ravizza, G.E., Dalai, T.K., Peucker-Ehrenbrink, B., 2008. Determining chondritic impactor size from the marine osmium isotope record. Science, 320(5873): 214-218.

Peucker-Ehrenbrink, B., Bach, W., Hart, S., Blusztajn, J., Abbruzzese, T. 2003. Rhenium-osmium isotope systematics and platinum group element concetrations in oceanic crust from DSDP/ODP Sites 504 and 417/418. Geochemistry Geophysics Geosystems, 4:8911-8939

Peucker-Ehrenbrink, B., Hannigan, R., 2000. Effects of black shale weathering on the mobility of rhenium and platinum group elements. Geology, 28(5): 475-478.

Peucker-Ehrenbrink, B., Jahn, B., 2001. Rhenium-osmium isotope systematics and platinum group element concentrations: Loess and the upper continental crust. Geochemistry Geophysics Geosystems, 2(10).

Peucker-Ehrenbrink, B., Ravizza, G., Hofmann, A., 1995. The marine 187Os/188Os record of the past 80 million years. Earth and Planetary Science Letters, 130(1-4): 155-167.

Quitté, G. et al., 2007. Osmium, tungsten, and chromium isotopes in sediments and in Ni-rich spinel at the K-T boundary: Signature of a chondritic impactor. Meteoritics & Planetary Science, 42(9): 1567-1580.

Racki, G., Machalski, M., Koeberl, C., Harasimiuk, M., 2011. The weathering-modified iridium record of a new Cretaceous-Palaeogene site at Lechowka near Chelm, SE Poland, and its Palaeobiologic implications. Acta Palaeontologica Polonica, 56(1): 205-215.

Ravizza, G., Paquay, F. 2008. Os isotope chemostratigraphy applied to organic-rich marine sediments from the Eocene-Oligocene transition on the West African margin (ODP Site 959). Paleoceanography, 23, PA2204.F

Ravizza, G., Peucker-Ehrenbrink, B., 2003. Chemostratigraphic Evidence of Deccan Volcanism from the Marine Osmium Isotope Record. Science, 302(5649): 1392-1395.

Ravizza, G. Pyle, D. 1997. PGE and Os isotopic analyses of single sample aliquots with NiS fire assay preconcentration. Chemical Geology, 141:251-268.

Ravizza, G., Turekian, K.K., 1989. Application of the 187Re-187Os system to black shale geochronometry. Geochimica et Cosmochimica Acta, 53(12): 3257-3262.

Ravizza, G., VonderHaar, D., 2012. A geochemical clock in earliest Paleogene pelagic carbonates based on the impact-induced Os isotope excursion at the Cretaceous-Paleogene boundary. Paleoceanography, 27(3).

Raynolds, R. 2002. Upper Cretaceous and Tertiary stratigraphy of the Denver Basin, Colorado. Rocky Mountain Geology, 37: 111-134.

Renne, P.R. et al., 2013. Time scales of critical events around the Cretaceous-Paleogene boundary. Science, 339(6120): 684-687.

Robinson, N., Ravizza, G., Coccioni, R., Peucker-Ehrenbrink, B., Norris, R. 2008. A high-resolution marine osmium isootpe reocrd from the late Maastrichtian: distinguishing the chemical fingerprints of the Deccan and KT impactor. Earth and Planetary Science Letters, 281: 159-168.

Sato, H., Onoue, T., Nozaki, T., Suzuki, K. 2013. Osmium isotope evidence for a large Late Triassic impact event. Nature communications, 4:2455-2462.

Sauvage, J., 2010. Distribution of Platinum Group Elements across the Cretaceous-Tertiary Boundary, Denver Basin (Colorado). Master's Thesis, Vrije Universiteit Brussel, Brussels, Belgium, 115 pp.

Sauvage, J., Goderis, S., Claeys, P., 2010. High-resolution platinum group elements and C-isotope analyses across the KT boundary in the Denver Basin (abstr.). Annual Meeting Geological Society of America, 42(#180696).

Schmitz, B., 1992. Chalcophile elements and Ir in continental Cretaceous/Tertiary boundary clays from the western interior of the USA. Geochimica et Cosmochimica Acta, 56(4): 1695-1703.

Schmitz, B. et al., 2004. Basaltic explosive volcanism, but no comet impact, at the Paleocene-Eocene boundary: high-resolution chemical and isotopic records from Egypt, Spain and Denmark. Earth and Planetary Science Letters, 225(1-2): 1-17.

Selby, D., 2007. Direct Rhenium-Osmium age of the Oxfordian-Kimmeridgian boundary, Staffin bay, Isle of Skye, U.K. and the late Jurassic timescale. Norsk Geologisk Tidsskrift, 87: 291-299.

Sharp, J.H. (1974) Improved analysis for "particulate" organic carbon and nitrogen from seawater. Limonology and Oceanography, 19:984-989.

Shukolyukov, A., Lugmair, G.W., 1998. Isotopic Evidence for the Cretaceous-Tertiary Impactor and Its Type. Science, 282: 927-929.

Smit, J. 1999. The global stratigraphy of the Cretaceous-Tertiary boundary impact ejecta. Annual Review of Earth and Planetary Science, 27: 75-113.

Smoliar, M.I., Walker, R.J., Morgan, J.W., 1996. Re-Os isotope constraints on the age of Group IIA, IVA, and IVB iron meteorites. Science, 271: 1099-1102.

Tagle, R., Claeys, P., 2005. An ordinary chondrite impactor for the Popigai crater, Siberia. Geochimica et Cosmochimica Acta, 69(11): 2877-2889.

Trinquier, A., Birck, J.-L., Allegre, C., 2006. The nature of the KT impactor. A 54Cr reappraisal. Earth and Planetary Science Letters, 241(3-4): 780-788.

Walker, R., Prichard, H., Ishiwatari, A., Pimentel, M., 2002. The osmium isotopic composition of convecting upper mantle deduced from ophiolite chromites. Geochimica et Cosmochimica Acta, 66(2): 329-345.

Chapter 3. Post-impact ^{187}Os/^{188}Os recovery across the K-Pg boundary in the southern Indian Ocean

Jessica Zaiss[1*], Greg Ravizza[1]

[1]Department of Geology and Geophysics, SOEST, University of Hawaii-Manoa Honolulu, HI USA

Abstract

Well-documented variations in the marine Os isotope record establish a decline in $^{187}Os/^{188}Os$ ratio of seawater from 0.6 to 0.4 in the latest Cretaceous (66.4 to 66.1 Ma) that is attributed to the onset of major Deccan volcanism. Soon thereafter (66.04 Ma) there is an abrupt decrease in $^{187}Os/^{188}Os$ to ~0.15 that results from the Chicxulub impact event , followed by recovery to pre-impact values of ~0.4 within the first ~200 kyr of the Paleogene. However, recent studies suggest that the modern global ocean may not be homogenous with respect to Os isotopes as previously assumed. Here we present new Os isotope and concentration data from two southern Indian Ocean sites across the Cretaceous-Paleogene (K-Pg) boundary . The post-impact $^{187}Os/^{188}Os$ ratio recovery profiles do not follow the global trend. At ODP site 738C, the post-impact $^{187}Os/^{188}Os$ ratio recovers to only ~0.35, more than 3 myr after the impact event. This must be a local effect as ODP site 761C, ~5000 km to the northeast of ODP site 738C, recovers fully to 0.4 by a maximum of 1.1 myr after the impact event. Biases due to mineral detritus and extraterrestrial Os can be dismissed requiring an alternative source of unradiogenic Os. We cannot rule out potential active sources of unradiogenic Os due to poor mass balance constraints, we favor the interpretation of lateral redistribution of impact related material as the cause of the persistently low $^{187}Os/^{188}Os$ ratios in the southern Indian Ocean.

3.1 Introduction

Recent changes in our understanding of the marine Os isotope record motivate detailed reconstruction of the marine Os isotope record of the Indian Ocean across the Cretaceous-Paleogene (K-Pg) boundary. Analyses of Quaternary marine sediments suggest that subtle regional differences in the seawater $^{187}Os/^{188}Os$ composition may exist in the modern ocean (Paquay and Ravizza 2012 and references there in) and data from older marine sediment imply much larger regional contrasts in seawater $^{187}Os/^{188}Os$ ratios are likely to have existed in the geologic past (DuVivier et al. 2014). These findings supersede earlier inferences that seawater $^{187}Os/^{188}Os$ composition was essentially homogenous throughout the Cenozoic and latest Cretaceous (See Peucker-Ehrenbrink and Ravizza 2000 for an overview). The composite record of $^{187}Os/^{188}Os$ ratio variation across the K-Pg (Robinson et al., 2009) is one of the better examples of coherent changes in seawater $^{187}Os/^{188}Os$ composition in different ocean basins. Eruption of the Deccan traps is believed to have caused a whole ocean shift to lower $^{187}Os/^{188}Os$ values, $^{187}Os/^{188}Os$ ratios in the latest Cretaceous and early Paleogene Indian Ocean might reflect Deccan influence by recording unusually low $^{187}Os/^{188}Os$ before and after the impact-induced Os isotope excursion at the K-Pg boundary. In this study, we explore this possibility for the first time.

Shifts to lower $^{187}Os/^{188}Os$ ratios in marine sediments are tracers of large impact events (Paquay et al. 2008, Sato et al., 2013) and large igneous province (LIP) eruptions (Cohen and Coe 2002,2007; Du Vivier et al., 2014; Kuroda et al., 2010; Ravizza and Peucker-Ehrenbrink, 2003; Tejada et al., 2009; Turgeon and Creaser, 2008). The seawater Os isotopic composition reflects a balance of radiogenic ($^{187}Os/^{188}Os \approx 1.2$) input from continental weathering and unradiogenic ($^{187}Os/^{188}Os \approx 0.127$) input from volcanic processes and extraterrestrial (ET) in flux (Peucker-Ehrenbrink and Ravizza, 2000; Sharma et al., 2007). During LIP and impact events, a large amount of unradiogenic Os is introduced to the global ocean causing the overall $^{187}Os/^{188}Os$ ratio to decline. The short residence time of Os (<10 - 40 kyr, Oxburgh, 2001;

Levasseur et al., 1999) allows the sedimentary record to capture rapid shifts in the marine Os isotope balance.

The mechanism by which the seawater $^{187}Os/^{188}Os$ composition changes is better understood for impact events than for LIP activity. In the event of chondrite impact event, vaporized, unradiogenic Os enters the ocean and mixes with ambient Os dissolved in seawater. The underlying sediment records the post-impact $^{187}Os/^{188}Os$ ratio minimum associated with the addition of ET Os, as well as the recovery to pre-impact, steady-state values (Paquay et al. 2008). The minimum $^{187}Os/^{188}Os$ ratio associated with impact events does not necessarily need to be chondritic due to mixing with the ambient ocean and can vary based on the pre-impact isotopic composition and size of the impactor (Sato et al., 2013; Paquay et al., 2008). The post-impact $^{187}Os/^{188}Os$ ratio decline is rapid and duration of the low $^{187}Os/^{188}Os$ ratio is short, consistent with an instantaneous addition of impact-derived Os followed by a relaxation to the pre-impact steady state. At three widely distributed sites, recovery to pre-impact $^{187}Os/^{188}Os$ values following the Chicxulub impact event at the Cretaceous-Paleogene (K-Pg) boundary occurs within roughly 200 kyr (Ravizza and VonderHaar, 2012), a time scale consistent with a marine residence time of 40 kyr. Iron meteorite or chondrite impact events are best for observing an Os excursion as they are enriched in highly siderophile elements, including Os (Koeberl and Shirey, 1997).

The influence of LIP emplacement on the seawater $^{187}Os/^{188}Os$ is inferred from correlating the timing of emplacement and a decline in the $^{187}Os/^{188}Os$ ratio of marine sediment cores. The actual mechanism responsible for transferring unradiogenic, mantle-derived Os to the global oceans during and after flood basalt volcanism events remains unclear. Hydrothermal alteration of basaltic flows (DuVivier et al., 2014; Tejada et al., 2009) and chemical weathering of large flood basalts (Cohen and Coe, 2007; Ravizza and Puecker-Ehrenbrink, 2003) have both been proposed to explain the direct release of mantle derived Os to seawater. Extensive continental flood basalt eruption may also influence the flux and isotopic

composition of Os delivered to the oceans by changing actively weathering terrains from old continental crust (relatively high $^{187}Os/^{188}Os$) to young basaltic flows (relatively low $^{187}Os/^{188}Os$). Ravizza and Peucker-Ehrenbrink (2003) suggested that this effect contributed to the decrease in seawater $^{187}Os/^{188}Os$ ratio during the initiation of major Deccan volcanism.

Regardless of the mechanism by which unradiogenic Os is introduced to the global ocean from LIPs, distinguishing the signature of LIPs from impacts in the marine Os isotope record is facilitated by the differences in the duration of low $^{187}Os/^{188}Os$ compositions; the duration of low $^{187}Os/^{188}Os$ ratios during LIP emplacement is greater than those associated with impact events. For example, the Os isotope excursion associated with the Caribbean LIP exhibits an abrupt decrease in $^{187}Os/^{188}Os$ ratio, followed by a broad minimum lasting approximately 200 kyr and a gradual recovery to higher ratios of similar duration (e.g. Du Vivier et al., 2014); the $^{187}Os/^{188}Os$ excursion of the Caribbean LIP is more than twice as long as impact-induced excursions. In the case of contemporaneous LIP eruption and a large impact event, such as the K-Pg impact event 66 Ma, the differences between the $^{187}Os/^{188}Os$ excursions allows the impact event to be imprinted on top of the Deccan LIP signature (Figure 3.1). The main phase of Deccan volcanism reduced the global seawater $^{187}Os/^{188}Os$ composition from 0.6 to 0.4 over ~200 kyr (Robinson et al. 2009). The ocean remained at 0.4 for a short amount of time and then the impact event brought the global seawater $^{187}Os/^{188}Os$ ratio down to ~0.15. Recovery to pre-impact $^{187}Os/^{188}Os$ ratios begins immediately and the total duration is short (see above), especially compared to the Deccan signature which seems to persist for more than a million years. Thus, although Deccan eruption and the Chicxulub impact event overlap in time, the influence of these two events on the marine Os isotope record can be differentiated.

ODP site 738 was selected for an Os isotope study for two reasons. First, the detailed Ir profile (Schmitz et al., 1991) across the K-Pg boundary indicated this site was well suited for further investigating the "Os

clock" proposed by Ravizza and VonderHaar (2012) for post-impact recovery. Second, the location of

this site in the Indian sector of the Southern Ocean places this site closer to the location of Deccan

volcanism than any previously studied deep ocean site. Results from this site were surprising in that the

post-impact seawater at this site did not return to the expected pre-impact value even after ~3.4 myr

after the impact. To determine if this is characteristic of the entire Indian and adjacent Southern Oceans,

we collected Os data from an ODP Site 761. This site sits ~5700 km (present –day) to the northeast of

ODP site 738C. Although the record we generated from ODP 761 is not densely sampled, it is sufficient

to establish that the low $^{187}Os/^{188}Os$ ratios expressed at Site 738 are not characteristic of the Indian

Ocean.

3.2 Geologic Setting

3.2-1 Ocean Drilling Program (ODP) site 738C

ODP hole 738C (62°42.54'S, 82°47.25'E, 2252.5 m water depth, Shipboard Scientific Party, 1989) is

located at a site of slow sediment accumulation on the southern portion of the Kerguelen Plateau

(Figure 3.2). This large plateau stretches 2500 km from southeast to northwest between the latitudes of

46°S and 64°S and stands 2-4 km above the neighboring African-Antarctic and Australian-Antarctic

basins (Barron et al. 1989). At the time of the K-Pg impact, the Indian sector of the Southern Ocean

hosted significant volcanic activity, most extensively from the large Deccan Traps, the Ninetyeast Ridge,

and Skiff bank (Coffin et al. 2002). For this study, we analyzed a closely spaced suite of samples from

core 20R, as well as spot analyses (1 sample per core) from cores 21R-24R, for a total depth range of

372.55 – 411.52 mbsf. The lower sampling resolution below Core 20R was due to very poor core

recovery and drilling disturbance related to the presence of cherts immediately below the K-Pg

boundary. Sediments spanning the K-Pg boundary at ODP site 738C are partially silicified and comprised

mostly greenish gray calcareous chalk with occasional chert nodules (Shipboard Scientific Party, 1989).

The biostratigraphically (Huber 1991, Wei and Pospichal, 1991) and chemically (Schmitz et al. 1991) complete K-Pg boundary lies within a 15 cm finely laminated, clay-rich section of the core with few nannofossils. ODP site 738C contains a large Ir anomaly, characterized by a maximum Ir concentration of 18 ng/g and an overall fluence of 320 ng Ir/cm^2 (Schmitz et al. 1991). Here, the term fluence refers to the integrated inventory of Ir in excess of background levels from top to bottom of the concentration anomaly. The global average Ir fluence for the K-Pg boundary is 55 ng/cm2 (Donaldson and Hildebrand 2001), and the Ir fluence at the K-Pg boundary in ODP site 738C is among the largest known.

3.2-2 Ocean Drilling Program (ODP) Site 761C

ODP 761, (16°44.23'S, 115°32.10'E, 2167.9 m water depth, Shipboard Scientific Party, 1990) located on the Wombat Plateau, encompasses a geochemically complete K-Pg excursion (Rocchia et al. 1992). Although this site contains a large and well-defined Ir anomaly (7.6 ng/g, Roccia et al., 1992), nannofossil biostratigraphy identifies a hiatus within the core approximately 23 cm above the Ir anomaly (Posphical and Bralower, 1992). The implications and extent of this hiatus are discussed below. This plateau, located ~5700 km to the northeast of ODP site 738C (Figure 3.2), is not a large igneous province like the Kerguelen plateau but rather a large marginal plateau surrounded by an abyssal plain which greatly reduces the amount of terrigenous input. The Ir anomaly for hole 761C is significantly smaller than at ODP site 738C (7.6 ng/g, Rocchia et al. 1992). Ir levels are elevated over a total thickness of 8 cm approximately centered about the K-Pg boundary yielding a total Ir flux of 80 ng Ir/cm^2 which is larger than the global mean fluence, but smaller than the Ir fluence at ODP site 738C (see above). Core material from the K-Pg boundary interval of ODP 761, as defined by the Ir anomaly, was depleted by the time of this study. However, published Ir data provide an invaluable context for the present study, allowing selection of samples that are unequivocally above or below the horizon influenced by impact-derived Ir. Samples analyzed were all within core 3R and ranged from 170.30 – 174.22 mbsf (Table 3.2).

3.3 Age Models

3.3-1 ODP site 738C

The age model for ODP site 738C is based solely on biostratigraphy (Figure 3.3 and Table 3.1). ODP 738 was one of seven Southern Ocean sites studied by Huber and Quillévéré (2005) during their revision of the Antarctic Paleogene planktonic foraminifer zonation scheme. Age constraints above the K-Pg boundary, as defined by the Ir anomaly, come directly from this revised zonal scheme. However, in an effort to be as accurate as possible, the ages for biostratigraphic datums come from Gradstein et al. (2012) rather than Huber and Quillévéré (2005). We still use the definitions for the zonal schemes from Huber and Quillévéré (2005). Our earliest-Paleogene samples cover planktonic foram zonal schemes AP0 through AP1c (Figure 3.4). The overlaps in depth between the biozones in Figure 3.4 are representative of the uncertainty in the exact depth of the specific biostratigraphic datums used to define zonal boundaries. Late-Cretaceous samples overlapped with the first and last appearance datums (FAD and LAD) of *Abathomphalus mayaroensis* (Huber, 1991). The age of these datums were obtained from Gradstein et al. (2012). Our sampling profile for this site ranges approximately between the ages of 69.1 Ma and 63.9 Ma. As noted above, samples above the K-Pg boundary are closely spaced in Core 20R (n = 46 over the first 3.4 million years of the Paleogene), but widely separated below the boundary in cores 21R to 24R (n = 4 in the last 3 myr of the Cretaceous). Biostratigraphic age controls yield an average sedimentation rate of ~0.17 cm/kyr for the first ~2 myr of the Paleogene. Below the boundary, the concept of average sedimentation rate is less useful because of poor core recovery. Instead, in the results section below we present the bounding age constraints for key samples below the boundary.

3.3-2 ODP site 761C

Age constraints for ODP Site 761C rely mostly on magnetostratigraphy. The use of biostratigraphic

datums is complicated by a hiatus ~23 cm above the Ir anomaly. Pospichal and Bralower (1992)

established that the 23 cm of sediment between the K-Pg boundary and the hiatus corresponds to

nannofossil subzone of CP1a in full. Many nannofossil datums that are widely spaced in time occur

suddenly at the top of this interval, marking a hiatus between CP1a and CP1b. Due to the hiatus, the age

model for this core relies solely on magnetostratigraphy. The C29r/C29n and C29n/C28r boundaries lie

between 0.54 - 1.2 m and 1.74 – 2.13 m above the Ir anomaly, respectively (Rocchia et al. 1992). The

ages for these boundaries were obtained from Gradstein et al. (2012). The top of C29r is 65.688 Ma and

the top of C29n is 64.958 Ma. Below the K-Pg boundary, the base of C29r chron was not fully recovered

in hole 761C but was reached in hole 761B (Galbrun, 1992). Calculating a sedimentation rate for the

earliest-Paleogene to the top of C29r would not be meaningful at ODP site 761C due to the uncertainty

in the temporal extent of the hiatus. However, bounding the top and bottom of C29n using ages from

Gradstein et al. (2012) we calculated a sedimentation rate of 0.16 cm/kyr through C29n. Assuming that

C29r has the same thickness for hole 761C as 761B, we can get a first-order approximation of the age-

depth relationship below the Ir anomaly. By doing so, we calculate an average sedimentation rate of 1.4

cm/kyr for the latest-Cretaceous. This constrains our sampling ages between 66.22 Ma and 65.69 Ma

(Figure 3.5).

3.3-3 Temporal overlap between ODP sites 761C and 738C

Although correlating ODP sites 738C and 761C in time is somewhat uncertain, we are confident that

there is significant temporal overlap of the early Paleogene and late Cretaceous intervals investigated

here. We cannot compare biostratigraphic datums between the two sites directly. ODP site 738C is a

high-latitude site where the biostratigraphic control is based on foraminiferal datums within the

Antarctic zonal scheme (Huber and Quillévéré, 2005). In contrast, biostratigraphic datums in ODP 761C

rely mainly on nannofossil and a few mid-latitude foraminiferal datums (Pospichal and Bralower, 1992).

However, the magnetic reversal stratigraphy (Rocchia et al 1992) provides useful age constraints in ODP

site 761C. Therefore, comparing temporal Os isotopic evolution between sites 738 and 761 was done in

the time domain opposed to direct comparison of biostratigraphic datums..

Using the zonal schemes in Huber and Quillévéré (2005), we determined that our most shallow sample

at ODP site 738C is 50 cm below the top of AP1b zone, which is marked by the FAD of *G. compressa*

(Figures 3.4 and 3.6). Although Site 738 did not yield a reliable magnetostratigraphy, Huber and

Quillévéré (2005) place the top of AP1b is within C28n. Our most shallow sample at ODP site 761C is 3

cm above the range of the C29n/C28r transition within C28r. According to Roccia et al. (1992), this is

within nannofossil zone NP2 (same as CP1b, Gradstein et al. 2012) which overlaps with the planktonic

foraminifer zone AP1b (Huber and Quillévéré, 2005). Thus, based on combined biostratigraphic and

magnetostratigraphic constraints, ODP holes 761C and 738B overlap for portions of C29r, C29n, and

C28r (Figure 3.6).

There is a remote possibility, suggested by the rare occurrence of *Chiasmolithus danicus* immediately

above the hiatus, that the hiatus in ODP site 761C is longer than proposed by Pospichal and Bralower

(1992) and extends into C28r rather than ending within C29r. If we assume this, the time interval of

overlap between ODP sites 761C and 738C shifts to younger ages encompassing the top of C28r, C28n

and the base of C27n (Figure 3.6).

Below the K-Pg boundary at ODP site 738C, our deepest sample is 1.12 m below the FAD of *A.

mayaroensis*. The age of this nannofossil datum has been placed at 69.118 Ma meaning our sample must

be older than this age. At 761, our deepest sample is still within C29r, the base of which has been place

at 66.398. Based on this, we are confident that our samples from these two sites overlap in time. Given

the poor core recovery in ODP site 738C below the boundary, the robustness of the age control for the youngest Cretaceous sample must be carefully evaluated. This sample lies below LAD of *A. mayaroensis* (66.35 Ma) implying an age greater than 66.35 Ma for our youngest Cretaceous sample from ODP site 738C. However, it is possible that this biodatum does not accurately reflect the age of the sediment at this depth as this site experienced extensive reworking. MacLeod and Huber (1996) estimated that up to 30% of the mass of foraminifers could be reworked based on Sr isotope analyses of foraminifera and the persistence of inoceramid remains above the K-Pg boundary.

3.4 Methods

3.4-1 Bulk Sediment Digestion

Bulk sediment digestions were carried out for samples from both ODP sites 738C and 761C. For the bulk digestions, crushed carbonate sample weights of ~0.3 g were digested in an H_2O_2/HNO_3 solution as outlined in Ravizza and VonderHaar (2012, Supplemental Material). Prior to sealing, the Carius tubes with samples were spiked with solutions enriched in [190]Os and [185]Re to allow Re and Os concentration measurements on same-sample aliquots by isotope dilution. Osmium isotope analyses were performed by transferring the digestion solution to a Teflon vial, followed by sparging the solution to introduce volatile OsO_4 into an ICP-MS (Hassler et al., 2002). Rhenium was obtained from the post-sparging solution via anion exchange chromatography, as described in Ravizza and Paquay (2007). These methods allow for making corrections for the in situ decay of [187]Re to [187]Os.

3.4-2 Partial digestion of sediment samples

A leaching method was also employed to minimize dissolution of mineral detritus phases which might bias Os isotopic composition data. Leaches were performed by loading 2-2.5 g of sample into 50 mL centrifuge tubes and adding dilute HNO_3 drop-wise until carbonate no longer reacted. The tube was

then placed in the centrifuge at 8000 rpm for 5 minutes. The liquid was decanted into Carius tube, 1 mL

of H_2O_2 was added and was then spiked for Os and Re. Note that concentrations determined from these

leach analyses represent the concentration of Re and Os in solution transferred to the Carius tube. If

there is significant sorption of Re or Os back onto remaining solids after the partial dissolution step but

before centrifugation, these concentrations may underrepresent the concentration of leachable Re and

Os. This method was applied to a subset of the samples from ODP site 738C that were located far above

the K-Pg boundary but still have bulk sediment $^{187}Os/^{188}Os$ far below the post-impact steady state value

of 0.4

3.5 Results

3.5-1 ODP site 738C

Pre-impact $^{187}Os/^{188}Os$ compositions are similar to late-Cretaceous Os profiles established for other

marine sites (Figure 3.7). The three deepest samples have $^{187}Os/^{188}Os$ ratios between 0.63 and 0.62. This

is nearly identical to the rest of the contemporaneous ocean (Figure 3.1). The impact-induced minimum

in $^{187}Os/^{188}Os$ (0.168) is also similar to that of other marine K-Pg impact records (Frei and Frei, 2002,

Paquay et al., 2008, Peucker-Ehrenbrink et al., 1995; Ravizza and Peucker-Ehrenbrink, 2003; Ravizza and

VonderHaar, 2012). ODP site 738C mimics an unexpected pattern observed at site 1262B (Ravizza and

VonderHaar, 2012) in that the maximum Os concentration occurs below the minimum $^{187}Os/^{188}Os$ ratio.

Post-impact $^{187}Os/^{188}Os$ ratio recovery does not follow the same trend as other K-Pg marine sites (Figure

3.8). Instead of recovering to a pre-impact steady-state value of 0.4, the $^{187}Os/^{188}Os$ ratios at ODP site

738C remain distinctly lower, only reaching to 0.32 after more than 4.5m/3 myr. The trend of relatively

low $^{187}Os/^{188}Os$ ratios occurs outside of the range of the Ir anomaly (Schmitz et al., 1991) indicating that

it is likely not emplaced impact-related material. Results for the partial digestions of samples yielded

very similar, but systematically higher $^{187}Os/^{188}Os$ ratios than the bulk digestions for all but two samples

(Figure 3.8). The highest ^{187}Os/^{188}Os ratio measured by the partial digestions was 0.357 but the majority remain ~0.32-0.33.

The maximum Os concentration is 2.057 ng/g (Table 3.1) and is at least two times larger than the impact induced Os maximum reported for other deep ocean K-Pg sites (Puecker-Ehrenbrink et al., 1995; Ravizza and VonderHaar, 2012), but more than 40 times lower than the highest Os cocnetration reported for a K-Pg boundary sample. Os concentrations remain elevated for ~1 m above the K-Pg boundary horizon before leveling off at background concentrations of 50-60 pg/g. This is consistent with elevated Ir concentrations that extend ~1.8 m above the maximum Ir concentration. The deepest samples in core 20R exhibit Os and Ir concentrations well above background levels. Concentrations from the leached samples were approximately half of those from bulk digestions (Table 3.1) but similar to other leaches performed on carbonates (Peucker-Ehrenbrink et al., 1995; Reusch et al., 1998).

Re concentrations were low and ranged from 2.2 pg/g to 150 pg/g. Because the Re concentrations were low compared to the Os concentration, age corrections for the ingrowth of ^{187}Os were small. Age corrections were less than 1% for all samples except two, 20R-5 13-15 cm and 20R-4 95-97cm, which were 2.9%and 2.8%, respectively.

3.5-2 ODP Site 761C

Overall, the general trend of the ^{187}Os/^{188}Os ratio through time at ODP site 761C is more similar to previously published data than ODP site 738C (Figure 3.9). Samples from ODP Hole 761C were not subjected to the partially digestion method used for some samples from ODP Hole 738C because the bulk sediment analyses conformed fairly well to the values expected based on previously published data (Paquay et al., 2008; Ravizza and VonderHaar, 2012). Pre-impact ^{187}Os/^{188}Os ratios exhibit a decreasing trend from ~0.45 to ~0.3, 1.76m to 40-15 cm, respectively, below the K-Pg horizon defined by the Ir anomaly (Figure 3.9). A similar, pre-impact, downward excursion from ~0.4 to impact-induced minima

has been reported for other marine sites (Ravizza and VonderHaar, 2012; Robinson et al., 2009). However, the onset of the downward excursion at ODP 761C is deeper than at other sites which typically start from ~0.5 to ~0.8 m below the K-Pg boundary (Figure 3.10).

Post-impact $^{187}Os/^{188}Os$ ratio results were again surprising but in a different way than ODP site 738C. At ODP site 761C, the $^{187}Os/^{188}Os$ ratio has recovered to the expected value of 0.4 by the first sample (34 cm) above the boundary. The $^{187}Os/^{188}Os$ ratio continues to rise through the most shallow sample (within 20cm above the C29n/C28r boundary) reaching ~0.5. Results from ODP 761C record some of the highest $^{187}Os/^{188}Os$ ratio for the time period investigated (Figure 3.11).

Background Os concentrations at ODP site 761C are similar to those at ODP site 738C ranging from 21.8 to 85.7 pg/g. Site 761C does not exhibit the broad influence of impact related Os that ODP site 738C does but this is not unexpected given elevated Ir concentrations only span a total of 8 cm, most of which is above the maximum concentration peak. Therefore, we would not expect to see elevated Os concentrations outside of this range.

3-5. Discussion

3.5-1 Pre-impact interpretations

One goal of this study was to determine if the Indian sector of the Southern Ocean was influenced by Deccan volcanism before the rest of the global ocean due to its proximity to the traps. However, it is hard to determine if ODP site 738C began to decline before the rest of the global ocean due to poor age constraint and sparse sampling density for this study. As noted above this is a consequence of poor core recovery below the K-Pg boundary at ODP site 738. The shallowest sample below the impact-derived material could be younger than biostratigraphy suggests as a result of reworking (MacLeod and Huber,

1996). A two component-mixing plot of Os data from ODP site 738C shows that impact related material from the K-Pg boundary could be reworked as much as 1.19 m up section (Figure 3.12). If we assume that *A. mayorensis* fossils exhibited a similar amount of reworking, this changes the age of sample 21R-01 12-13 cm from 66.4 Ma to 66.3 Ma. This places the pre-impact ^{187}Os/^{188}Os ratio at ODP site 738C slightly lower than other marine sites at ~66.4 - 66.3 Ma.   Sampling for site 761C begins at 66.1 Ma where the ^{187}Os/^{188}Os ratio is 0.45, well above the recorded ^{187}Os/^{188}Os ratio of 0.36 for ODP site 738C, 300 kyr prior. This suggests that emplacement of the Deccan Traps created local heterogeneities in seawater ^{187}Os/^{188}Os compositions within the Indian Ocean before homogenizing with other ocean basins.

The transition of ^{187}Os/^{188}Os ratios from >0.4 to <0.4 at ODP site 761C started at least 1.37 m below the K-Pg boundary. This is outside the expected range for this excursion to begin. Typically, this decline begins between 0.5 and 0.8 m below the Ir anomaly (Robinson et al., 2009; Ravizza and VonderHaar, 2012). Competing explanations for this secondary interval of decreasing ^{187}Os/^{188}Os ratios at other marine sites include redistribution of impact-related Os, through either diffusion or bioturbation (Robinson et al., 2009; Ravizza and VonderHaar, 2012). Other workers argue that the global decline in ^{187}Os/^{188}Os ratios immediately below the K-Pg boundary reflects a pulse of Deccan volcanism immediately prior to the K-Pg boundary (Husson et al., 2014). While we remain skeptical of this interpretation, our data from ODP 761 are consistent with it.

3.5-2 Post-Impact interpretations

At the K-Pg boundary horizon at ODP site 738C there is an offset between the highest Os concentration and the lowest ^{187}Os/^{188}Os ratio. We interpret this to mean that there are two phases of impact associated Os, one water soluble phase and another insoluble phase. Physical mixing model of impact derived and ambient materials require that samples with the highest Os concentration have the lowest

^{187}Os/^{188}Os ratios. However, as seen here and at 1262B, this need not be the case. If there was a soluble component, this would likely be more diagenetically mobile which would lower the measured ^{187}Os/^{188}Os ratio of samples but not necessarily to the local minimum. Conversely, if there is a phase of impact derived Os bound in insoluble phases that make up the majority of the sediment at an impact horizon, then this would record local minimum ^{187}Os/^{188}Os ratios but not necessarily have the highest concentration.

 The extended period of unradiogenic ^{187}Os/^{188}Os ratios for sediments at ODP site 738C could be caused by an elevated proportion of ET Os due to a slow accumulation rate or Os with low ^{187}Os/^{188}Os bound in mineral phases. It is important to investigate whether the ^{187}Os/^{188}Os composition recorded in sediments at ODP site 738C reflects the composition of the overlying seawater or if it is an artifact of the sediments themselves. In the following sections, we will address the ^{187}Os/^{188}Os ratio of the overlying seawater, the geographical extent of the unradiogenic ^{187}Os/^{188}Os compostions, as well as discuss possible causes for persistent unradiogenic ^{187}Os/^{188}Os values.

3.5-2a Extraterrestrial Os

At ODP site 738C, ^{187}Os/^{188}Os ratios remain lower than expected for at least the first ~3.4 myr of the Paleogene. A recently proposed model suggests that ^{187}Os/^{188}Os values should recover on a timescale of ~200 kyr (Ravizza and VonderHaar, 2012). One possible explanation could be upward reworking of impact derived Os. However, two-component mixing between ambient ocean and impact related Os is only valid for samples between 375.97 mbsf and 377.22 mbsf (Figure 3.12), a length scale consistent with the extent of the Ir anomaly. A second explanation is the slow sedimentation rate (~0.2 cm/kyr, Huber and Quillévéré, 2005) found at this site. In pelagic sites with low accumulation rates and low Os concentrations, the background flux of cosmic dust can shift the bulk sediment ^{187}Os/^{188}Os ratio lower than the seawater ^{187}Os/^{188}Os ratio (Esser and Turekian, 1988). It is important to consider ET Os when

reconstructing paleo-seawater ^{187}Os/^{188}Os profiles. If sediment accumulation rate is known, the contribution of ET Os to the bulk sediment can be estimated by employing estimated burial rates of ET Os (Equation 1).

$$^{188}Os_{ET} = \text{(Os burial flux)} * \text{(sediment density)}^{-1} * \text{(sedimentation rate)}^{-1} \qquad \text{(Equation 1)}$$

This calculation used a ^{188}Os$_{ET}$ burial flux of 0.186 pg ^{188}Os cm^{-2} kyr^{-1} (Ravizza, 2007), a bulk sediment density of 1 g cm^{-3}, and sedimentation rates were calculated on a per sample basis from the biostratigraphically determined ages and associated sample depths (Figure 3.8). Differences from this correction and ^{3}He corrected ratios are a reflection of the difference between sedimentation rates used for each method. The leaching method we used varied from the typical method employed for He analyses. It is possible that some of the ^{3}He data was released during our procedure and future work should redo He analyses to make sure the He corrected ^{187}Os/^{188}Os ratios are accurate.

Results from the above calculations preclude the notion that the lowered ^{187}Os/^{188}Os ratios of the earliest-Paleogene are due solely to increased ET Os influence (Figure 3.8). The corrected samples remained below the expected value of 0.4. However, using average sedimentation rates as we have done in equation 3 likely yields an over estimate of ET Os inventories because intervals of slow sedimentation or hiatuses are less likely to be sampled than interval of the core that accumulated at above average rates. Based on this, we dismiss significant ET Os contribution to these sediments.

3.5-2b Mineral Detritus

Mantle Os bound in mineral phases associated with igneous activities, such as chromites, could lower the bulk ^{187}Os/^{188}Os composition. Typically these grains have elevated Os concentrations (on the order of 1-100~~3~~ ng/g) with a mantle/chondritic composition (^{187}Os/^{188}Os ≈ 0.127) (Lambert et al. 1994; Walker

et al. 1996, Walker et al. 2002). The large difference in concentration between typical carbonates and mantle chromite grains would require only a small concentration of chromite to lower the bulk $^{187}Os/^{188}Os$ ratio. The gentle leach procedure performed for this study was not harsh enough to dissolve chromite grains. The results from the leach procedure indicate that mantle Os is not responsible for sustained low $^{187}Os/^{188}Os$ ratios as all samples were, again, distinctly lower than the expected minimum of 0.4 but were also systematically higher than the $^{187}Os/^{188}Os$ ratio of the bulk sediments. The two samples in which the leach produced slightly lower $^{187}Os/^{188}Os$ than the corresponding bulk sediment data suggest that the leaching method is not simply consistently dissolving a fraction of the unradiogenic detrital Os in the sediment . If all samples had yielded slightly higher $^{187}Os/^{188}Os$ ratios, it would have been more likely that the leach was not gentle enough and dissolved a constant portion of mineral detritus. Additionally, the $^{187}Os/^{188}Os$ results from the leaches show a smoother profile than the Carius tube digestions. Detrital matter can cause $^{187}Os/^{188}Os$ profiles to appear more noisy. The smoother leach $^{187}Os/^{188}Os$ ratio profile indicates that the leaches captured the $^{187}Os/^{188}Os$ composition of seawater more accurately than Carius tube digestions. Given that ^3He data indicate the ET contributions are unimportant to the Os budget of ODP 738C samples, and that leach data eliminate detrital influence, we conclude that the persistently low $^{187}Os/^{188}Os$ ratios reflect the Os isotopic composition of overlying seawater.

3.5-3 Spatial Extent of sustained low $^{187}Os/^{188}Os$ ratios

To determine if the low $^{187}Os/^{188}Os$ ratios at ODP site 738C extend northward into the Indian Ocean, we compare to other lower latitude sites with in the Indian Ocean during the same time. The available samples provide evidence that the paleo-east Indian Ocean (Figure 3.2) fully recovers from the Os impact signature to pre-impact values and beyond. This is unexpected as it is the highest recorded $^{187}Os/^{188}Os$ ratio recorded over this time interval. One cause could be due to its close proximity to the

actively rifting Australian continent. Neodymium isotopes suggest that the sediments at nearby site 762 record an increase in weathering of Gondwana during this time (Houedec et al., 2012). If this land mass had experienced an increase in weathering as suggested, this would contribute significantly more radiogenic Os to the proximal ocean raising the ^{187}Os/^{188}Os ratio beyond open water sites.

Further evidence that ODP site 738C does not reflect the entire southern Indian Ocean during this time comes from DSDP site 245. Though data are sparse here (only three samples), they show that this part of the ocean recovers to 0.40-0.41 after the impact event (Ravizza and Peucker-Ehrenbrink, 2003). The ages for these samples range from 64.6 Ma to 63.9 Ma. Reported ^{187}Os/^{188}Os composition data for DSDP 245 and ODP 761C constrain the spatial extent of the anomalously low ^{187}Os/^{188}Os values to exclude the western and eastern limits of the Indian Ocean.

3.5-4 Possible sources of unradiogenic Os

Accounting for sources of unradiogenic Os to the modern ocean is not a trivial exercise and still requires much work. There is a disparity between the calculated amount of unradiogenic Os required to balance the riverine input and the measured contributions of unradiogenic Os from ET and submarine mantle sources (e.g. Sharma et al., 2007). However, analyses of Os in hydrothermal fluids yield low concentrations alluding to no obvious source of unradiogenic Os to balance the modern marine Os budget. Counter to the modern ocean, sediment records show that there is an unradiogenic source from LIP eruption events.

The Southern-Indian Ocean hosted extensive magmatism during the late-Cretaceous/early-Paleogene. LIP eruption dominated the total volume produced, the largest being the Deccan traps but also the Kerguelen Plateau. Data from DSDP 245, which was proximal to the Deccan Traps, and ODP 761C do not support Deccan as being a main source of unradiogenic Os to ODP site 738C as the post-impact, Os recovery at these sites mimics the global ocean. Volcanism from the Kerguelen plume can be traced

from ~110 Ma to as late as ~35 Ma, much of which was sub-aerial (Frey et al., 2000). Hydrothermal

alteration, chemical weathering of Kerguelen Plateau lavas, as well as sub-aerial volcanism, could be

considered as likely candidates for an unradiogenic Os source. However, if any or all of these possibilities

were the missing source, we would expect that low $^{187}Os/^{188}Os$ ratios would be apparent throughout the

entire ODP site 738C record. Our study shows that at ~67.3 Ma the seawater $^{187}Os/^{188}Os$ ratio at the

southern Kerguelen Plateau was identical to other sites around the world. Our results do not show

Kerguelen as a pre-impact unradiogenic source and as such, there is no reason to believe it would have

such a profound effect on the post-impact seawater $^{187}Os/^{188}Os$ composition unless there was a

previously unidentified eruption pulse on the Kerguelen Plateau in the earliest Paleogene. There is an

important caveat to this argument. It makes the implicit assumption that our knowledge of the eruptive

history of Kerguelen is complete enough to preclude a pulse of activity immediately after the K-Pg

impact event. Several studies have speculated that impact events may stimulate plume volcanism

(Boslough et al., 1996; Meschede et al., 2011). While our results do not contribute directly to

addressing this question, proponents of this view could construe our results from ODP Site 738 as

permissive evidence that Kerguelen plume volcanism was stimulated by the Chicxulub impact event.

LIP eruption events were not the sole source of magmatism in the Southern/Indian Ocean during the

late Cretaceous and early Paleogene. The Ssoutheast Indian ridge (SEIR) was starting to ramp up to its

maximum spreading rate and Australia was continuing its slow drift from Antarctica. However, modern

day metalliferous sediments near the super-fast spreading south East Pacific Rise have $^{187}Os/^{188}Os$

compositions similar to that of seawater (Oxburgh, 1998).   The most likely source of mantle Os would

be weathering of peridotite hosted hydrothermal systems (Cave et al., 2003, Sharma et al., 2007) more

likely present at ridges with slow spreading rates (Liu et al., 2008). The rifting of Australia from

Antarctica, which is proximal to site ODP site 738C, was characterized as a slow magmatic process

(Mutter et al., 1985). Calculations predict that Os lost from peridotites during weathering could nearly

equal that of riverine input to the ocean (Snow and Reisberg, 1995). In a study of five fresh peridotites with a small, weathered outer layer, the change in Os concentration between the weathered and fresh portions was small (Liu et al., 2008). Three samples experienced Os losses of 0.08, 0.13, and 1.16 ng/g from fresh to weathered portions while two samples experienced Os gain. $^{187}Os/^{188}Os$ values remained nearly constant across all samples. Although this study seems to suggest that Os loss during weathering of mantle rocks is small, it is hard to constrain the total surface area of peridotites experiencing weathering annually. It is possible that the amount of readily available peridotite, as possibly exposed from slow rifting Australia, increased during the earliest Paleogene. Until further research is conducted to investigate this, we cannot exclude slow spreading ridges as a source of mantle Os to the Indian sector of the Southern Ocean in the earliest Paleogene. Alternative to direct weathering, mantle Os has been discovered in condensates from magmatic volatiles (Yudovskaya et al., 2008). This could also be a source of unradiogenic Os to the southern Indian Ocean.

3.5-5 Sediment redistribution

An alternative possibility does not require an additional source of unradiogenic Os, but rather that the persistent low $^{187}Os/^{188}Os$ ratios at ODP site 738C are the result of sediment reworking. MacLeod and Huber (1996) report findings of inoceramid remains with distinctly older Sr isotope ratios in sediments millions of years after their expected extinction date. A 15 cm thick laminated interval that encompasses the K-Pg boundary at ODP site 738C precludes the possibility of bioturbation as a reworking mechanism and requires deposition of winnowed sediment. Emplacement of impact related material to ODP site 738C from proximal locations would create the illusion of low $^{187}Os/^{188}Os$ ratios further up the sediment record than expected. If this is the source of the additional unradiogenic Os, the system becomes multi-component versus binary rendering it unnecessary for reworked samples to follow a two-component mixing model (Figure 3.12). The presence of the inoceramid fossils make it impossible to dismiss

sediment reworking. We suggest that one of the main causes of the persistently low ^{187}Os/^{188}Os ratios at

ODP site 738C lateral redistribution of sediments that reflect an older seawater ^{187}Os/^{188}Os composition.

By assuming that the bulk measured ^{187}Os/^{188}Os ratio is a mixture of sediment recording the expected

ambient ^{187}Os/^{188}Os ratio of 0.4 and impact related sediment with a ^{187}Os/^{188}Os composition of ~0.17, it

is possible to calculate the fraction of reworked impact sediment required to obtained the measured

values. Samples near the top of the suite analyzed here require ~30-40% of the total sediment is

reworked impact material. This is in good agreement with the 30% predicted for foraminifera by

MacLeod and Huber (1996). As expected, as the K-Pg boundary horizon is approached, the fraction of

impact related material required increases. Redistribution of impact related sediment for ~3.4 myr is not

inconsistent with the timescales of redistribution based on the inoceramids. The gradual rise in

^{187}Os/^{188}Os ratio, coupled with the decreasing fraction of impact related sediment required might reflect

depletion of impact sediment being reworked resulting in the winnowing of sediments that began

recording post-impact recovery. Alternatively, gradual changes in ocean currents moving sediments

could allow the impact-related material to be deposited elsewhere.

3.6 Conclusions

Before the onset of Deccan volcanism, the global ocean was homogeneous with respect to ^{187}Os/^{188}Os

compositions with sites all around the world recording a seawater composition of 0.6. Between the

onset of Deccan volcanism and the K-Pg impact event, the southern Indian ocean may have exhibit a

drop in ^{187}Os/^{188}Os ratio before the rest of the global ocean possibly due to a second eruption of the

Deccan Traps just prior to the K-Pg impact event. Post-impact the sediments in the southern Indian

Ocean suggest an extended period of relatively unradiogenic ^{187}Os/^{188}Os composition for at least the

first ~3.4 myr of the Paleogene. Once biases due to elevated fraction ET Os and detrital matter with a

low ^{187}Os/^{188}Os ratio were eliminated, the persistently low ^{187}Os/^{188}Os ratios in the southern Indian

Ocean required additional explanation. Due to poor understanding of the mechanism(s) by which unradiogenic Os is introduced to the global ocean, we cannot rule out the possibility that the extended period of low $^{187}Os/^{188}Os$ ratios at ODP site 738C are due to local inputs of unradiogenic Os. However, based on the presence of inoceramid remains from a previous study, we favor the interpretation that these sediments reflect lateral redistribution of impact related material.

Future Work

Further investigations of the anomalously low $^{187}Os/^{188}Os$ ratios should include obtaining tighter constraints on the regional distribution. One possible location would be ODP site 750 as it encompasses a complete K-Pg section. This site would be ideal as it is also located on the Kerguelen Plateau. ODP site 752 offers an expanded K-Pg section but lies within volcanic ash. Gentle leaching of these samples might allow for the acquisition of the overlying seawater compositions as well.

Better constraints on the global ocean Os mass balance, specifically the sources of mantle Os, are needed to more accurately pinpoint sources to the Southern-Indian Ocean. This would require a better understanding of how and when mantle rocks are weathered annually, as well as the total surface area available for weathering. Specifically future work should focus on constraining how weathering of peridotites can supply unradiogenic Os to the ocean.

Other work on elements that are tracers for mantle related processes should also be considered. It has been shown that Mg is released during peridotite weathering in an amounts that could be similar to its annual riverine influx (Snow and Dick, 1995). As such, Mg could potentially be a tracer of weathered peridotite at ODP 738C. Additionally, metals and metalloids such as Se, Hg, Cd, As, Cu, and Bi are released during degassing at mid-ocean ridges (Rubin, 1997 and references therein). These elements have a sufficient residence time that would allow them to possibly act as a tracer for enhanced ridge activity. If the large amount of volcanic/magmatic activity present in the Indian Ocean is the source of

the additional unradiogenic Os at ODP 738C, then perhaps metal/metalloid concentrations would also

be increased in these waters.

Barron, J., Larson, B., et al., 1989, *Proc. ODP, Init. Repts.,* 119: College Station, TX (Ocean Drilling Program)

Cave, R.R., Ravizza, G.E., German, C.R., Thomson, J., Nesbitt, R.W. 2003. Deposition of osmium and other platinum-group elements beneath the ultramafic-hosted Rainbow hydrothermal plume. Earth and Planetary Science Letters, 210: 65-79.

Coffin, M. F., Pringle, M.S., Duncan, R.A., Gladczenko T.P., Storey, M., Mueller R.D., Gahagan, L.A. 2002. Kerguelen Hotspot Magma Output since 130 Ma. Journal of Petrology, 43: 1121-1139.

Cohen, A., Coe, A., 2002. New geochemical evidence for the onset of volcanism in the Central Atlantic magmatic province and environmental change at the Triassic-Jurrassic boundary. Geology, 30: 267-270.

Cohen, A. and Coe, A. 2007. The impact of the Central Atlantic Magmatic Province on climate and on the Sr- and Os-isotope evolution of seawater. Palaeogeography, Palaeoclimate, Palaeoecology, 244: 374-390.

Dalai, T.K., Suzuki, K., Minagawa, M., Nozaki, Y., 2005. Variations in seawater osmium isotope composition since the last glacial maximum: A case study from the Japan Sea. Chemical Geology, 220: 303-314.

Donaldson, S., Hildebrand, A.R. 2001. The global fluence of Ir at the Cretaceous-Tertiary Boundary. Meteoritics and Planetary Science, 36: A50.

Du Vivier, A.D.C., Selby, D., Sageman, B.B., Jarvis, I., Gröcke, Voigt, S. 2014. Marine ^{187}Os/^{188}Os isotope stratigraphy reveals the interaction of volcanism and ocean circulation during Ocean Anoxic Event 2. Earth and Planetary Science Letters, 389: 23-33.

Esser, B.K., Turekian, K.K. 1988. Accretion rate of extraterrestrial particles determined from osmium isoopte systematics of pacific pelagic clay and manganese nodules. Geochimica et Cosmochimica Acta, 52: 1383-1388.

Exon, N.F., Haq, B.U., von Rad, U., 1992. Exmouth Plateau Revisited: Scientific Drilling and Geological Framework. Proceedings of the Ocean Drilling Program, Scientific Results, 122: 3-20.

Frei, R., Frei, K.M. 2002. A multi-isotopic and trace element investigation of the Cretaceous-Tertiary boundary layer at Stevns Klint, Denmark – inferences for the origin and nature of siderophile and lithophile element geochemical anomalies. Earth and Planetary Science Letters, 203: 691-708.

Frey, F., Coffin, M., Wallace, P., Weis, D., 2003. Leg 183 synthesis Kerguelen Plateau-Broken Ridge-a large igneous province. Proceedings of the Ocean Drilling Program, Scientific Results, 183: 1-48.

Frey, F.A., Coffin, M.F., Wallace, P.J., Weis, D., Zhao, X., Wise Jr., S.W., Wähnert, V., Teagle, D.A.H., Saccocia, P.J., Reusch, D.N., Pringle, M.S., Nicolaysen, K.E., Neal, C.R., Müller, R.D., Moore, C.L., Mahoney, J.J., Kesztheylyi, L., Inokuchi, H., Duncan, R.A., Delius, H., Damuth, J.E., Damasceno, D., Coxall, H.K., Borre, M.K., Boehm, F., Barling, J., Arndt, N.T., Antretter, M. 2000. Origin and evolution of a

submarine large igneous province: the Kerguelen Plataeau and Broken Ridge, southern Indian Ocean. Earth and Planetary Science Letters, 176: 73-89.

Galbrun, B. 1992. Magnetostratigraphy of Upper Cretaceous and Lower Tertiary Sediments, Sites 761 and 762, Exmouth Plateau, Northwest Australia. *In* von Rad, U. Haq, B.U., et al., *Proc ODP, Sci Results*, 122: College Station, TX (Ocean Drilling Program), 699 – 716.

Gradstein, F.M., Ogg, J.G., Schmitz, M.D., Ogg, G.M. 2012. *The Geologic Time Scale Volume 2.* Elsevier BV, Kidlington, Oxford, United Kingdom.

Gramlich, J., Murphy, T., Garner, E., Shields, W. 1973. Absolute isotopic abundance ratio and atomic weight of a reference sample of rhenium. Journal of Research National Bureau of Standards, 77A: 691-698.

Horan, M., Walker, R., Morgan, J., Grossman, J., Rubin, A., 2003. Highly siderophile elements in chondrites. Chemical Geology, 196(1-4): 27-42.

Hoeudec, S.L., Meynadier, L., Cogné, J.P., Allégre, C.J., Gourlan, A.T. 2012. Oceanwide imprint of large techtonic and oceanic events on seawater Nd isotope composition in the Indian Ocean from 90 to 40 Ma. Geochemistry Geophysics Geosystems, 13: Q06008. doi:10.1029/2011GC003963

Huber, B. 1991. Maestrichtian planktonic foraminifer biostratigraphy and the Cretaceous/Tertiary boundary at hole 738C (Kerguelen Plateau, Southern Indian Ocean). *In* Barron, J., Larsen, B. et al., *Proc. ODP, Sci Results*, 119: College Station, TX (Ocean Drilling Program), 771-794.

Huber, B., Quillévéré, F., 2005. Revised Paleogene planktonic foraminiferal biozonation for the Austral realm. Journal of Foraminiferal Research, 35: 299-314.

Keller, G., Adatte, T., Gardin, S., Bartolini, A., Bajpai, S., 2008. Main Deccan volcanism phase ends near the K-T boundary: Evidence from the Krishna-Godavari Basin, SE India. Earth and Planetary Science Letters, 268: 293-311.

Koeberl, C., and Shirey, S. 1997. Re-Os isotope systematics as a diagnostic tool for the study of impact craters and distal ejecta. Palaeogeography, Palaeoclimatology, Palaeoecology, 132: 25-46.

Kuroda, J., Hori, R.S., Suzuki, K., Gröcke, D.R., Ohkouchi, N. 2010. Marine osmium isotope record across the Triassic-Jurassic boundary from a Pacific pelagic site. Geology, 38: 1095-1098.

Lambert, D. et al., 1994. Re-Os and Sm-Nd Isotope Geochemistry of the Stillwater Complex, Montana: Implications for the Petrogenesis of the J-M Reef. Journal of Petrology, 35: 1717-1753.

Levasseur, S. Birck, J.L., Allégre C.J. 1999. The osmium riverine flux and the oceanic mass balance of osmium. Earth and Planetary Science Letters, 174: 7-23.

Liu, C.Z., Snow, J.E., Hellebrand, E., Brügmann, G., von der Handt, A., Büchl, A., Hoffman, A., W., 2008. Ancient, highly heterogeneous mantle beneath Gakkel ridge, Arctic Ocean. Nature, 452: 311 – 316.

MacLeod, K.G., Huber, B.T. 1996. Strontium isotopic evidence for extensive reworking in sediments spanning the Cretaceous-Tertiary boundary at ODP site 738. Geology, 24: 463-466.

Müller, C., 1974. Calcareous Nannoplankton, Leg 25 (Western Indian Ocean). Initial Reports Deep Sea Drilling Project, 25: 579-633.

Mutter, J.C., Hegarty, K.A., Cande, S.C., Weissel, J.K. 1985. Breakup between Australia and Antarctica: A brief review in the light of new data. Tectonophysics, 114: 255-279.

Oxburgh, R. 2001. Residence time of osmium in the oceans. Geochemistry, Geophysics, Geosystems, 2. 2000GC00010.

Paquay, F.S., Ravizza, G., 2012. Heterogeneous seawater ^{187}Os/^{188}Os during the late Pleistocene glaciations. Earth and Planetary Science Letters, 349-350: 126-138.

Peucker-Ehrenbrink, B. and Ravizza G. 2000. The marine osmium isotope record. Terre Nova, 12: 205-219.

Peucker-Ehrenbrink, B., Ravizza, G., Hofmann, A., 1995. The marine 187Os/188Os record of the past 80 million years. Earth and Planetary Science Letters, 130(1-4): 155-167.

Pospichal, J., Bralower, T., 1992. Calcareous Nannofossils Across the Cretaceous/Tertiary Boundary, Site 761, Northwest Australian Margin. *In* von Rad, U., Haq, B.U. et al., *Proc, ODP, Sci. Results*, 122: 735-751.

Ravizza, G. 2007. Reconstructing the marine ^{187}Os/^{188}Os record and particulate flux of meteoritic osmium during the late Cretaceous. Geochimica Cosmochimica Acta, 71: 1355-1369.

Ravizza, G., and Peucker-Ehrenbrink B. 2003. Chemostratigraphic Evidence of Deccan Volcanism from the Marine Osmium Isotope Record. Science, 302: 1392-1395.

Ravizza, G. and VonderHaar, D. 2012. A geochemical clock in earliest Paleogene pelagic carbonates based on the impact-induced Os isotope excursion at the Cretaceous-Paleogene boundary. Paleoceanography, 27: PA3219. doi:10.1029/2012PA002301

Reusch, D., Ravizza G., Maasch, K.A., Wright, J.D. 1998. Miocene seawater ^{187}Os/^{188}Os ratios inferred from metalliferous carbonates. Earth and Planetary Science Letters, 160: 163-178.

Robinson, N. Ravizza, G., Coccioni, R., Peucker-Ehrenbrink, B., Norris, R. 2009. A high-resolution marine ^{187}Os/^{188}Os record for the late Maastrichtian: Distinguishing the chemical fingerprints of Deccan volcanism and the KP impact event. Earth and Planetary Science Letters, 281: 159-168.

Rocchia, R., Boclet, D., Bonté, P., Froget, L.,Galbrun, B., Jéhanno, C., and Robin, E. 1992. Iridium and Other Element Distributions, Mineralogy, and Magnetostratigraphy Near the Cretaceous/Tertiary Boundary in Hole 761C. *In* von Rad, U. Haq, B.U. et al. *Proc. ODP, Sci. Results*, 122: 753-762.

Rubin, K. 1997. Degassing ofmetals and metalloids from erupting seamount and mid-ocean ridge volcanoes: Observations and predictions. Geochimica Cosmochimica Acta, 61: 3525-3542.

Sato, H., Onoue, T., Nozaki, T., Suzuki, K., 2013. Osmium isotope evidence for a large Late Triassic impact event. Nature Communications, 4, 2455. doi:10.1038/ncomms3455

Schmitz, B., Asaro, F., Michel H.V., Thierstein H.R., Huber B.T. 1991 Element stratigraphy across the Cretaceous/Tertiary boundary in Hole 738C. *In* Barron J., Larsen B., et al., 1989. *Proc. ODP Init. Repts.*, 119: College Station TX (Ocean Drilling Program)

Sharma, M., Rosenberg, E.J., Butterfield, D.A. 2007. Search for the proverbial mantle osmium sources to the oceans: Hydrothermal alteration of mid-ocean ridge basalt. Geochimica Cosmochimica Acta, 71: 4655-4667.

Shipboard Scientific Party, 1989, Site 738. *In* Barron J., Larsen B., et al., 1989. *Proc. ODP Init. Repts.*, 119: College Station TX (Ocean Drilling Program)

Shipboard Scientific Party, 1990. Site 761. *In* Haq, B.U., von Rad, U., O'Connel S., et al., *Proc. ODP, Init. Repts.,* 122: College Station, TX (Ocean Drilling Program)

Snow, J.E., Reisberg, L. 1995. Erratum of "Os isotopic systematics of the MORB mantle: results from altered abyssal peridotites". Earth and Planetary Science Letters, 136: 723-733.

Snow, J.E., Dick, J.B., 1995. Pervasive magnesium loss by marine weathering of peridotite. Geochimica Cosmochimica Acta, 59, 4219-4235.

Tejada, M. et al., 2009. Ontong Java Plateau eruption as a trigger for the early Aptian oceanic anoxic event. Geology, 37: 855-858.

Turgeon, S., Creaser, R., 2008. Cretaceous oceanic anoxic event 2 triggered by a massive magmatic episode. Nature, 454: 323-326.

Walker, R., Hanski, E., Vuollo, J., Liipo, J., 1996. The Os isotopic composition of Proterozoic upper mantle: evidence of chondritic upper mantle from the Outokumpu ophiolite, Finland. Earth and Planetary Science Letters, 141: 161-173.

Walker, R., Prichard, H., Ishiwatari, A., Pimentel, M., 2002. The osmium isotopic composition of convecting upper mantle deduced from ophiolite chromites. Geochimica et Cosmochimica Acta, 66(2): 329-345.

Wei, W., Pospichal, J., 1991. Danian calcareous nannofossil succession at site 738 in the southern Indian Ocean. *In* Barron, J. Larsen, B. et al., Proc. ODP, Sci. Results, 119: College Station, TX (Ocean Drilling Program), 495-512.

Williams, G., Turekian, K., 2004. The glacial–interglacial variation of seawater osmium isotopes as recorded in Santa Barbara Basin. Earth and Planetary Science Letters, 228: 379-389.

Yudovskaya, M., Tessalina, S., Distler, V., Chaplygin, I., Chugaev, A. Dikov, Y. 2008. Behavior of highly-siderophile elements during magma degassing: A case study at the Kudryavy volcano. Chemical Geology, 248: 318-341.

Chapter 4. Conclusions and future work

The large differences in the isotopic composition and concentration of Os in most extraterrestrial materials compared to typical UCC rocks make the Re-Os isotopic system ideal to study impact events. These events create unique isotopic excursions across sediment horizons that are distinguishable from LIP or other volcanic events.

Results from the Bowring Pit study indicate that the impactor could be up to two times larger based on ^{187}Os/^{188}Os estimations. This study also requires that future work reexamine the basic assumption that the K-Pg impact fallout is both homogeneous and chondritic with respect to ^{187}Os/^{188}Os composition. Additionally, results from this study indicate that much of the Os delivered to the Bowring Pit site was in a water-soluble form, evident from significant remobilization down section, as well as bound in insoluble particulates. This could possibly explain the phenomenon seen at some marine sites where the maximum Os concentration does not align with the lowest ^{187}Os/^{188}Os ratio.

There are two possible explanations for the persistently low ^{187}Os/^{188}Os ratios at ODP 738C: first, sediment reworking and re-deposition of impact related material, and second, seawater is locally heterogeneous. If option one is correct it implies that sediment redistribution could have a large effect on measured ^{187}Os/^{188}Os ratios and should be considered when reconstructing past ^{187}Os/^{188}Os records. Based on the Indian Ocean study, pelagic sediments appears to record the ^{187}Os/^{188}Os composition of the overlying seawater of when they were originally deposited and do not acquire a new ^{187}Os/^{188}Os composition when redeposited. However, the results of this study do not preclude the possibility that the southern Indian Ocean experienced a local input of unradiogenic Os, as suggested by option number two. One potential cause of heterogeneity could be via a previously unrecognized eruption of the Deccan Traps. Because this cannot dismissed, this study also has potential implications on the

69

heterogeneity of global seawater with respect to Os. If the pre-impact ^{187}Os/^{188}Os ratio at 738C was found to be lower than the rest of the global ocean at the same time, this means that the Deccan Traps were supplying unradiogenic Os to the global oceans in an amount so large that thermohaline circulation could not efficiently mix the unradiogenic signature. This could have potential implications on the constraints of total ocean mixing time in the latest-Cretaceous.

Future work

Future work should strive to continue collecting full Os isotopic and concentration profiles across terrestrial K-Pg sites to further quantify the amount of impact-related Os that is bound in soluble and insoluble phases. This is imperative for making impactor size estimations from Os isotopes. The Os in the ejecta plume is a mixture of target rock and extraterrestrial Os. In order to more accurately estimate the size of the impacting bolide, future work should strive to estimate the fraction of the Os in the ejecta plume that is associated with target rock. Furthermore, this work assumes that the ejecta plume is homogeneous with respect to Os. To justify this assumption, future work should include terrestrial Os profiles at sites that are also distal to the Chicxulub impact crater.

More work should be done on ODP 738C, core 21 and at other sites in the Indian sector of the Southern Ocean, both pre- and post-impact. Denser sampling of pre-impact 738, and older 761 sediments would help determine if the southern Indian Ocean experienced an initial decline in ^{187}Os/^{188}Os composition due to Deccan volcanism before the rest of the world. Additional studies should be performed to constrain the spatial extent of persistently low, post-impact ^{187}Os/^{188}Os ratios. Other drill sites on the Kerguelen Plateau offer a good opportunity to study the K-Pg boundary but some lie within ash layers. Future work on these sites should be meticulous to separate the seawater signature from the signature of the volcanic activity associated with the ash layers.

Further analyses should be done that employ different tracers to determine if the persistently low $^{187}Os/^{188}Os$ ratios are due to mantle processes or reworked impact material. Due to the concentrated amount of volcanic and magmatic processes in the Indian Ocean, other elements such as Mg, Se, Hg, Cd, As, Cu, and Bi that are released during active volcanism and weathering of peridotite could act as potential tracers of these processes at ODP site 738C. If it is a mantle process introducing unradiogenic Os, analyses should investigate whether the process influencing the $^{187}Os/^{188}Os$ of the sediment is related to spreading ridges or hot spot volcanism. Generally, better constraints on the processes by which unradiogenic Os is supplied to global seawater are required to better understand the Os mass balance.
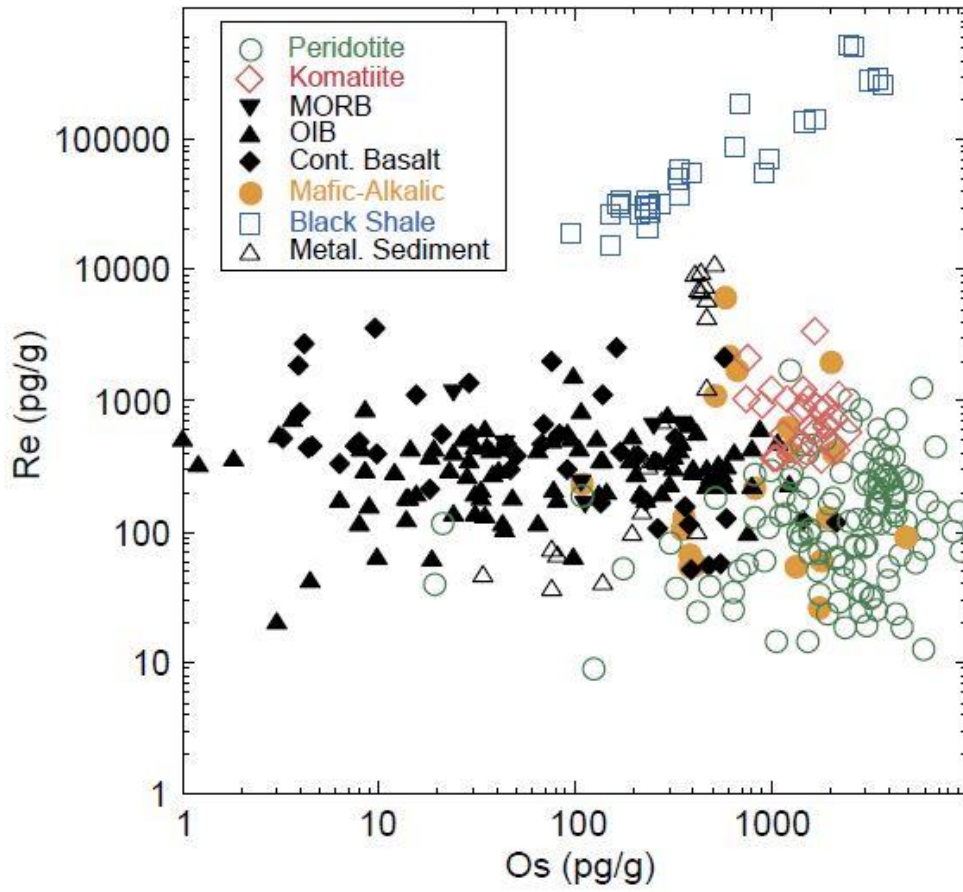
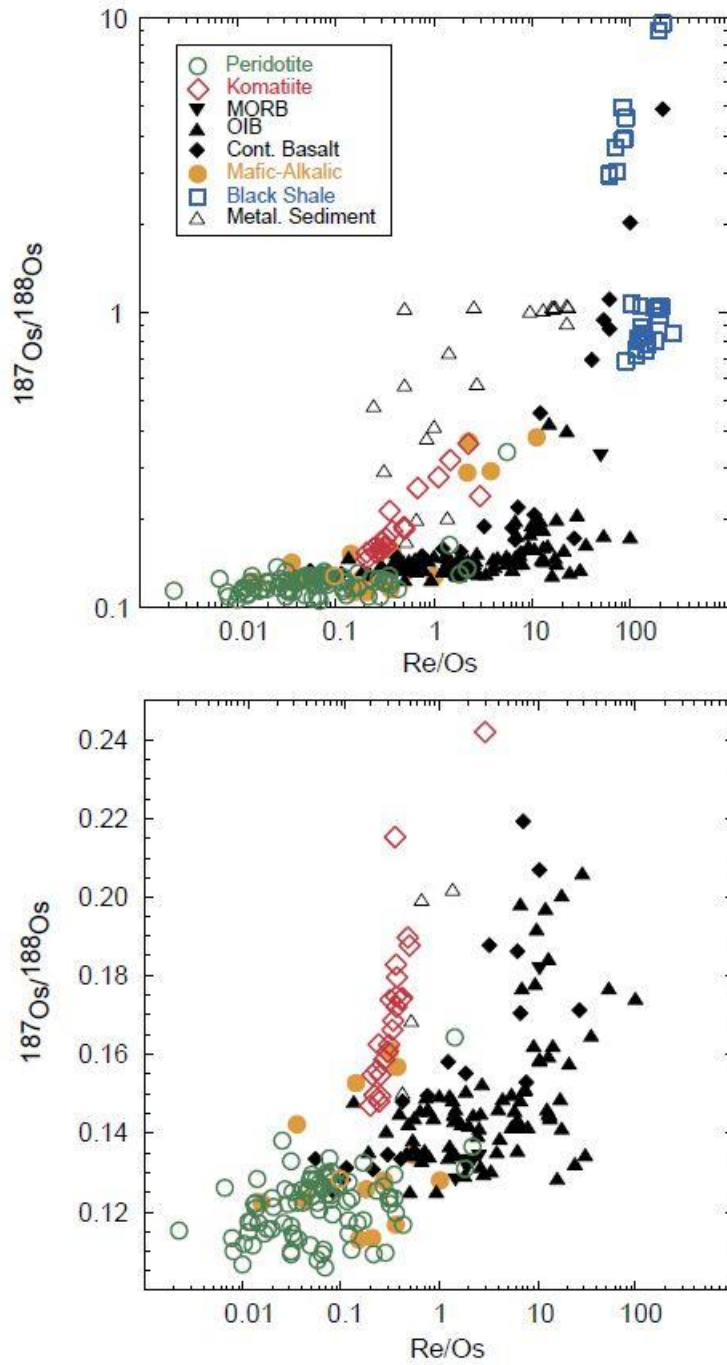**Figure 1.1** Rhenium and Os concentrations for various rock types. Taken from Carlson (2005).

Figure 1.2 ^{187}Os/^{188}Os ratios versus Re/Os for various rock types. These plots show the large range in Os isotopic composition between mantle and UCC type rocks. Additionally, these data points reflect the unpredicted near chondritic composition of the mantle. Taken from Carlson (2005).
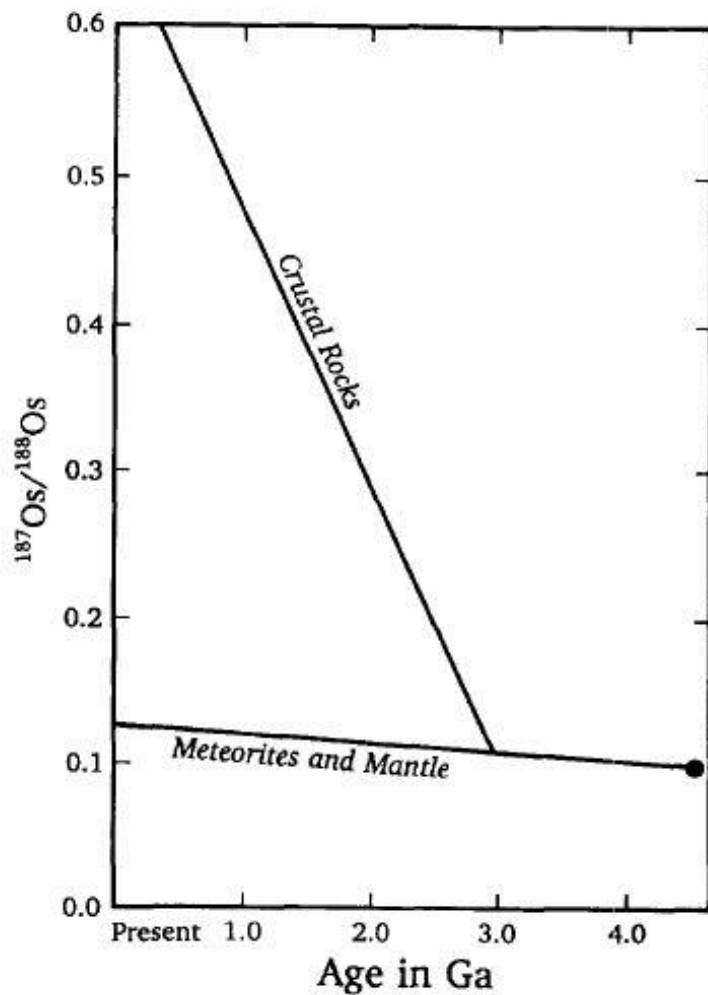
Figure 1.3. A schematic of the evolution of $^{187}Os/^{188}Os$ through time comparing the differences between crustal rocks and meteorites/mantle. Taken from Keoberl and Shirey (1997). This figure demonstrates the large difference between the $^{187}Os/^{188}Os$ compositions over time, mainly as a result of the differences in compatibility of Re and Os. Rhenium is moderately incompatible element whereas Os is a highly compatible element that would have stayed behind in the melt residue as the earth's crust was forming. Subsequent *in situ* decay of ^{187}Re to ^{187}Os causes the $^{187}Os/^{188}Os$ of the upper continental crust to be significantly more radiogenic than the mantle with time.
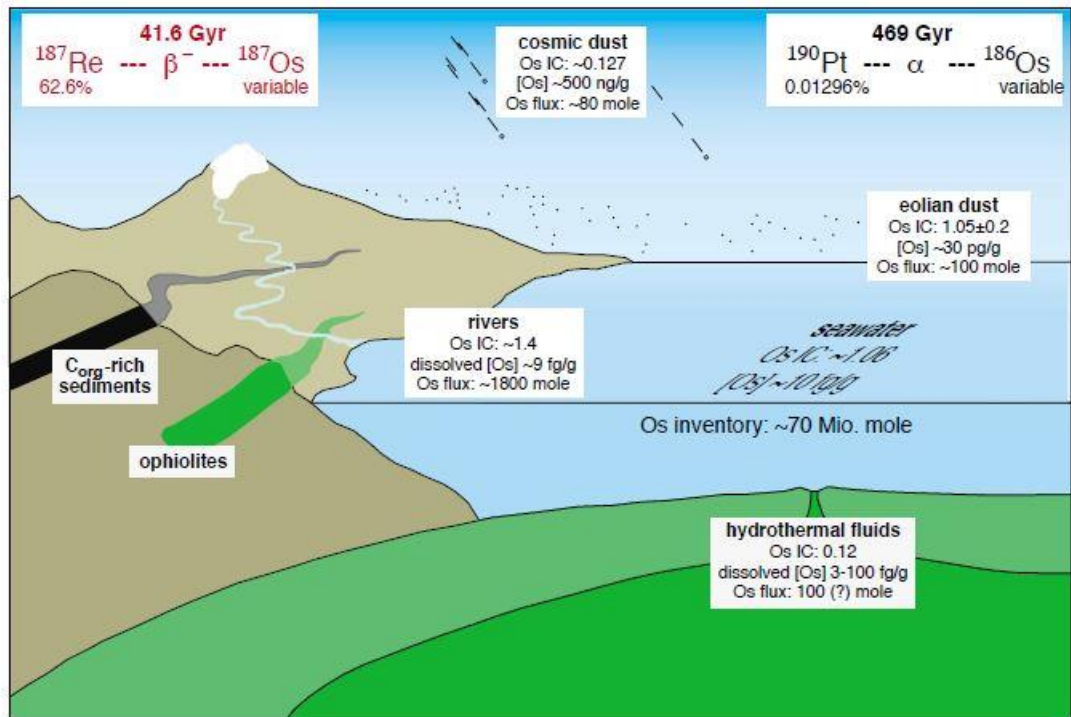
Figure 1.4. A schematic of the sources of Os to the global ocean as well as the decay scheme of the two modern radiogenic isotopes of Os. Rivers are the dominant source of Os to the ocean and typically exhibit very radiogenic $^{187}Os/^{188}Os$ compositions due to silicate weathering. The sources of unradiogenic Os to the oceans remains ill-constrained. However mass balance calculations assert that hydrothermal fluids/mantle processes are the dominant source of unradiogenic Os to the oceans. Figure taken from Peucker-Ehrenbrink and Ravizza (2000).
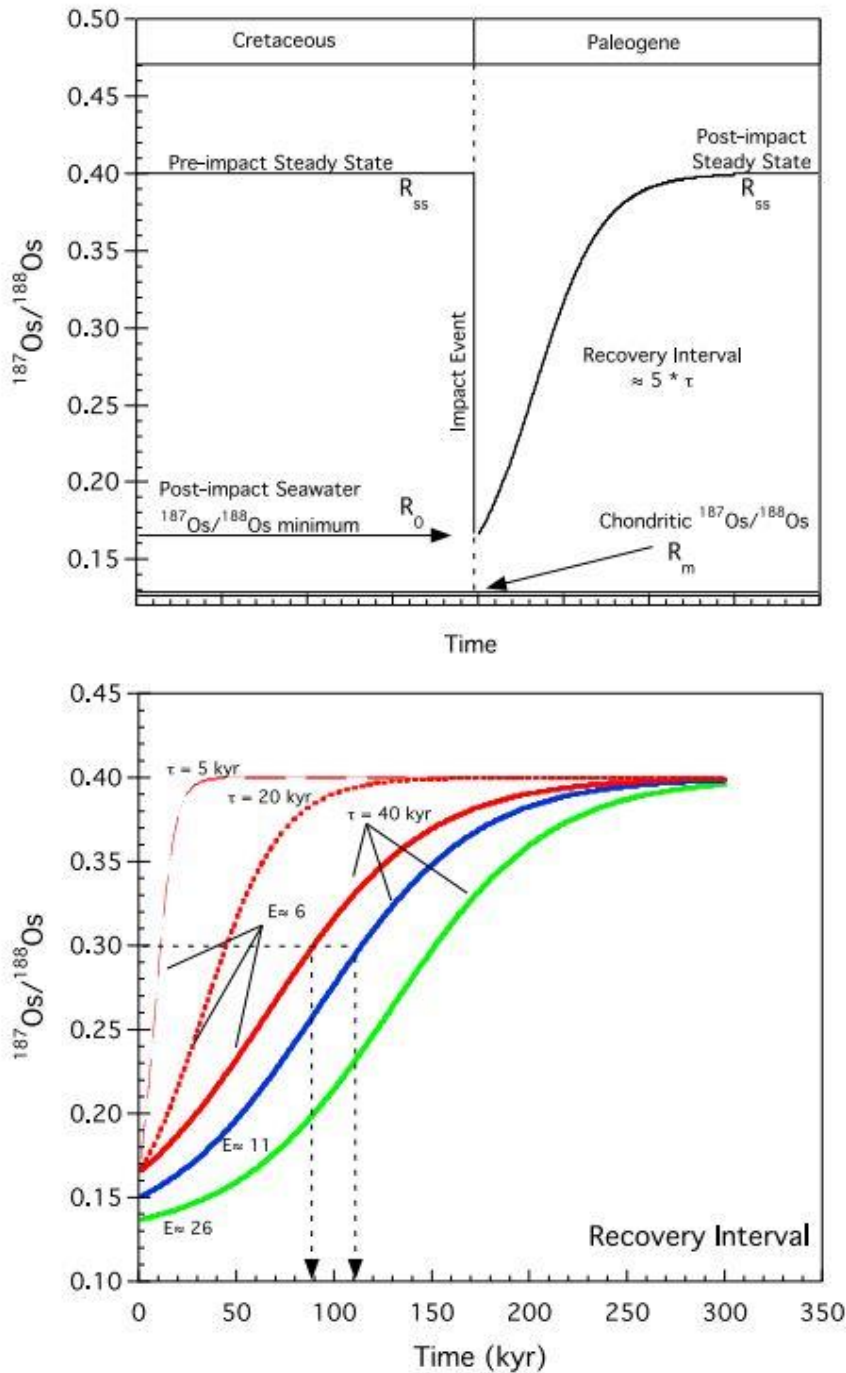
Figure 1.5. Idealized seawater ^{187}Os/^{188}Os response to the K-Pg impact event (top) and the effects of residence time (τ) and enrichment (E) of Os in the post-impact seawater relative to the pre-impact seawater on the post-impact recovery of ^{187}Os/^{188}Os values to pre-impact, steady state values (bottom). An enrichment factors between 6-11 are common for the K-Pg impact event. The recovery profiles at sites that this model has been tested on are consistent with a 40 kyr residence time of Os in the global ocean. This figure is taken from Ravizza and VonderHaar (2012).
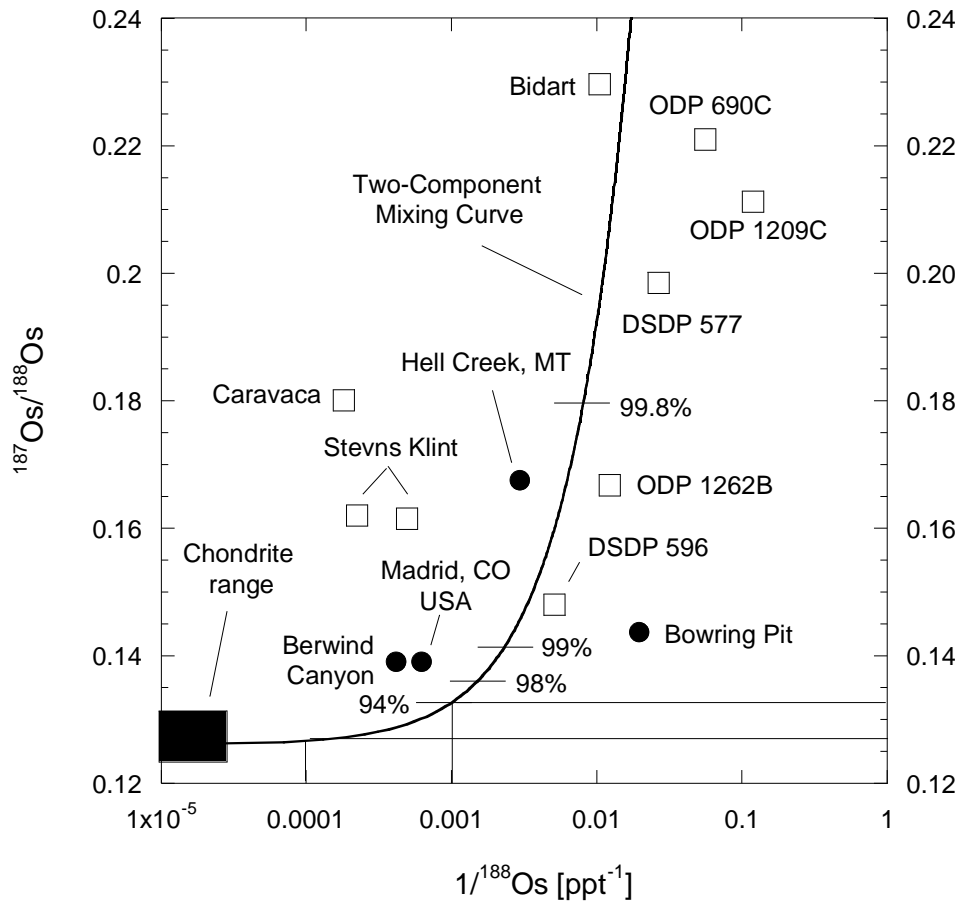
Figure 1.6. Two-component mixing curve between average upper continental crust and chondrites is shown with age corrected $^{187}Os/^{188}Os$ ratios for K-Pg boundary samples falling in between the two end members. Note that the age corrected $^{187}Os/^{188}Os$ ratios of the K-Pg boundary samples with the highest Os concentrations plot above the trend predicted by the physical mixing model. Percentages along the mixing line refer to the percent by mass of continental crust within the mixture. The thinner black lines show that for nearly an order of magnitude difference in Os concentration, the mixing model predicts that the isotopic composition should exhibit minimal change and should remain close to chondritic. The boxed area represents the field in which chondrites fall, marine K-Pg samples are represented by the squares and terrestrial K-Pg sites are circles. For site references, see Table 2 in Chapter 4
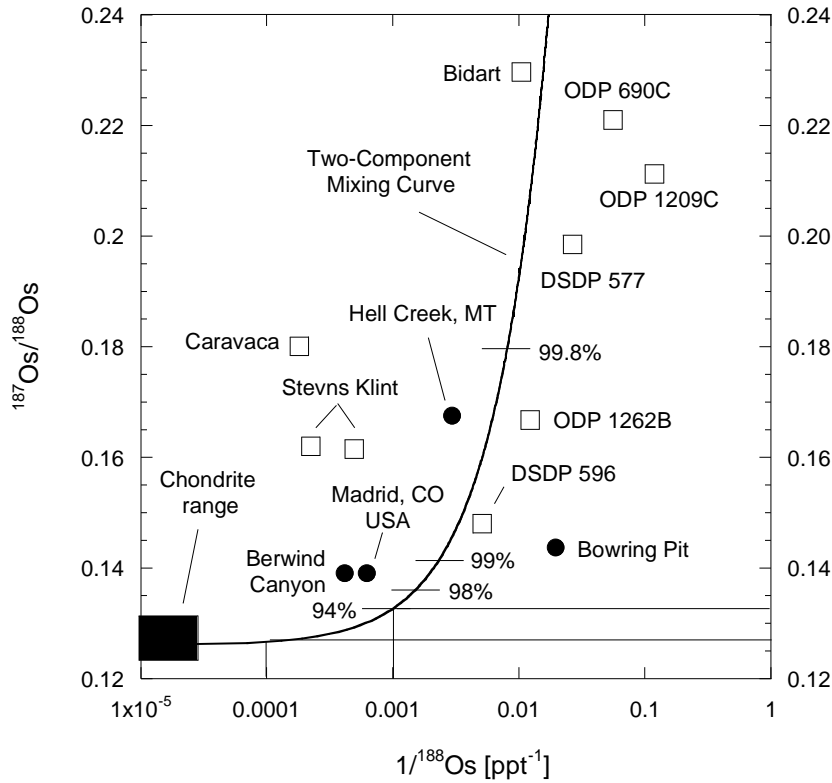
Figure 2.1. Two-component mixing curve between average upper continental crust and chondrites is shown with age corrected $^{187}Os/^{188}Os$ ratios for K-Pg boundary samples falling in between the two end members. Note that the age corrected $^{187}Os/^{188}Os$ ratios of the K-Pg boundary samples with the highest Os concentrations plot above the trend predicted by the physical mixing model. Percentages along the mixing line refer to the percent by mass of continental crust within the mixture. The thinner black lines show that for nearly an order of magnitude difference in Os concentration, the mixing model predicts that the isotopic composition should exhibit minimal change and should remain close to chondritic. The boxed area represents the field in which chondrites fall, marine K-Pg samples are represented by the squares and terrestrial K-Pg sites are circles. For site references, see Table 2.

Figure 2.2 (Left) Photo of the Bowring Pit outcrop exposing the West Bijou K-Pg section taken Summer 2012 with 10 cm scale bars for reference. (Right) Adapted from Barclay and Johnson (2004) to show the lithostratigraphic and fernspore (Nichols and Fleming, 2002), and shocked quartz distribution as it correlates to the Bowring Pit outcrop.
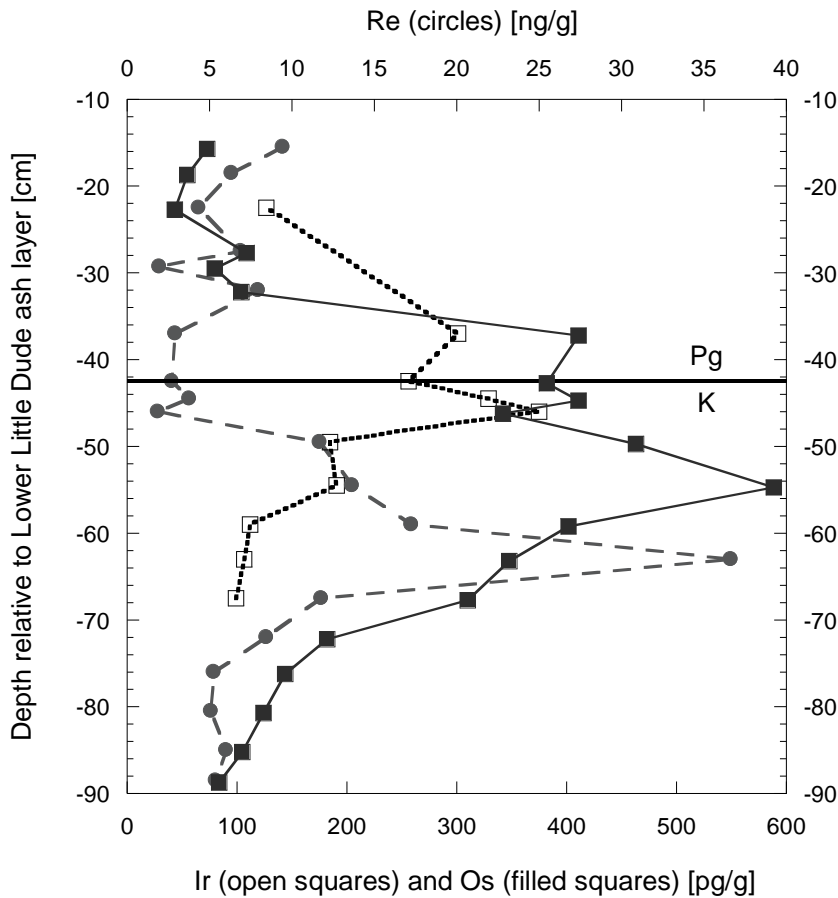
Figure 2.3. Osmium, Re, and Ir concentration profiles. Ir data is from Sauvage (2010) in which the remobilization of Ir down section of the K-Pg boundary is noted. Osmium shows a similar remobilization but peaks further down section than Ir. The differing depths of Os and Ir concentration peaks support diagenesis rather than bioturbation as the proxy through which remobilization occurred. Note the separate y-axis for Re.
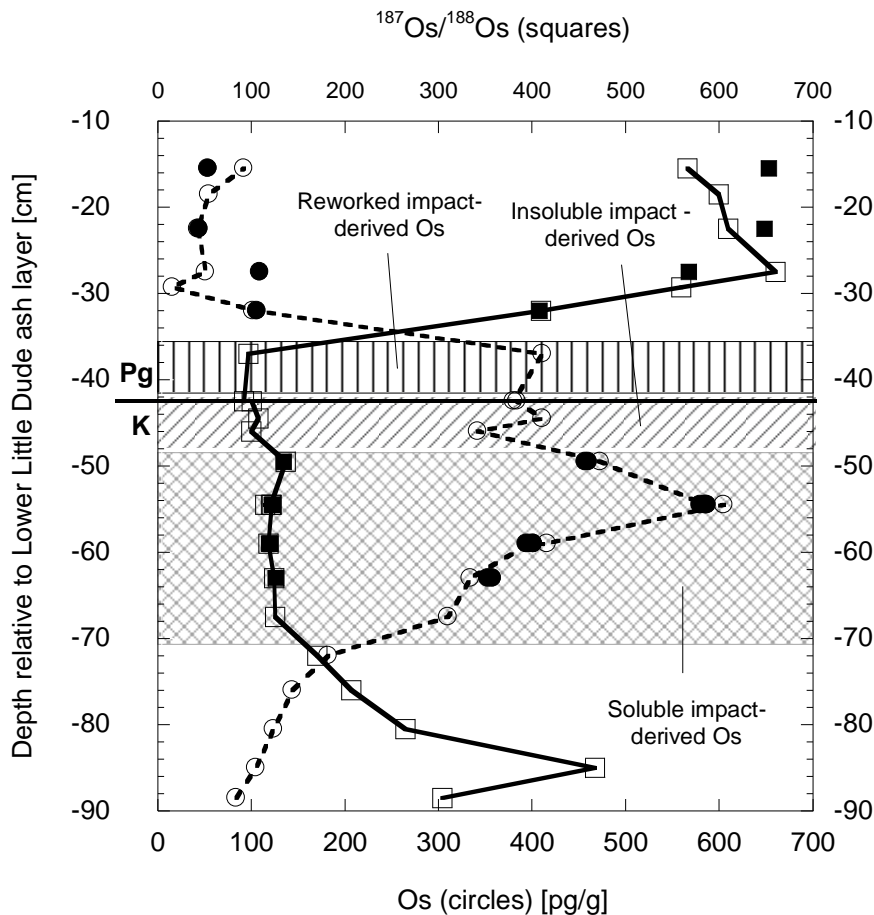
Figure 2.4. The K-Pg boundary Os excursion at the Bowring Pit. Fusion data is plotted as filled in points in the shape that corresponds to the data type; circles represent concentration data and squares show [187]Os/[188]Os ratios. This plot emphasizes the large concentration anomaly relative to background sediments towards the shallower portion of the section as well as the drastic drop in measured [187]Os/[188]Os ratios associated with extraterrestrial input. Here, the maximum concentration occurs approximately 12 cm below the boundary and is part of a broad interval of elevated Os concentrations (~ 10x average crustal values) that begins immediately above the boundary and continues through the depth of the samples. Downward remobilization of impact-derived Os indicates that there is a soluble form of chondritic Os from the ejecta plume fallout that is mobile in the reducing sediments of the Bowring Pit. As expected, the minimum [187]Os/[188]Os ratio occurs directly at the boundary (-42.5 cm) and is part of a region that shows minimal mobility of impact derived Os.
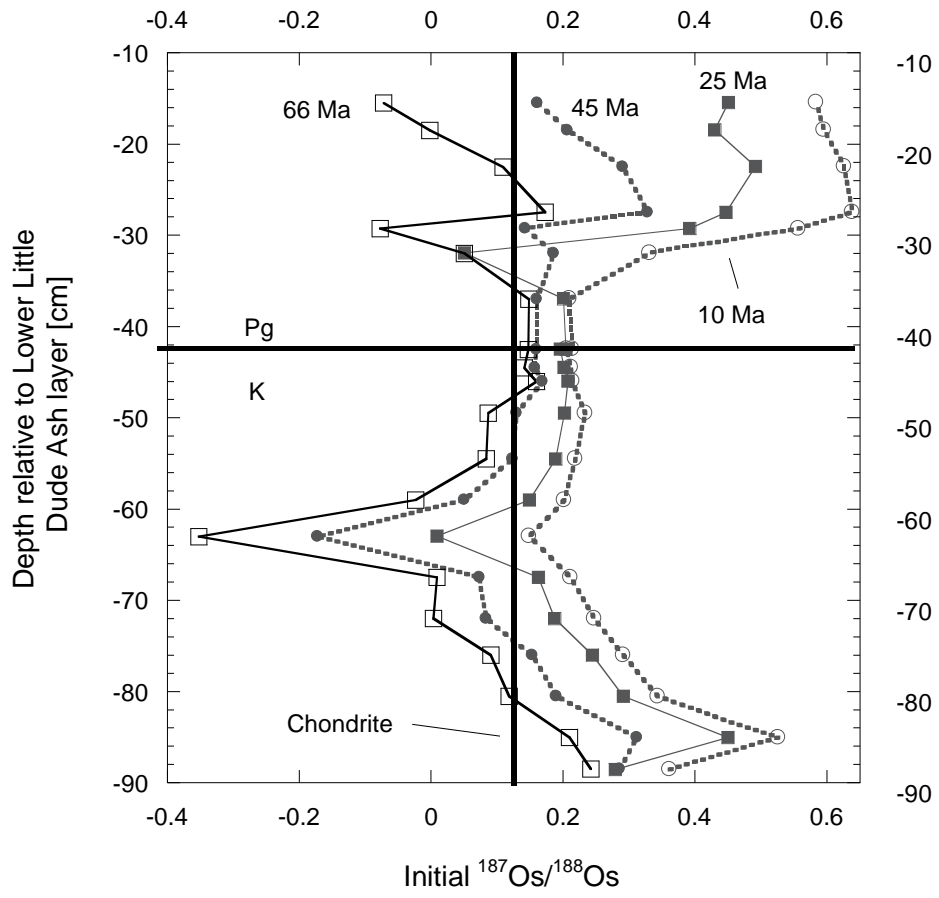
Figure 2.5. Age corrections for successively younger ages until all samples reach a plausible initial $^{187}Os/^{188}Os$ value. At 10 Ma, all samples are above the chondritic line indicating either Re addition or Os loss within the last 10 Ma.
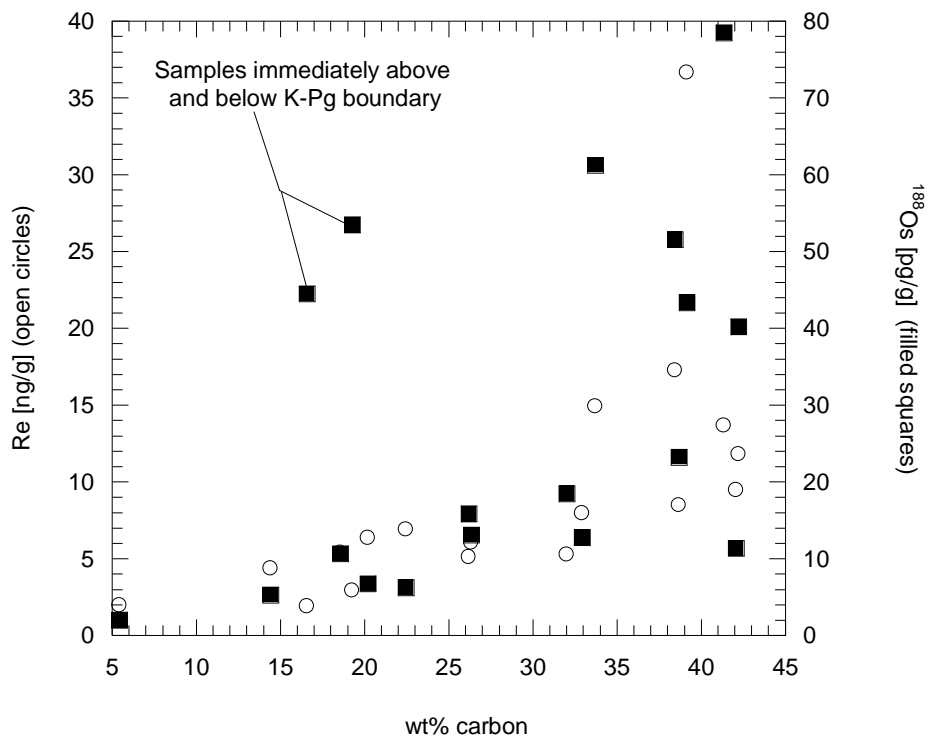
Figure 2.6. Osmium and Re concentrations as they vary with wt% carbon. The concentrations are positively correlated with wt% carbon with the exception of the two samples immediately surrounding the K-Pg boundary. These samples have higher Os concentrations than other samples with similar wt% carbon. This is consistent with impact derived Os.

Table 2.1. Depth, measured and initial ^{187}Os /^{188}Os (with 2σ uncertainties) and ^{187}Re/^{188}Os and Os/Ir values, Os, Re, and Ir concentrations across the Bowring Pit K-Pg boundary section.

| Sample	Depth[1]	Analysis Method[2]	^{187}Os/^{188}Os[3]	Os [pg/g]	Re [ng/g][4]	^{187}Re/^{188}Os	Initial ^{187}Os/^{188}Os[3]	Ir [pg/g][6]	Os/Ir	Wt% C
BP 20	-17 : -14	CT	0.6218 (45)	92	9.16 (0.11)	509	0.0623 (085)			42.07
		F	0.7024 (25)	54						
BP 19	-20 : -17	CT	0.6524 (06)	55	6.75 (0.13)	629	-0.0397 (141)			20.20
BP 18	-25 : -20	CT	0.6620 (74)	43	4.28 (0.31)	511	0.0996 (419)	127	0.339	14.43
		F	0.6984 (29)	44						
BP 17	-30 : -25	CT	0.7091 (98)	51	7.18 (0.12)	727	-0.0898 (161)			22.48
		F	0.6233 (24)	109						
BP 16	-30 : -28.5	CT	0.6156 (104)	16	1.97 (0.08)	627	-0.0741 (307)			5.45
BP 15	-34 : -30	CT	0.4750 (44)	102	21.77 (0.41)	1071	-0.7024 (228)			32.94
		F	0.4763 (13)	106						
BP 14	-40 : -34	CT	0.1862 (08)	411	2.92 (0.54)	34	0.1484 (011)	301	1.365	19.29
BP 13*	-45 : -40	CT	0.1819 (31)	387	2.79 (0.08)	35	0.1436 (033)	256	1.512	
		CT [r,sa]	0.1901 (18)	384		35	0.1515 (021)			
BP 12	-45 : -44	CT	0.1906 (24)	411	3.78 (0.10)	45	0.1417 (027)	330	1.245	
BP 11	-47 : -45	CT	0.1890 (09)	342	1.88 (0.03)	27	0.1597 (010)	375	0.912	16.60
BP 10	-52 : -47	CT	0.2232 (16)	473	11.72 (0.14)	120	0.0909 (023)	185	2.557	33.71
		F	0.2214 (07)	457						
		F [r]	0.2218 (03)	460						
BP 9	-57: -52	CT	0.2093 (24)	605				191	3.168	41.35
		CT [r,sa]	0.2027 (26)	586						
		CT [r]	0.2082 (13)	585	13.73 (0.20)	114	0.0830 (022)			
		F	0.2094 (06)	580						
		F [r]	0.2103 (10)	587						
BP 8	-61 : -57	CT	0.2062 (12)	397				112	3.545	38.47
		CT [r]	0.2067 (16)	416	17.26 (0.22)	201	-0.0145 (032)			
		F	0.2071 (03)	394						

		F [r,sa]	0.2080 (04)	401						
BP 7	-65 : -61	CT	0.2115 (08)	334	36.65 (1.12)	532	-0.3740 (178)	107	3.121	39.14
		F	0.2135 (13)	358						
		F [r,sa]	0.2132 (05)	353						
BP 6	-70 : -65	CT	0.2126 (17)	310	11.79 (0.17)	185	0.0097 (034)	99	3.131	42.23
BP 5	-74 : -70	CT	0.2537 (38)	182	8.46 (0.11)	227	0.0042 (036)			38.10
BP 4	-78 : -74	CT	0.2881 (14)	144	5.26 (0.17)	179	0.0914 (064)			32.02
BP 3	-83 : -78	CT	0.3420 (32)	124	5.09 (0.24)	202	0.1195 (111)			26.22
BP 2	-87 : -83	CT	0.5301 (40)	105	6.02 (0.21)	290	0.2115 (117)			26.35
BP 1	-90 : -80	CT	0.3786 (25)	84	5.39 (0.16)	318	0.0287 (106)			18.56

[1] Sample depths and intervals from bottom : top referenced to the Lower Little Dude ash layer, [2] Indicates the method used for each sample. CT – carius tube digestion; F – Ni-S fire assay through fusion; r – replicate analysis; r,sa – replicate analysis on same sample aliquot as previously listed , [3] Number in parenthesis represent 2σ uncertainty in the last digits, [4] Number in parenthesis represents 2σ uncertainties in pg/g, [5] Ir data from Sauvage (2010), *Indicates K-Pg boundary sample

Table 2.2. Compilation of K-Pg boundary data

	Ir [ng/g]	Re [ng/g]	Os [pg/g]	Os/Ir	Measured ^{187}Os/^{188}Os	Initial ^{187}Os/^{188}Os	Reference
Marine							
Bidart		0.912	737		0.2364	0.2297	Quitte et al. (2007)
Caravaca		4.011	42,355	0.74†	0.1806	0.1801	Quitte et al. (2007)
	56.9	2.7	46,000	0.81			Kyte et al. (1985)
DSDP 596		0.625	1492	0.11†	0.1502	0.1480	Peucker-Ehrenbrink et al. (1995)
	13.6		809	0.06			Lee et al. (2003)
	14						Zhou et al. (1991)
DSDP 577			521	1.93†	0.1570		Ravizza and Peucker-Ehrenbrink (2003)
		0.73	290	1.07†	0.2120	0.1985	Walker in Meisel et al. (1995)
	7.09		439	0.06	0.1570		Paquay et al. (2008)
Mid-Waipara	0.321		1200	3.74	0.2693		Ferrow et al. (2011)
ODP 690C	1.25	0.091	123	0.098	0.2250	0.2210	Ravizza and VonderHaar (2012)
ODP 886C	1.88		2377	1.26	0.3200		Ravizza (2007)
ODP 1209C		0.032	64.6		0.2140	0.2114	Ravizza and VonderHaar (2012)
ODP 1262B		0.487	622		0.1710	0.1668	Ravizza and VonderHaar (2012)
Stevns Klint		8.01	15,523	0.44†	0.1642	0.1615	Quitte et al. (2007)
	35.3	0.372	34,200	0.97	0.1621	0.1620	Frei and Frei (2002)
Sumbar			40,000		0.1369		Meisel et al. (1995)
Woodside Creek	127		60,000	0.47	0.1342*		Lichte et al. (1986)
Terrestrial							
Berwind Canyon, CO		2.05	18,230		0.1395	0.1389	Esser and Turekian (1989)

Bowring Pit, CO		3.95	387	1.51†	0.1819	0.1436	this study
	0.256						Sauvage (2010)
Compressor Creek	0.176		172	0.98	0.2040		Ferrow et al. (2011)
Madrid, CO		2.09	12,160	0.46†	0.1398	0.1389	Esser and Turekian (1989)
	26.4						Schmitz (1992)
Raton, NM			36,691	33.36†	0.1372		Esser and Turekian (1989)
	1.1						Schmitz (1992)
Starkville South, CO			21,220	2.21†	0.1476		Esser and Turekian (1989)
			12,590	1.31†	0.1466		Esser and Turekian (1989)
					0.155*		Luck and Turekian (1983)
	9.6						Schmitz (1992)

†Value was calculated using Ir data from same location but different reference
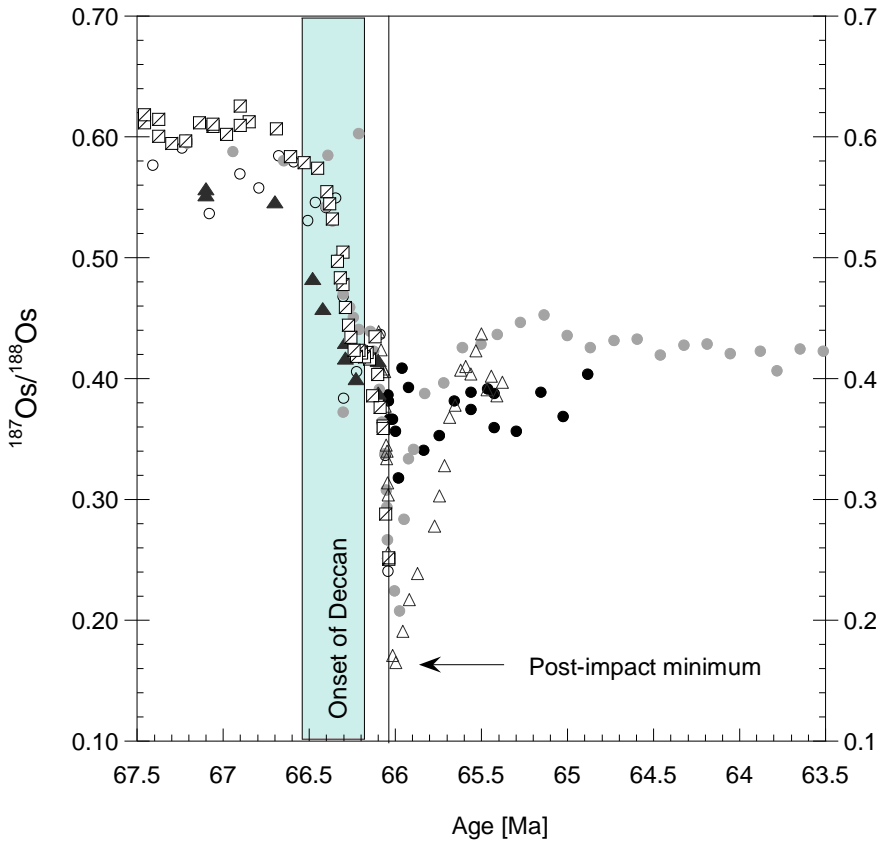*Calculated from reported $^{186}Os/^{188}Os$ ratio by multiplying by 0.120

Figure 3.1. ^{187}Os/^{188}Os recovery profiles from the west Pacific, Southern-Atlantic, and south Atlantic oceans, and the proto-Tethys sea (Robinson et al., 2009; Ravizza and VonderHaar, 2012). These sedimentary records so that for most of the global oceans, there is a pre-Deccan steady state composition of ~0.6 that rapidly declines to ~0.4 after the onset of Deccan volcanism. Coincidently with the K-Pg impact event, the global ocean ^{187}Os/^{188}Os ratio declines as a result of the sudden influx of chondritic Os (^{187}Os/^{188}Os ≈ 0.12, Horan et al., 2003). As Os is removed from the water column, the ^{187}Os/^{188}Os composition returns to the pre-impact steady state value.
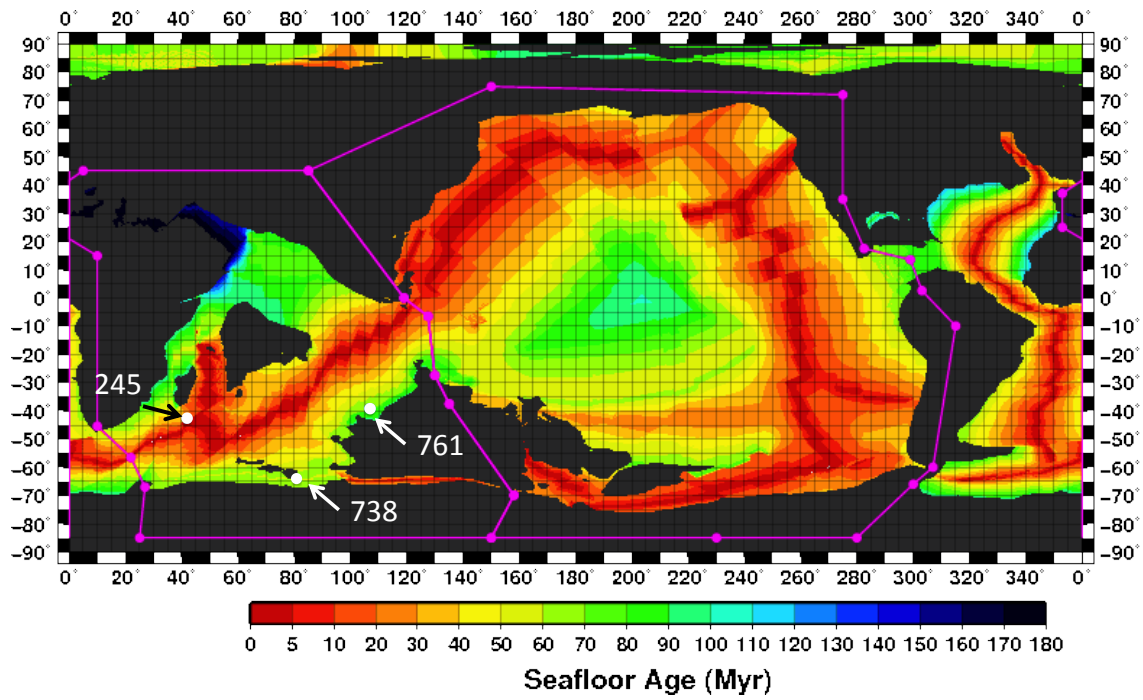
Figure 3.2. Paleoreconstruction of the Southern-Indian Ocean with seafloor ages at 66 Ma. Paleolocations of ODP sites 738, 761, and 245 are shown.
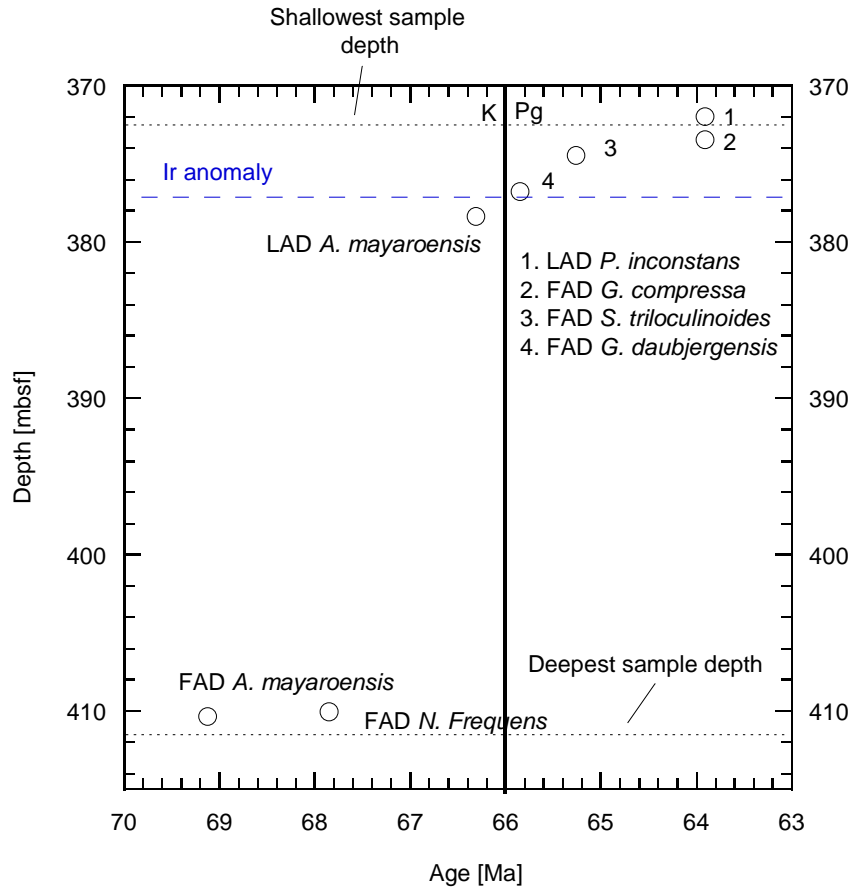
Figure 3.3. Age versus depth for site 738C. Age – depth relationship was established for this site using biostratigraphic depths (Huber, 1991; Huber and Quillévéré, 2005) and the ages from Gradstein et al. (2012). Depths of the Ir anomaly, the shallowest and deepest samples are labeled as well.
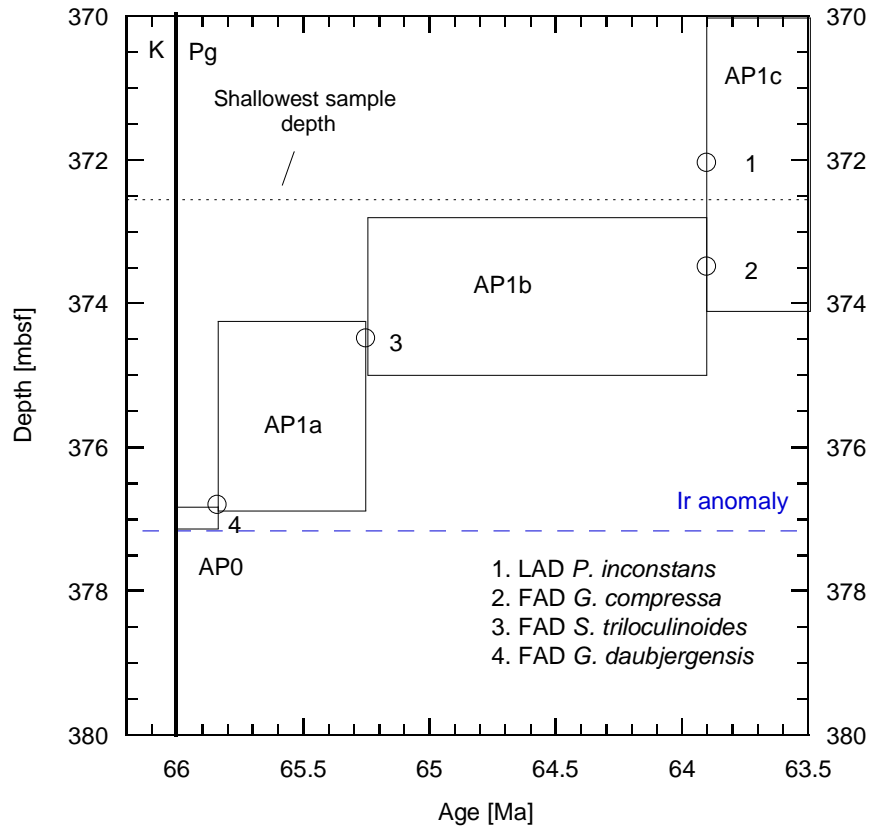
Figure 3.4. Age versus depth for the earliest Paleogene at site 738C. Biozones were established using the revised Antarctic Paleogene scheme as defined by Huber and Quillévéré (2005). Absolute ages are from Gradstein et al. (2012). Overlap in depth between the successional zones represents the uncertainty in specific planktonic foraminifer depth used to define the biozones. Also shown are the depths of the Ir anomaly and the shallowest sample.
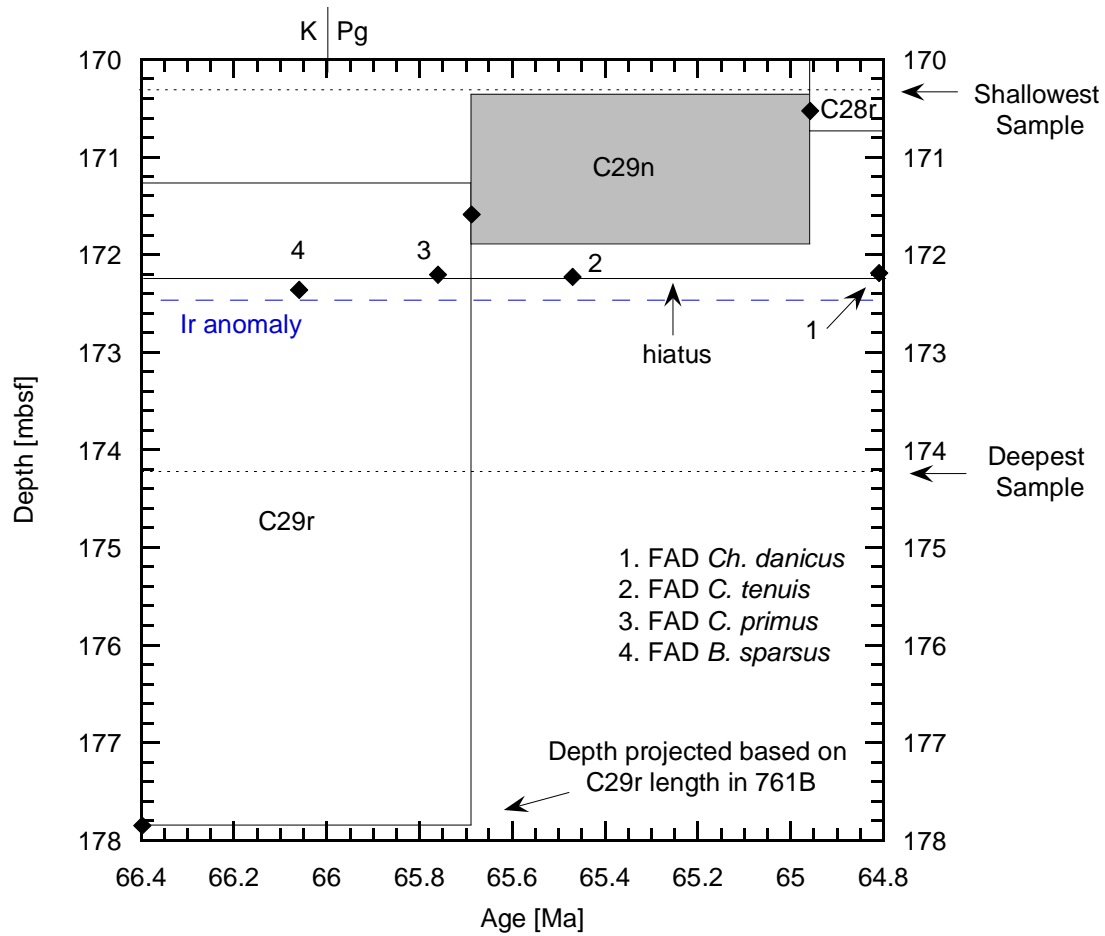
Figure 3.5. Age versus depth for site 761C. Age constraints come from magnetostratigraphy (Rocchia et al., 1992). Earliest Paleogene biostratigraphy at this site is of little use due to a hiatus ~23 cm above the K-Pg boundary as defined by the Ir anomaly.
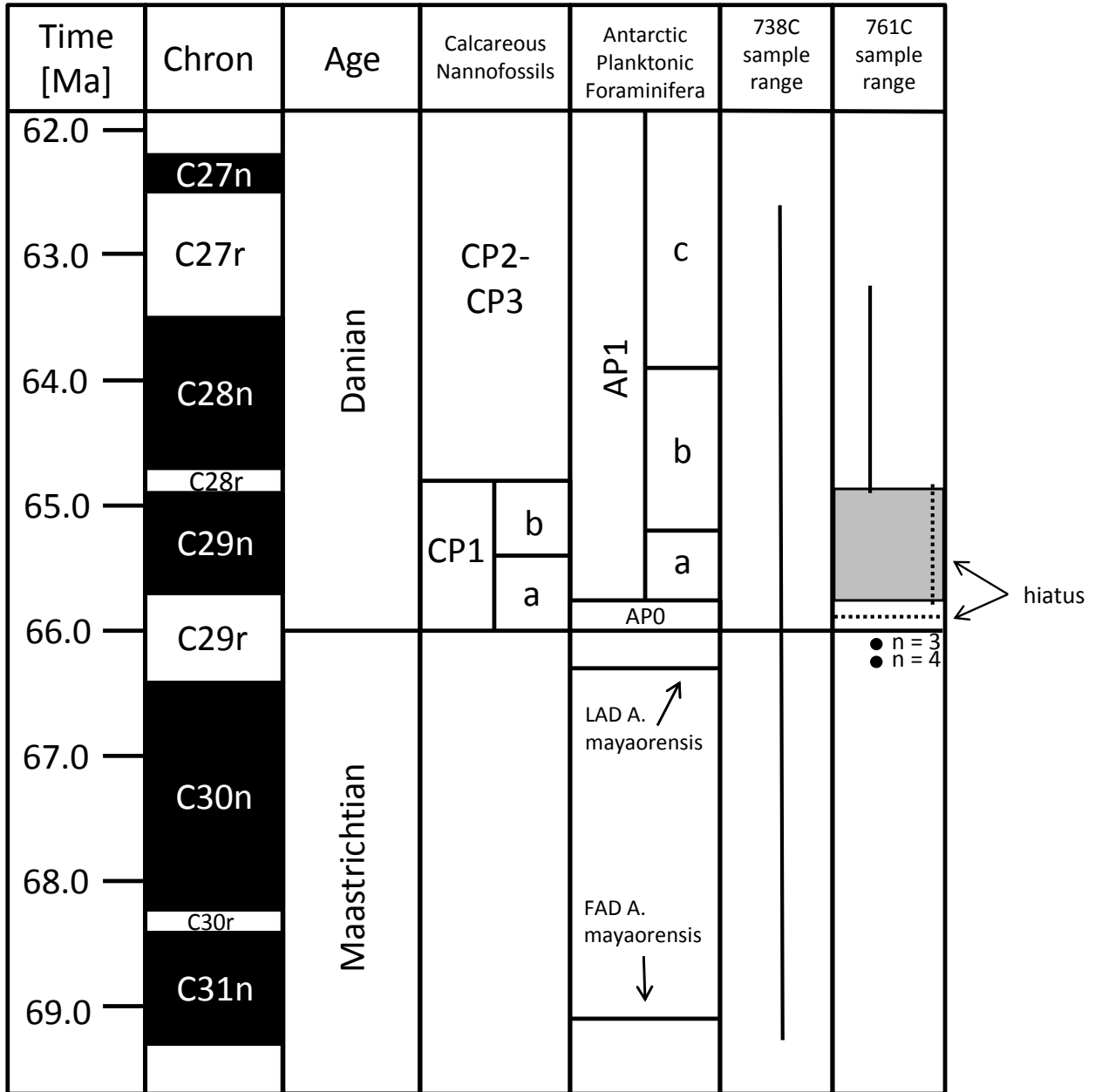
Figure 3.6. Correlation of biozone schemes, magnetochrons, and core recovery across 738C and 761C. Ages for the magnetochrons and calcareous nannofossil zonations come from Gradstein et al. (2012). Antarctic planktonic foraminifera zonations are from Huber and Quillévéré (2005). The black line in the 738C sample range column represents the total depth spanned by our suite of samples. In the 761C sample range column, there are two different sample ranges corresponding to different durations of the hiatus present at site 761C. The solid line corresponds to the hiatus extending from C29n through C28n, represented by the grey box. The dotted line represents the sample ages if the hiatus were to only occur within C29r.
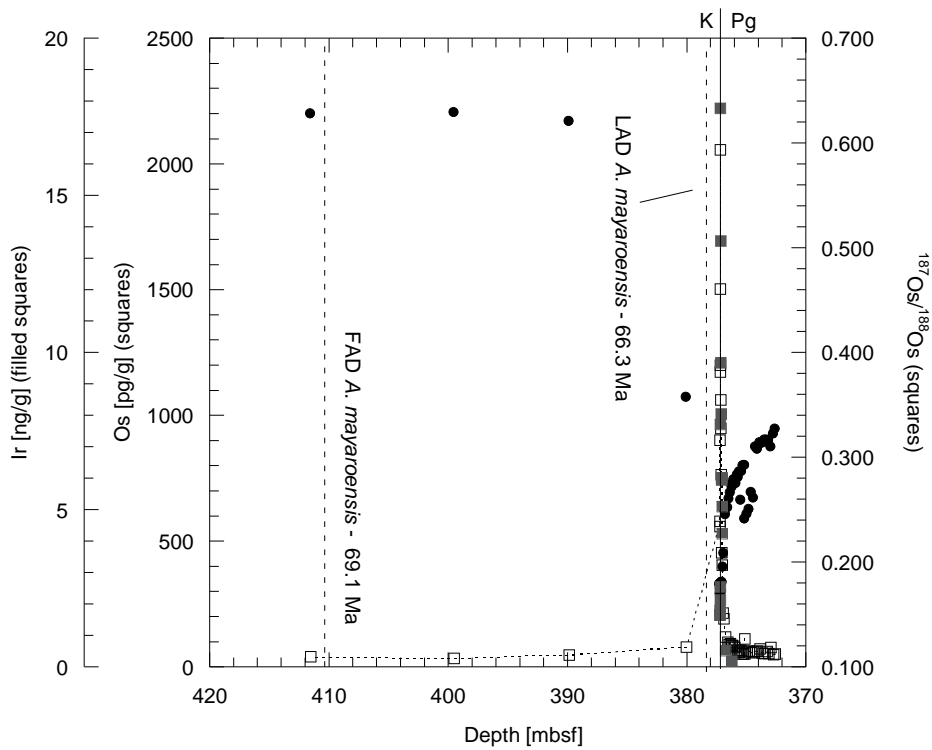
Figure 3.7. ODP site 738C bulk Os IC (diamonds), and Os and Ir anomalies (open and filled squares, respectively) versus depth. Pre-impact Os IC compositions, as well as the impact-induce IC minimum, are similar to values reported for other sites. Age constraints for the upper-most Cretaceous may be biased to older ages by nannofossil redistribution (MacLeod and Huber, 1996). However, the LAD of *A. mayaroensis* has not been subjected to extensive redistribution, the Os IC of the Southern Ocean at site 738C was slightly lower than the rest of the global ocean at this time. However, it is hard to determine the extent to which redistribution may have occurred. Post-impact Os IC recovery at 738C is unexpected in that it does not reach the pre-impact steady state value of ~0.4 as established by other marine sites globally. Ir data comes from Schmitz et al. (1991).
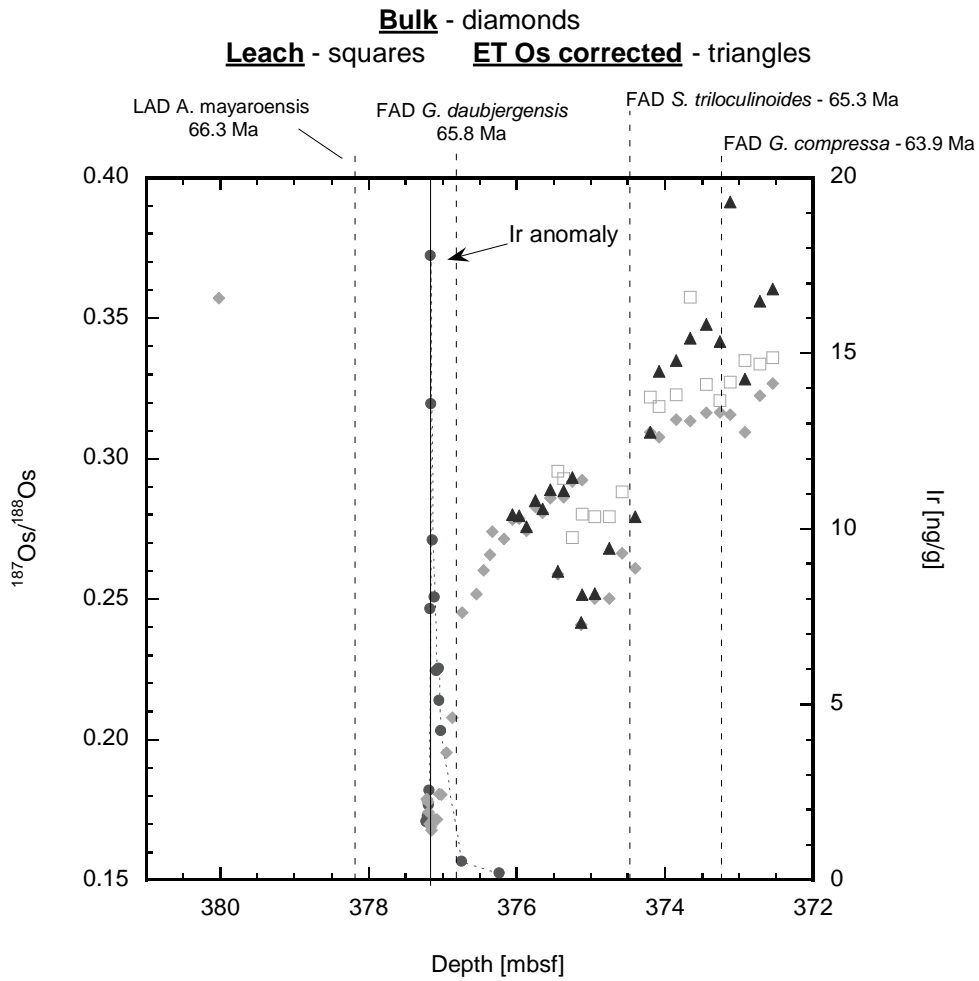
Figure 3.8. Zoomed in plot of the 738C Os IC profile with Ir anomaly. Biostratigraphic datums are also plotted to show that after more than 3 myr after the impact event, the Os IC does not reach the expected value of ~0.4. The extended period of low Os IC reaches beyond the extent of the Ir anomaly indicating that it is not likely due to emplaced impact-related material.
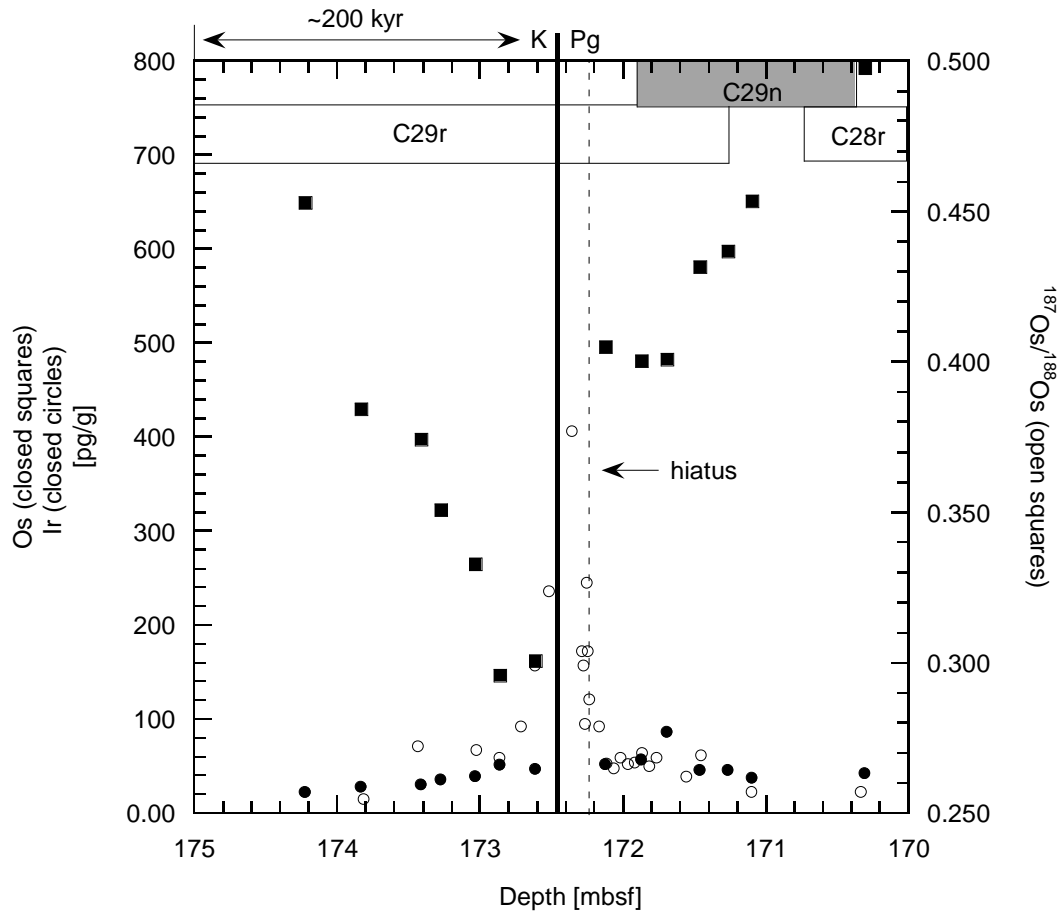
Figure 3.9. ODP site 761C bulk ^{187}Os/^{188}Os composition and Os and Ir (Roccia et al., 1992) concentrations versus depth. It should be noted that a significant portion of the Ir anomaly has been truncated to allow details of the Os concentration to be seen. The Ir anomaly goes as high as 7600 pg/g. Although sampling did not allow for a full impact-induced Os excursion to be obtained, available samples exhibit a ^{187}Os/^{188}Os ratio decline from ~0.4 before the impact as well as a full recovery to pre-impact values of at least 0.4. This site shows an exceptional continued recovery to 0.45. The base of the C29r chron is inferred from 761B. The overlap in magnetocrhons on this plot is a result of the uncertainty in reported data.
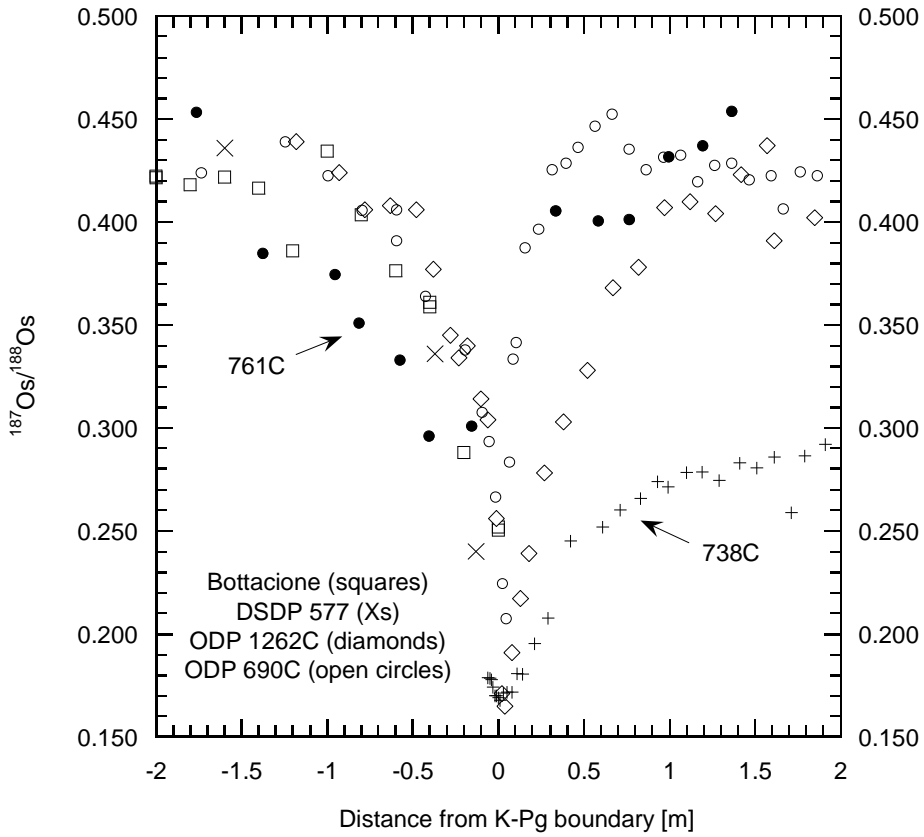
Figure 3.10. ^{187}Os/^{188}Os versus distance from K-Pg boundary. Site 761C begins to decline from ~0.4 deeper than other marine K-Pg sites which typically exhibit a similar decline within a maximum of 0.8 m below the K-Pg boundary.
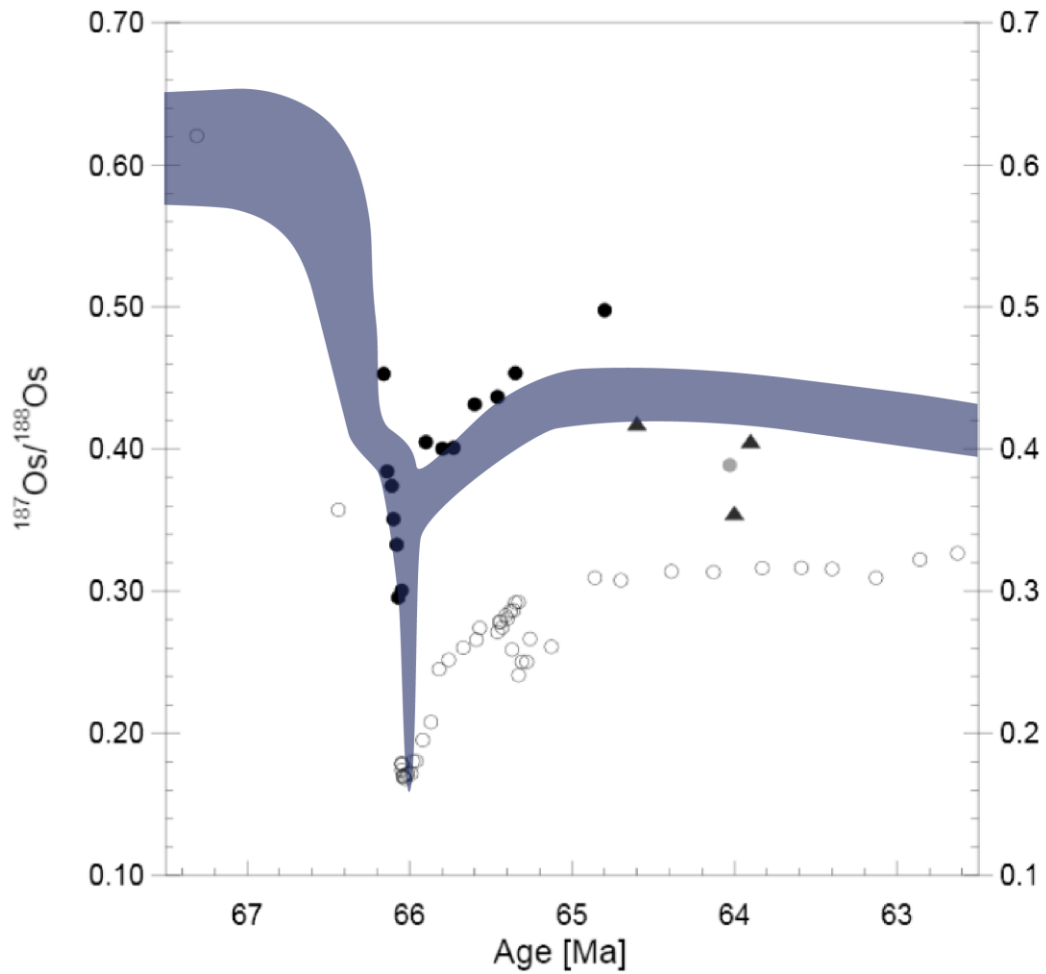
Figure 3.11. Age versus ^{187}Os/^{188}Os for Indian Ocean sites 738C (open circles), 761C (filled black circles) and DSDP sites 245 (triangles, Ravizza and Peucker-Ehrenbrink, 2003) as well as Pacific Ocean site 323 (filled grey circle, Peucker-Ehrenbrink et al., 1995). Also shown is a field representing the general trend of the global ocean for comparison. 738C exhibits anomalously low ^{187}Os/^{188}Os ratios for an extended period of time compared not only to the global ocean but also local sites. However, 761C exhibits early paleogene ^{187}Os/^{188}Os ratios above the expected trend and local sites.
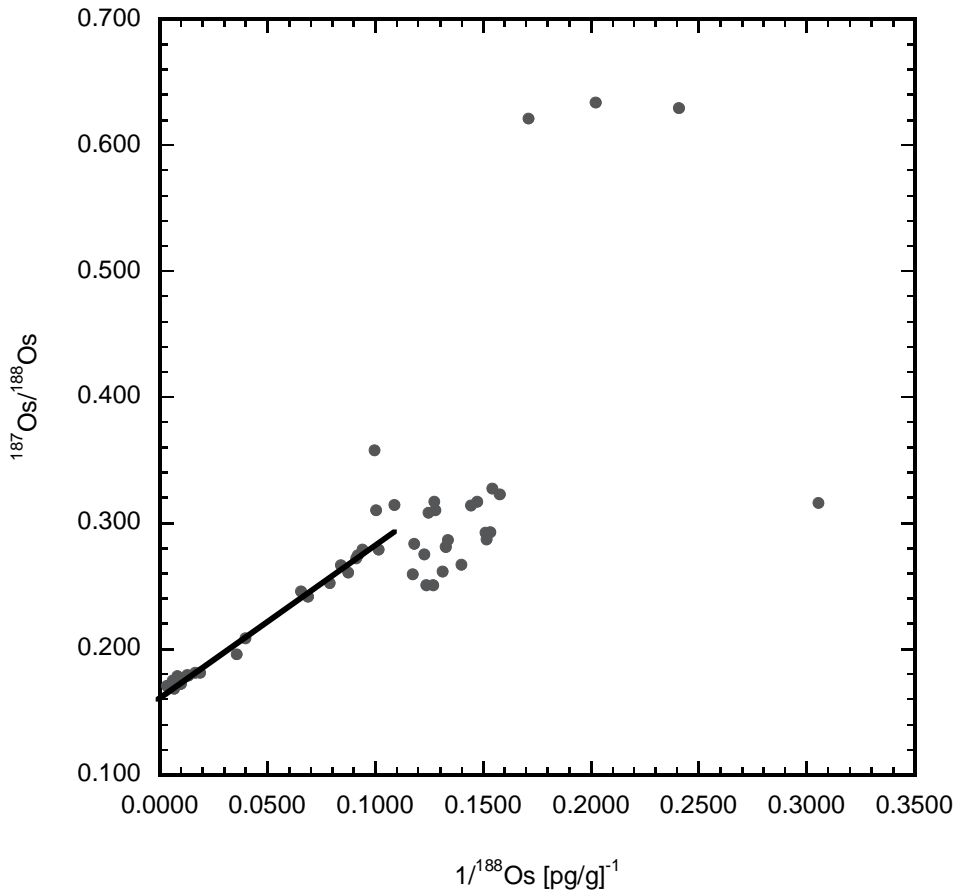
Figure 3.12. Mixing plot showing $^{187}Os/^{188}Os$ versus inverse ^{188}Os concentration. Samples with the line drawn through them represent samples that exhibit two component mixing between ambient seawater and impact derived Os. These samples span from core 20R-4 127-129 cm to 20R-5 101-102 cm (375.97 – 377.22 mbsf). This figure supports the notion that anomalously low $^{187}Os/^{188}Os$ compositions at 738C above 375.97 mbsf are not the direct result of reworking impact derived Os but rather reflect relatively low ambient seawater $^{187}Os/^{188}Os$ ratios.

Table 3.1. ODP 738C data

Core-Section	Depth Interval	mbsf	Depth relative to KPB [m]	Carius tube Os [pg/g][1]	Carius Tube $^{187}Os/^{188}Os$ [2]	Leach Os [pg/g][1]	Leach $^{187}Os/^{188}Os$ [2]	Re [pg/g]	Initial $^{187}Os/^{188}Os$	Age [Ma]	Fraction of impact-related sediment
20R-2	83.5-85.5	372.55	4.61	50.60 (0.12)	0.3268 (68)	23.90 (0.13)	0.3359 (46)			62.63	0.32
	100-102	372.72	4.44	49.51 (0.27)	0.3224 (56)	26.00 (0.17)	0.3337 (46)			62.86	0.34
	120-122	372.92	4.24	77.58 (0.39)	0.3094 (39)	27.31 (0.61)	0.3350 (52)			63.13	0.39
	140-142	373.12	4.04	25.55 (0.18)	0.3157 (59)	21.26 (0.07)	0.3273 (60)			63.40	0.37
20R-3	6-8	373.26	3.90	61.26 (0.44)	0.3165 (54)	20.60 (1.06)	0.3207 (143)			63.59	0.36
	24-26	373.44	3.72	52.96 (0.20)	0.3163 (58)	24.78 (0.06)	0.3265 (47)			63.83	0.36
FAD *G. compressa*	**373.49**									***63.90**	
	46-48	373.66	3.50	54.00 (0.30)	0.3135 (55)	23.43 (0.18)	0.3574 (597)			64.13	0.38
	65-67	373.85	3.31	71.50 (0.22)	0.3139 (44)	24.54 (0.84)	0.3227 (55)			64.39	0.37
	88-90	374.08	3.08	62.49 (0.31)	0.3076 (54)	28.95 (0.08)	0.3185 (40)			64.70	0.40
	100-102	374.20	2.96	60.90 (1.01)	0.3094 (53)	36.84 (0.21)	0.3219 (32)			64.86	0.39
	120-122	374.40	2.76	58.97 (0.30)	0.2609 (90)					65.13	0.60
FAD *S. trilonucliodes*	**374.49**									***65.25**	
	138-140	374.58	2.58	55.38 (0.34)	0.2664 (64)	22.75 (0.07)	0.2882 (45)			65.26	0.58

20R-4	5-7	374.75	2.41	62.47 (0.25)	0.2503 (81)	27.20 (0.10)	0.2794 (48)			65.28	0.65
	25-27	374.95	2.21	60.89 (0.21)	0.2503 (81)					65.31	0.65
	42-44	375.12	2.04	50.67 (0.11)	0.2923 (26)	30.53 (0.09)	0.2802 (40)	3.8	0.2919	65.33	0.47
	43-45	375.13	2.03	112.02 (2.14)	0.2408 (17)			7.0	0.2405	65.33	0.69
	55-57	375.25	1.91	51.47 (0.13)	0.2919 (23)	26.94 (0.10)	0.2719 (55)	2.4	0.2916	65.35	0.47
	67-69	375.37	1.79	51.23 (0.14)	0.2864 (19)	27.37 (0.09)	0.2929 (35)	3.0	0.2861	65.36	0.49
	75-77	375.45	1.71	65.89 (0.21)	0.2589 (21)	27.20	0.2955 (35)	16.4	0.2576	65.37	0.61
	85-87	375.55	1.61	58.12 (0.15)	0.2860 (25)			2.3	0.2858	65.38	0.50
	95-97	375.65	1.51	58.45 (0.19)	0.2807 (21)			85.8	0.2728	65.40	0.52
	105-107	375.75	1.41	65.69 (0.34)	0.2829 (26)			7.6	0.2823	65.41	0.51
	117-119	375.87	1.29	63.21 (0.18)	0.2744 (20)			2.8	0.2742	65.43	0.55
	127-129	375.97	1.19	76.35 (0.35)	0.2786 (21)			2.2	0.2784	65.44	0.53
	136-138	376.06	1.10	82.34 (0.16)	0.2783 (15)			8.5	0.2777	65.45	0.53
	147-149	376.17	0.99	85.00 (0.30)	0.2713 (17)			10.8	0.2706	65.46	0.56
20R-5	3-5	376.33	0.93	84.44 (0.16)	0.2740 (18)			11.6	0.2733	65.57	0.55
	13-15	376.36	0.83	92.18 (0.46)	0.2658 (26)			132.9	0.2581	65.59	0.58
	25.5-27.5	376.45	0.71	88.46 (0.19)	0.2602 (11)			9.8	0.2596	65.67	0.61

FAD *C. primus*	**35-37**	**376.55**	**0.61**	**97.76 (0.15)**	**0.2518 (11)**	23.3	0.2505	65.76	0.64
	54-56	376.74	0.42	117.49 (0.24)	0.2451 (13)	15.3	0.2444	65.82	0.67
FAD *G. daubjergensis*		**376.81**						***65.84**	
	67-69	376.87	0.29	191.37 (0.48)	0.2078 (11)	32.5	0.2069	65.87	0.84
	75-77	376.95	0.21	213.79 (0.56)	0.1953 (11)	19.3	0.1948	65.92	0.89
	82-83	377.02	0.14	404.97 (0.56)	0.1804 (70)	10.1	0.1803	65.96	0.95
	85-86	377.05	0.11	454.24 (0.62)	0.1806 (07)	50.6	0.1800	65.98	0.95
	88-89	377.08	0.08	749.63 (6.22)	0.1716 (05)	38.9	0.1713	65.99	0.99
	91-92	377.11	0.05	765.10 (1.43)	0.1716 (05)	28.5	0.1714	66.01	0.99
	93-94	377.13	0.03	947.74 (2.01)	0.1712 (06)	36.7	0.1710	66.02	0.99
Pg - Danian	95-96	377.15	0.01	1,061.83 (1.21)	0.1680 (06)	33.7	0.1678	66.03	1.01
	96-96.2	377.16	0.00	1,172.72 (3.13)	0.1690 (07)	27.0	0.1689	***66.04**	1.00
K - Maastrichtian	96.2-97	377.17	-0.01	2,056.61 (3.93)	0.1699 (06)	54.4	0.1698	66.04	1.00
	97-98	377.18	-0.02	1,501.74 (5.44)	0.1700 (06)	43.1	0.1698	66.04	1.00
	98-99	377.19	-0.03	1,200.40 (2.11)	0.1742 (05)	150.0	0.1735	66.05	0.98
	99-100	377.20	-0.04	901.61 (1.13)	0.1778 (07)	29.5	0.1776	66.05	0.97
	100-101	377.21	-0.05	558.52 (1.06)	0.1786 (05)	24.1	0.1784	66.05	0.96

	Interval	Depth						Age	
	101-102	377.22	-0.06	579.34 (2.32)	0.1788 (14)	26.7	0.1786	66.05	0.96
LAD *A. mayaroensis*		**378.40**						66.30	
21R-1	12-13	380.02	-2.86	78.51 (0.35)	0.3572 (126)			66.44	
22R-1	25-26	389.85	-12.69	47.32 (0.35)	0.6205 (267)			67.31	
23R-1	30.5-31.5	399.51	-22.35	33.69 (0.18)	0.6289 (311)			68.16	
K - Campanian									
FAD *A. mayaroensis*		**410.40**						***69.12**	
24R-2	111-112	411.52	-34.36	40.16 (0.27)	0.6335 (245)			69.22	

*Represents tie points used during interpolations to get ages for sample, [1] Number in parenthesis represents 2σ uncertainties in pg/g, [2] Number in parenthesis represents 2σ uncertainties in the last digits represented

Table 3.2. 761C Data

	Core	Section	Depth Interval	Abs. depth [mbsf]	Depth relative to KPB [m]	Carius tube Os [pg/g][1]	Carius Tube[2] $^{187}Os/^{188}Os$	Age 1 [Ma]	Age 2 [Ma]
	3R	1	60.5-61.5	170.30	2.16	41.54 (0.71)	0.4976 (75)	64.80	63.24
Top C29n (Top of C28n)				170.43 ± 0.10				64.96	63.49
			140-141	171.10	1.37	36.65 (0.45)	0.4534 (80)	65.35	64.12
		2	6-7	171.26	1.20	45.27 (0.24)	0.4366 (29)	65.46	64.30
			26-27	171.46	1.00	45.07 (0.28)	0.4314 (28)	65.60	64.52
Top C29r (top of C28r)				171.59 ± 0.33				65.69	64.67
			49-50	171.69	0.77	85.65 (0.28)	0.4008 (26)	65.73	64.72
		3	16-17	171.87	0.59	56.36 (0.24)	0.4002 (23)	65.80	64.80
Pg			41-42	172.12	0.34	51.50 (0.28)	0.4049 (26)	65.90	64.91
			75.5- 75.8	172.46				66.04	
K			90-91	172.61	-0.15	46.31 (0.96)	0.3006 (44)	66.05	
			115-116	172.86	-0.40	50.36 (0.27)	0.2956 (22)	66.07	
			132-133	173.03	-0.57	38.26 (0.28)	0.3326 (23)	66.08	
		4	5-6	173.27	-0.81	35.33 (0.27)	0.3507 (32)	66.10	

19-20	173.41	-0.95	29.68 (0.31)	0.3742 (46)	66.11
61-62	173.83	-1.37	27.42 (0.44)	0.3843 (52)	66.14
100-101	174.22	-1.76	21.79 (0.88)	0.4529 (103)	66.16
Bottom C29r		*177.58			66.40
				29r/29n	28r/28n

The Age 1 column represents the ages of the samples if the reversal above the hiatus is the C28r/C29n reversal. Age 2 represents the age of the samples if the hiatus extends into C28r resulting in the reversal above the hiatus being the C28r/C28n reversal.

*The bottom of C29r is based on the total length of C29r in hole 761B as the base of C29r was not recovered in 761C. [1] Number in parenthesis represents 2σ uncertainties in pg/g, [2] Number in parenthesis represents 2σ uncertainties in the last digits represented

Alvarez, L., Alvarez, W., Asaro, F., Michel, H., 1980. Extraterrestrial Cause for the Cretaceous-Tertiary Extinction. Science, 208: 1095-1108.

Berglund, M., Wieser, M.E. 2011. Isotopic compositions of the elements 2009 (IUPAC Technical Report). Pure Appl. Chem., 83: 397-410.

Burton, K.W., Gannoun, A., Parkinson, I.J. 2010. Climate driven glacial-interglacial variations in the osmium isotope composition of seawater recorded by planktic foraminifera. Earth and Plant. Sci. Lett., 295: 58-68.

Carlson, R.W., Shirey, S.B., Schönbächler, M. 2008. Applications of PGE radioisotope systems in geo- and cosmochemistry. Elements, 4: 239-245.

Chen, J.H., Papanastassiou, D.A., Wasserburg, G.J. 1998. Re-Os systematics in chondrites and the fractionation of the platinum group elements in the early solar system. Geochimica et Cosmochimica Acta, 62: 3379-3392.

Chen, C., Mukul, S. 2009. High precision and high sensitivity measurements of osmium in seawater. Anal. Chem., 81: 5400-5406.

Cohen, A.S., Coe, A.L., Harding, S.M. Schwark, L. 2004. Osmium isotope evidence for the regulation of atmospheric CO_2 by continental weathering. Geology, 32: 157-160.

Colodner, D., Sachs, J., Ravizza, G., Turekian, K., Edmond, J., Boyle, E. 1993. The geochemical cycle of rhenium – a reconnaissance. Earth and Planet. Scie. Lett. 117: 205-221.

Dalai, T.K., Suzuki, K., Minagawa, M., Nozaki, Y. 2005. Variations in seawater osmium composition since the last glacial maximum: A case study from the Japan Sea. Chem. Geol., 220: 303-314.

Horan, M., Walker, R., Morgan, J., Grossman, J., Rubin, A., 2003. Highly siderophile elements in chondrites. Chemical Geology, 196(1-4): 27-42.

Hull, P., Franks, P.J.S., Norris, R.D. 2011. Mechanism and models of iridium anomaly shape across the Cretaceous-Paleogene boundary. Earth and Planet. Sci. Lett. 301: 98-106.

Koeberl, C., Claeys, P., Hecht, L., McDonald, I. 2012. Geochemistry of Impactites. Elements, 8: 37-24.

Koeberl, C., Shirey, S.B. 1997. Re-Os systematics as a diagnostic tool for the study of impact craters and distal ejecta. Palaeogeo. Palaeoclimat. Palaeoecol. 132: 25-46.

Kuroda, J., Hori, R.S., Suzuki, K., Gröcke, D.R., Ohkouchi, N. 2010. Marine osmium isotope record across the Triassic-Jurassic boundary from a Pacific pelagic site. Geology, 38: 1095-1098.

Lee, C.-T., Wasserburg, G.J., Kyte, F.T. 2002. Platinum-group elements (PGE) and rhenium in marine sediments across the Cretaceous-Tertiary boundary: Constraints on Re-PGE transport in the marine environment. Geochim. Cosmochim. Acta. 67: 655-670.

Levasseur, S. Birck, J.L., Allégre C.J. 1999. The osmium riverine flux and the oceanic mass balance of osmium. Earth and Planetary Science Letters, 174: 7-23.

Luguet, A., Lorand, J.-P., Seyler, M. 2003. Sulfide petrology and highly siderophile element geochemistry of abyssal peridotites: A coupled study of samples form the Kane Fracture Zone (45°W 23°20N, MARK area, Atlantic Ocean). Geochim. Cosmochim. Acta, 67: 1553-1570.

Luguet, A., Shirey, S.B., Lorand, J.-P., Horan, M.F., Carlson, R.W. 2007. Residual platinum group minerals from highly depleted harzburgites of the Lherz massif (France) and their role in HSE fractionation of the mantle. Geochim. Cosmochim. Acta 71: 3082-3097.

Martin, C., Peucker-Ehrenbrink, B., Brunskill, G., Szymczak R. 2001. Osmium isotope geochemistry of a tropical estuary. Geochim. Cosmochim. Acta., 65: 3193-3200.

Meisel, T., Krähenbühl, U., Nazarov, M.A. 1995. Combined osmium and strontium isotopic study of the Cretaceous-Tertiary boundary at Sumbar, Turkmenistan: A test for impact vs volcanic hypothesis. Geology, 23: 313-316.

Meisel, T., Walker, R.J., Irving, A.J., Lorand, J.P. 2001. Osmium isotopic compositions of mantle xenoliths: A global perspective. Geochim. Cosmochim. Acta, 65: 1311-1323.

Meisel, T., Walker, R.J., Morgan, J.W. 1996. The osmium isotopic composition of the Earth's primitive upper mantle. Nature, 383: 517-520.

Moore, J., Wilson, G.P., Sharma, M., Hallock, H., Braman, D.R., Renne, P.R. 2014. Assessing the relationship of the Hell Creek - Fort Union contact, Cretaceous-Paleogene boundary, and Chicxulub impact ejecta horizon at the Hell Creek Formation lectostratotype, Montana, USA. Geol. Soc. Am. Spec. Papers, 503: 123-135.

Morford, J.L., Martin, W.R., Carney, C.M. 2012. Rhenium geochemical cycling: insights from continental margins. Chem. Geol., 324: 73-86.

Morgan, J. 2008. Comment on "Determining Chondritic Impactor Size from the Marine Osmium Isotope Record". Science, 321: 1158.

Oxburgh, R. 2001. Residence time of osmium in the oceans. Geochemistry, Geophysics, Geosystems, 2. 2000GC00010.

Oxburgh, R., Pierson-Wickmann, A.-C., Reisberg, L., Hemming, S. 2007. Climate-correlated variations in seawater Os-187/Os-188 over the past 200,000 yr: Evidence from the Cariaco Basin, Venezuela. Earth and Planet. Scie. Lett., 263: 246-258.

Palme, H. 2008. Platinum-group elements in cosmochemistry. Elements, 4: 233-238.

Paquay, F.S., Ravizza, G., 2012. Heterogeneous seawater 187Os/188Os during the late Pleistocene glaciations. Earth and Planetary Science Letters, 349-350: 126-138.

Paquay, F.S., Ravizza, G.E., Dalai, T.K., Peucker-Ehrenbrink, B. 2008. Determining chondritic impactor size from the marine osmium isotope record. Science, 320: 214- 218.

Peregoedova, A., Barnes, S.-J., Baker, D.R. 2004. The formation of Pt-Ir alloys and Cu-Pd-rich sulfide melts by partial desulfurization of Fe-Ni-Cu sulfides: results of experiments and implications for natural systems. Chem. Geol., 208: 247-264.

Puecker-Ehrenbrink, B., Blum, J.D. 1998. Re-Os isotope systematics and weathering of Precambrian crustal rocks: Implications for the marine osmium isotope record. Geochimica et Cosmochimica Acta, 62: 3193-3203. 1998. Annu. Rev. Earth Planet. Sci., 26: 423-500.

Puecker-Ehrenbrink, B., Jahn, B. 2001. Rhenium-osmium isotope systematics and platinum group element concentrations: Loess and the upper continental crust. Geochem. Geophys. Geosys., 2001GC000172.

Puchtel, I.S., Humayun, M. 2001. Platinum group element fractionation in a komatiitic basalt lava lake. Geochim. Cosmochim. Acta, 65:2979-2993.

Ravizza, G., Norris, R.N., Blusztajn, J., Aubry, M.P. An osmium isotope excursion associated with the late-Paleocene thermal maximum: Evidence of intensified chemical weathering. Paleoceanography, 16: 155-163.

Ravizza, G., Turekian, K.K. 1992. The osmium isotopic composition of organic-rich marine sediments. Earth and Planet. Sci. Lett., 110: 1-6.

Roy-Barman, M. Wasserburg, G.J., Papanastassiou, D.A., Chaussidon, M. 1998. Osmium isotope composotions and Re-Os concentrations in sulfide globules from basaltic glasses. Earth and Planet. Sci. Letters, 154: 331-347.

Sato, H., Onoue, T., Nozaki, T., Suzuki, K., 2013. Osmium isotope evidence for a large Late Triassic impact event. Nature Communications, 4, 2455. doi:10.1038/ncomms3455

Schmitz, B., Asaro, F., Michel H.V., Thierstein H.R., Huber B.T. 1991 Element stratigraphy across the Cretaceous/Tertiary boundary in Hole 738C. In Barron J., Larsen B., et al., 1989. Proc. ODP Init. Repts., 119: College Station TX (Ocean Drilling Program)

Sharma M., Papanastassiou D.A., and Wasserburg G.J. 1997. The concentration and isotopic composition of osmium in the oceans. Geochim. Cosmochim. Acta, 61: 3287-3299.

Sharma, M., Wasserburg, G.J., Hofmann, A.W., Butterfield, D.A. 2000. Osmium isotopes in hydrothermal fluids from the Juan de Fuca Ridge. Earth and Planet. Sci. Letters, 179: 139-152.

Shen, J.J., Papanastassiou, D.A., Wasserberg, G.J. 1996. Precise Re-Os determinations and systematics of iron meteorites. Geochimica et Cosmochimica Acta, 60: 2887-2900.

Shirey, S., Walker, R. 1998. The Re-Os isotope system in cosmochemistry and high-temperature geochemistry. Annu. Rev. Earth Planet. Sci., 26: 423-500.

Smoliar, M.I., Walker, R.J., Morgan, J.W., 1996. Re-Os isotope constraints on the age of Group IIA, IVA, and IVB iron meteorites. Science, 271: 1099-1102.

Turgeon, S.C., Creaser, R.A. 2008. Cretaceous ocean anoxic event 2 triggered by a massive magmatic episode. Nature, 454: 323-326.

Walker, R.J., Morgan, J.W., Beary, E.S., Smoliar, M.I., Czamanske, G.K., Horan, M.F. 1997. Applications of the ^{190}Pt-^{186}Os isotope system to geochemistry and cosmochemistry. Geochim. Cosmochim. Acta, 61: 4799-4807.

Wasson, J.T. 1985. Meteorites: their record of early solar system history. San Franscisco: Freeman. 267 pgs.

Woodhouse, O.B., Ravizza, G., Kenison Falkner, K., Statham, P.J., Peucker-Ehrenbrink, B. 1999. Osmium in seawater: vertical profiles of concentration and isotopic composition in the eastern Pacific Ocean. Earth and Plant. Sci. Lett., 173: 223-233.